

NIST Technical Note 2159

Laboratory Method for Recording AWS-3 LTE Waveforms

Aric W. Sanders
M. Keith Forsyth
Robert D. Horansky
Azizollah Kord
Duncan A. McGillivray

This publication is available free of charge from:
<https://doi.org/10.6028/NIST.TN.2159>

NIST
**National Institute of
Standards and Technology**
U.S. Department of Commerce

NIST Technical Note 2159

Laboratory Method for Recording AWS-3 LTE Waveforms

Aric W. Sanders
M. Keith Forsyth
Robert D. Horansky
Azizollah Kord
Duncan A. McGillivray
*Communications Technology Laboratory
NIST*

This publication is available free of charge from:
<https://doi.org/10.6028/NIST.TN.2159>

May 2021



U.S. Department of Commerce
Gina M. Raimondo, Secretary

National Institute of Standards and Technology
*James K. Olthoff, Performing the Non-Exclusive Functions and Duties of the Under Secretary of Commerce
for Standards and Technology & Director, National Institute of Standards and Technology*

Laboratory Method for Recording AWS-3 LTE Waveforms

Aric W. Sanders, M. Keith Forsyth, Robert D. Horansky,
Azizollah Kord, Duncan A. McGillivray

NASCTN Project Manager: Fabio C.S. da Silva
NASCTN Program Manager: Melissa M. Midzor

May 11, 2021



NASCTN

National Advanced Spectrum and
Communications Test Network

DISCLAIMER

Certain commercial entities, equipment, or materials may be identified in this document in order to describe an experimental procedure or concept adequately. Such identification does not imply any recommendation or endorsement by National Institute of Standards and Technology (NIST) or National Advanced Spectrum and Communications Test Network (NASCTN), nor is it intended to imply that the materials or equipment identified are necessarily the best available for the purpose.

National Institute of Standards and Technology Technical Note 2159
Natl. Inst. Stand. Technol. Tech. Note 2159, 106 pages (May 2021)
CODEN: NTNOEF

This publication is available free of charge from:
<https://doi.org/10.6028/NIST.TN.2159>

Preface

The work described herein was performed as a result of a spectrum sharing project request submitted to the National Advanced Spectrum and Communications Test Network (NASCTN). NIST is a founding charter member of NASCTN. This work was sponsored by Edwards Airforce Base, and conducted by NIST with support by MITRE. A summary of each organization's technical contributions follows.

The project underwent formal screening and approval by the NASCTN Steering Committee. A description of NASCTN and listing of Charter Members at the time of publication of this report follows.

National Advanced Spectrum and Communications Test Network (NASCTN)

The mission of the National Advanced Spectrum and Communications Test Network (NASCTN) is to provide, through its members, a network for robust test processes and validated measurement data necessary to develop, evaluate and deploy spectrum sharing technologies that can improve access to the spectrum by both federal agencies and non-federal spectrum users.

NASCTN is a member organization under a charter agreement. Members

- Facilitate and coordinate work with federal, academic, and industry spectrum users to rapidly and cooperatively facilitate spectrum sharing and co-existence studies;
- Work as a partnership to address the interests and equities of all spectrum stakeholders in a fair, equitable, and non-preferential manner; and
- Through sharing of technical resources, with consideration for cost, provide liaison and support to coordinate and leverage existing national capabilities supporting government, academic, and industry testing and evaluation known to improve and expedite spectrum sharing and coexistence.

Charter members at the time of publication of this report are (in alphabetical order):

- Department of Defense Chief Information Officer (DoD CIO)
- National Aeronautics and Space Administration (NASA)
- National Institute of Standards and Technology (NIST)
- National Oceanic and Atmospheric Administration (NOAA)
- National Science Foundation (NSF)
- National Telecommunications and Information Administration (NTIA)

NIST hosts the NASCTN capability at the Department of Commerce Boulder Laboratories in Boulder, Colorado.

Technical Contributors

Contributor	Organization	Contribution
Forsyth, M. K.	NIST	Development of testbed
Horansky, R. D.	NIST	Radiated measurements of testbed
Kord, A.	NIST	LTE network setup and testbed Implementation
Kuester, D.	NIST	LTE Waveform processing
McGillivray, D. A.	NIST	Test implementation lead, design, coordination, and planning
Sanders, A. W.	NIST ¹	Development of testbed and software design
Krangle, M.	MITRE	Waveform processing
Young, W. F.	MITRE	Project technical lead

¹ Currently employed at the University of Colorado, Boulder

Acknowledgments

The technical team thanks Barbara Wheaton and Kenneth Temple of Edwards Air Force Base for their support and sponsoring of the National Advanced Spectrum and Communications Test Network (NASCTN) test on "AWS-3 LTE impacts on AMT" of which this report is an addendum.

Furthermore, the team acknowledges the NASCTN program manager, Dr. Melissa Midzor and the NASCTN project manager Dr. Fabio da Silva for their support of the project.

It is important to recognize that the methodology used to create the library of user equipment (UE) emission captures leverages previous testbed implementations and we hereby recognize the experimental expertise of Jason Coder, Dr. Daniel Kuester and many others that participated in the "Characterizing LTE User Equipment Emissions: Factor Screening" project [1]. Also, Dr. Adam Wunderlich provided key experimental analysis and guidance.

Executive Summary

The National Advanced Spectrum and Communications Test Network (NASCTN)'s "AWS-3 LTE impacts on AMT" study required in-phase and quadrature (IQ) recordings of user equipment (UE) uplink band (UL) traffic from advanced wireless services 3 (AWS-3) (1755 MHz - 1780 MHz) equipment for playback in a susceptibility analysis. These IQ recordings were a combination of field IQ recordings and IQ recordings in a laboratory environment. It was determined that an extended library of laboratory based IQ recordings of UE UL traffic would benefit other projects and research in communications and spectrum usage. These laboratory IQ recordings provide a database that is: free from potential personal identifying information, are recorded with a high signal-to-noise ratio, have corresponding UE diagnostic information, and have control and documentation of key network configurations. Therefore, National Institute of Standards and Technology (NIST) and the NASCTN program office commissioned this work. The focus of this work is to provide a library of IQ recordings of actual UE UL emissions with sufficient time resolution and dynamic range for use in spectrum sharing and interference susceptibility studies. The IQ recordings of the UE UL emissions were performed in the NIST Broadband Interoperability Testbed (NBIT) facility, where one UE was in connection to a fully emulated long-term evolution (LTE) network with a commercial off-the-shelf (COTS) evolved Node B (eNB), or LTE base station. In select cases a second UE was attached to the network. NBIT's testbed allows for a radiated free-space connection in an anechoic chamber to the UE in conjunction with a cabled user equipment traffic generator (UTG) for control of cell loading conditions.

IQ recordings are presented under configurations that represent different channel conditions and cell loading. Seven conditions include a second radiating UE. The device under test (DUT) UEs are placed in a static location designed to have a reference signal received power (RSRP) of approximately -85 dBm. In the seven cases with a second radiating UE, the additional UE is placed in a location designed to have an approximate RSRP of -95 dBm. The eNB was configured to have a reference signal power (RSP) of -11 dBm. The conditions span a changing set of input factors, without being fully factorial:

- Power control, with: open loop and closed loop power control methods.
- Resource blanking mask, with: none, upper 6% of allocation, upper 10% of allocation, and center 10% of allocation.
- Uplink channel allocation, with: 5 MHz, 10 MHz and 20 MHz.
- Number of loading UEs, with: 3, 7, and 15 loading UEs.
- Data rate of DUT UE, varying among: 0.5, 1, 5, and 10 megabits per second (Mbit/s).
- Number of radiating UEs, either: 1 or 2.

These IQ recordings are captured at a sampling rate of 61.44 MS/s, in an experiment designed to selectively increase the dynamic range of the emissions from the DUT UE. Each IQ recording includes 5 seconds of data or 307.2 million data points. Every IQ recording is time-aligned to the communication system by using user equipment self-reported diagnostics (USRD) data and confirmed with an independent recording of the power spectrum at a lower sampling rate. These well characterized IQ recordings are designed to be introduced into susceptibility studies. The recordings are available at <https://doi.org/10.18434/mds2-2395>.

Contents

Technical Contributors	iii
Executive Summary	v
List of Acronyms	ix
List of Figures	x
List of Tables	xiii
1 Introduction	1
1.1 Motivation	1
1.2 Overview	1
2 Testbed	2
2.1 Overview	2
2.2 Testbed Design	2
2.2.1 Testbed Equipment	3
2.2.1.1 LTE Infrastructure	3
2.2.1.2 LTE eNB	5
2.2.1.3 LTE UE Traffic Generator	5
2.2.1.4 Vector Signal Analyzer	5
2.2.1.5 DUT UEs - Devices and Traffic	5
2.2.1.6 USRD Monitoring Software	6
2.2.1.7 Vector Signal Transceiver	6
2.3 Testbed Radiated Path	6
3 Test Implementation	9
3.1 LTE Configuration	9
3.1.1 Factors	9
3.1.2 eNB Configuration	9
3.1.3 UE Configuration	9
3.1.4 UTG Configuration	9
3.1.5 Use Cases	10
3.2 Testbed Automation	10
3.2.1 Python Automation	10
3.2.2 LabVIEW Automation	11
4 Test Execution	13
4.1 Test Sequence	13
4.2 Testbed-Log Collection	13
4.2.1 Data Flow and Storage	13
4.3 Test Matrix	14

5	Test Verification and Data Synchronization	16
5.1	Data Parsing & Processing	16
5.1.1	Diagnostic Data (USRD)	16
5.1.2	VSA Data	16
5.1.3	IQ Recordings	17
5.1.4	Time Alignment	17
6	Conclusion	20
A	Calibration and Verification Measurements	21
A.1	Over-the-Air Link Budget Measurements	21
A.2	Conducted Path Link Budget Measurement	23
A.3	Cable Verification	23
A.4	Total System Losses and Uncertainty	23
B	Graphical Overview of IQ Recordings	30
	Bibliography	87

Acronyms

3GPP	3rd-Generation Partnership Project		
AMT	aeronautical mobile telemetry	NVRAM	nonvolatile random-access memory
ADB	Android Debug Bridge	OLPC	open loop power control
AWS-3	advanced wireless services 3	PC	personal computer
CLI	command line interface	PGW	packet gateway
CLPC	closed loop power control	PII	personally identifiable information
COTS	commercial off-the-shelf	PRB	physical resource block
CSV	comma separated value	PSCRD	Public Safety Communications Research Division
DL	downlink band	QCI	quality of service class identifier
DUT	device under test	RAN	radio access network
EEPROM	electrically erasable programmable read-only memory	RF	radio frequency
eNB	evolved Node B	RSP	reference signal power
EPC	evolved packet core	RSRP	reference signal received power
FFT	Fast Fourier Transform	SCPI	standard commands for programmable instruments
GUI	graphical user interface	SGW	serving gateway
HSS	home subscriber server	SINR	signal-to-interference-plus-noise ratio
IP	internet protocol	SVSWR	site voltage standing wave ratio
IQ	in-phase and quadrature	TCP	transmission control protocol
kbit/s	kilobits per second	TDMS	technical data management streaming
LAN	local area network	TTI	transmission time interval
LO	local oscillator	UDP	user datagram protocol
LTE	long-term evolution	UE	user equipment
Mbit/s	megabits per second	UI	user interface
MCS	modulation coding scheme	UL	uplink band
MME	mobility management entity	US	United States
ms	millisecond	USB	universal serial bus
MXI	multisystem extension interface	USRD	user equipment self-reported diagnostics
.NET	Microsoft .NET framework	UTG	user equipment traffic generator
NASCTN	National Advanced Spectrum and Communications Test Network	VNA	vector network analyzer
NBIT	NIST Broadband Interoperability Testbed	VSA	vector signal analyzer
NI	National Instruments	VST	vector signal transceiver
NIST	National Institute of Standards and Technology	XML	extensible markup language

List of Figures

2.1	Overview of the experimental setup.	3
2.2	Schematic diagram of the laboratory capture.	8
3.1	Data and control connections within the testbed network.	11
3.2	VST IQ recording-capture software user interface.	12
4.1	High-level test sequence specification.	14
5.1	Cross correlation of the UE synthetic spectrogram and the IQ recording generated spectrogram.	18
5.2	Aligned spectrograms of IQ from the VST, VSA , and UE generated spectrograms from USRD.	19
A.1	Overview of Anechoic Chamber Setup.	25
A.2	Plot of the relative power loss between the vector signal transceiver (VST) and UE1 horn antennas.	26
A.3	Plot of the relative power loss between the VST and UE2 horn antennas.	27
A.4	Plot of the relative power loss between the VST antenna and the UE2 antenna.	28
A.5	Electrical schematic of the NASCTN LTE Testbed.	29
B.1	140 milliseconds of IQ Recording 1 of Configuration Number 1.	31
B.2	140 milliseconds of IQ Recording 1 of Configuration Number 2.	32
B.3	140 milliseconds of IQ Recording 1 of Configuration Number 3.	33
B.4	140 milliseconds of IQ Recording 1 of Configuration Number 4.	34
B.5	140 milliseconds of IQ Recording 1 of Configuration Number 5.	35
B.6	140 milliseconds of IQ Recording 1 of Configuration Number 6.	36
B.7	140 milliseconds of IQ Recording 1 of Configuration Number 7.	37
B.8	140 milliseconds of IQ Recording 1 of Configuration Number 8.	38
B.9	140 milliseconds of IQ Recording 1 of Configuration Number 9.	39
B.10	140 milliseconds of IQ Recording 1 of Configuration Number 10.	40
B.11	140 milliseconds of IQ Recording 1 of Configuration Number 11.	41
B.12	140 milliseconds of IQ Recording 1 of Configuration Number 12.	42
B.13	140 milliseconds of IQ Recording 1 of Configuration Number 13.	43
B.14	140 milliseconds of IQ Recording 1 of Configuration Number 14.	44
B.15	140 milliseconds of IQ Recording 1 of Configuration Number 15.	45
B.16	140 milliseconds of IQ Recording 1 of Configuration Number 16.	46
B.17	140 milliseconds of IQ Recording 1 of Configuration Number 17.	47
B.18	140 milliseconds of IQ Recording 1 of Configuration Number 18.	48
B.19	140 milliseconds of IQ Recording 1 of Configuration Number 19.	49
B.20	140 milliseconds of IQ Recording 1 of Configuration Number 20.	50
B.21	140 milliseconds of IQ Recording 1 of Configuration Number 21.	51
B.22	140 milliseconds of IQ Recording 1 of Configuration Number 22.	52
B.23	140 milliseconds of IQ Recording 1 of Configuration Number 23.	53
B.24	140 milliseconds of IQ Recording 1 of Configuration Number 24.	54
B.25	140 milliseconds of IQ Recording 1 of Configuration Number 25.	55
B.26	140 milliseconds of IQ Recording 1 of Configuration Number 26.	56
B.27	140 milliseconds of IQ Recording 1 of Configuration Number 27.	57
B.28	140 milliseconds of IQ Recording 1 of Configuration Number 28.	58
B.29	140 milliseconds of IQ Recording 1 of Configuration Number 29.	59
B.30	140 milliseconds of IQ Recording 1 of Configuration Number 30.	60
B.31	140 milliseconds of IQ Recording 1 of Configuration Number 31.	61
B.32	140 milliseconds of IQ Recording 1 of Configuration Number 32.	62
B.33	140 milliseconds of IQ Recording 1 of Configuration Number 33.	63

B.34	140 milliseconds of IQ Recording 1 of Configuration Number 34.	64
B.35	140 milliseconds of IQ Recording 1 of Configuration Number 35.	65
B.36	140 milliseconds of IQ Recording 1 of Configuration Number 36.	66
B.37	140 milliseconds of IQ Recording 1 of Configuration Number 37.	67
B.38	140 milliseconds of IQ Recording 1 of Configuration Number 38.	68
B.39	140 milliseconds of IQ Recording 1 of Configuration Number 39.	69
B.40	140 milliseconds of IQ Recording 1 of Configuration Number 40.	70
B.41	140 milliseconds of IQ Recording 1 of Configuration Number 41.	71
B.42	140 milliseconds of IQ Recording 1 of Configuration Number 42.	72
B.43	140 milliseconds of IQ Recording 1 of Configuration Number 43.	73
B.44	140 milliseconds of IQ Recording 1 of Configuration Number 44.	74
B.45	140 milliseconds of IQ Recording 1 of Configuration Number 45.	75
B.46	140 milliseconds of IQ Recording 1 of Configuration Number 46.	76
B.47	140 milliseconds of IQ Recording 1 of Configuration Number 47.	77
B.48	140 milliseconds of IQ Recording 1 of Configuration Number 48.	78
B.49	140 milliseconds of IQ Recording 1 of Configuration Number 49.	79
B.50	140 milliseconds of IQ Recording 1 of Configuration Number 50.	80
B.51	140 milliseconds of IQ Recording 1 of Configuration Number 51.	81
B.52	140 milliseconds of IQ Recording 1 of Configuration Number 52.	82
B.53	140 milliseconds of IQ Recording 1 of Configuration Number 53.	83
B.54	140 milliseconds of IQ Recording 1 of Configuration Number 54.	84
B.55	140 milliseconds of IQ Recording 1 of Configuration Number 55.	85
B.56	140 milliseconds of IQ Recording 1 of Configuration Number 56.	86

List of Tables

2.1	Summary of testbed components.	4
4.1	Test Configurations.	15
5.1	VSA acquisition bandwidth per allocation.	16
A.1	Radiated path loss measurement accounting for uncertainty due to antenna placement and frequency averaging. . .	22
A.2	Conducted path loss measurements.	23
A.3	Summary of system losses and associated uncertainties.	24

Chapter 1

Introduction

1.1 Motivation

In many spectrum sharing tests, a recording of interfering traffic is captured and played back to assess the detrimental impact on a communication system that is coincident in frequency (co-channel interference) or in an adjacent band (out-of-band interference). This method was used to measure the impacts of long-term evolution (LTE) user equipment (UE) emissions in the United States advanced wireless services 3 (AWS-3) frequency band (1755 MHz - 1780 MHz) on aeronautical mobile telemetry (AMT) systems in the adjacent L band (1780 MHz - 1850 MHz), for the "AWS-3 LTE Impacts on AMT" project proposed by Edwards Air Force Base. To benefit this and future studies, the National Advanced Spectrum and Communications Test Network (NASCTN) identified a need for providing a methodology to reliably acquire in-phase and quadrature (IQ) recordings of UE uplink band (UL) emissions in a laboratory setting for receiver susceptibility studies. This document focuses on recording radiated AWS-3 cellular LTE UL emissions from UE. The LTE network configurations affecting the physical layer addressed in this effort were informed by findings of NASCTN's report on "Characterizing LTE User Equipment: Factor Screening Report" [1], as well as the in-field capture campaign [2] for the "LTE Impacts on AMT" project.

1.2 Overview

In this technical note we describe a process to acquire IQ recordings of radiated cellular UL traffic of UEs in a fully emulated LTE network using a commercial off-the-shelf (COTS) evolved Node B (eNB). An anechoic chamber in the NIST Broadband Interoperability Testbed (NBIT) facility serves as a radiated test environment. The eNB is used in conjunction with a user equipment traffic generator (UTG) to subject the device under test (DUT) UEs to various LTE traffic conditions and capture a series of IQ recordings. The recordings are time-aligned with diagnostic information from the chip-set of a DUT UE and reporting from the UTG. When compared to field captures, this method allows greater insight and control of the network configuration and leads to recordings that are optimized to be free of incidental and unwarranted content, such as personally identifiable information (PII). Furthermore, the methodology presented here describes how to capture IQ recordings of UE UL traffic with high signal-to-noise floor ratios (> 35 dB). We chose different configurations of the LTE network that are well within the performance envelope of LTE deployments. For a detailed discussion of the experimental factors, see Section 3.

The remainder of this report is laid out as follows:

- Testbed (Chapter 2) : an overview of the test architecture, including test circuitry, radiated path layout, and test automation
- Test implementation (Chapter 3) : a description of the order of execution and how the testbed was implemented
- Test execution (Chapter 4): a description of the test sequence and test matrix
- Test verification (Chapter 5) : processes developed to verify the IQ recordings
- Uncertainty evaluation (Appendix A) : an analysis of the expected radio frequency (RF) uncertainty in the IQ acquisition process
- IQ graphic library (Appendix B) : a visual representation of the IQ recordings captured for a selected time

Chapter 2

Testbed

2.1 Overview

This research leverages NBIT which includes a fully emulated LTE network using a COTS eNB, utilized for spectrum sharing and coexistence testing, and an anechoic chamber with a $3\text{ m} \times 3\text{ m} \times 3\text{ m}$ quiet zone. This facility is configured to support a radiated emissions capture campaign of UL transmissions. NBIT was augmented with test circuitry between the radio-to-air interface, traffic generation, diagnostic tools, and RF measurement hardware necessary to perform laboratory captures. The testbed details are outlined in the sections below. The measurement of relevant path losses in the system is covered in detail in Appendix A.

2.2 Testbed Design

The testbed was designed to have a wide dynamic range control of the UE power as well as to be able to capture DUT UE UL emissions. The capture of the DUT UE UL emissions are performed simultaneously and include: the UE diagnostic information, a spectrogram from a vector signal analyzer (VSA), and a time series of IQ recordings. These repetitive data streams are recorded on instruments with slightly different clock times and have timestamps that must be aligned (see chapter 5) but once they are aligned to the LTE system time, they give independent measurements of the UE UL transmissions. These multiple independent measurements give additional confidence in the integrity of the test methodology. The UE UL diagnostic data were used as the primary time basis to correctly align all other captured data sources. Figure 2.1 shows a block diagram overview of the experimental setup. In Figure 2.1, five major logical blocks are highlighted: the radiated path, the RF test circuit, the LTE network loading and monitoring equipment, the control network, and IQ acquisition. The first logical block is the radiated path or the physical layout of the anechoic chamber. This consists of two horn antennas and two UEs inside of the anechoic chamber. The second logical block is the RF test circuit that contains the appropriate attenuation, splitting/combining and phase shifting to both direct the UL and downlink band (DL) traffic to LTE and RF measurement equipment. The third logical block, denoted as LTE, consists of the eNB, UTG and the VSA. The LTE network behavior is controlled by the eNB which is loaded by the UTG and UEs and monitored by the VSA. The fourth logical block contains the a combination of local area network (LAN) and universal serial bus (USB) connections reporting to a control personal computer (PC) for testbed automation. The fifth and last logical block consists of the vector signal transceiver (VST) and RAID drive. Experimentally, two independent recordings of UL are acquired simultaneously, one in coordination with the LTE block and one electrically triggered by this event, but through a separate RF path. The recording from the VSA is designed to capture only the set channel bandwidth of the eNB and serves as a power measurement independent of the UE diagnostic information to ensure that the experiment is properly executing. The IQ recording from the VST captures a larger fixed bandwidth with a smaller total path loss from the UE and is the primary data included in the IQ library. The RF path for the IQ recordings includes the VST antenna leading to the VST. The VST then streams data to a RAID drive and is identified as the IQ acquisition block. Each component of this test bed is detailed in Table 2.1 and discussed in detail in the proceeding sections.

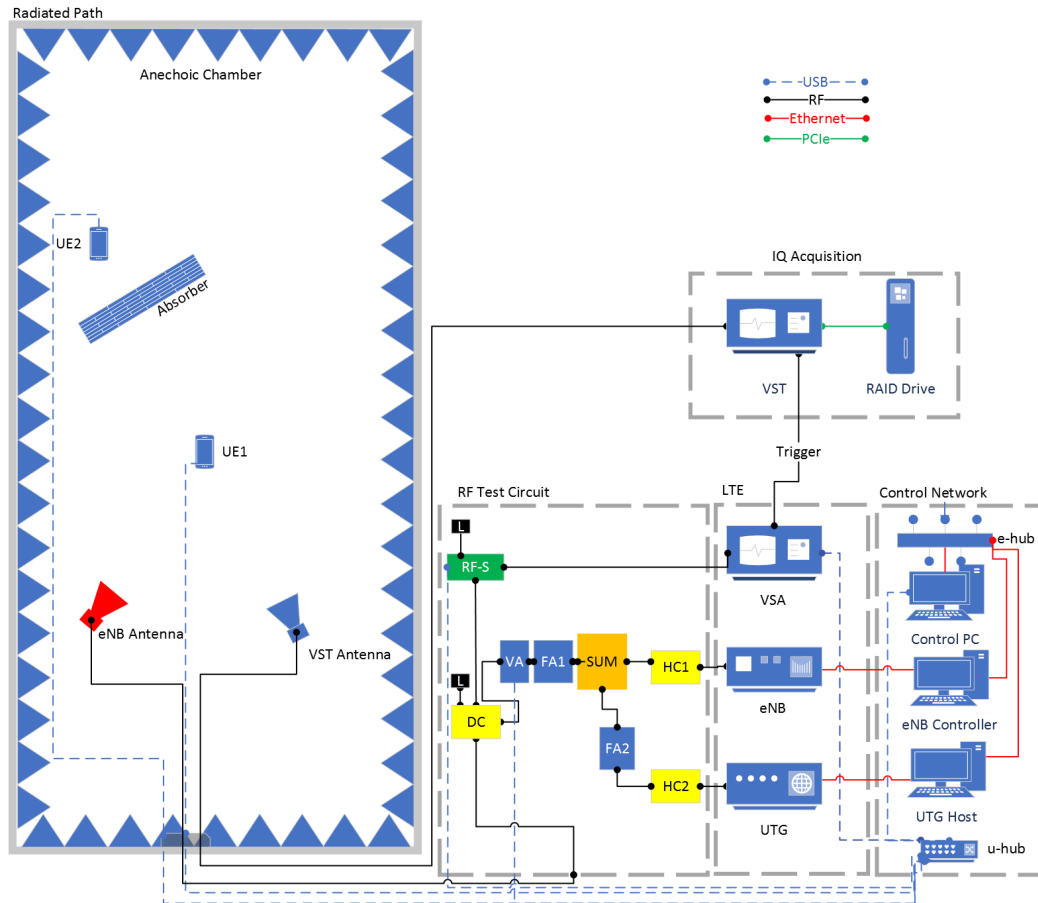


Figure 2.1: Overview of the experimental setup. The test made use of a hybrid measurement setup. Radiated anechoic portion treated the DUT UEs as black box entities while the cabled setup allowed for harmonized balancing of reference signal received power (RSRP) between the UTG and the DUT UEs.

2.2.1 Testbed Equipment

The testbed unifies core pieces of NBIT's LTE infrastructure, telecommunication diagnostic equipment, as well as RF measurement hardware to capture diagnostic information and IQ recordings. To that end, the testbed used a hybrid test approach using cabled and radiated connections to record LTE communications. The communications came from a DUT UE, and optionally a separate loading UE, while a host computer with USRD Monitoring Software was used to capture diagnostic log files from the DUT UE. A VSA and VST were used to capture IQ recordings of the UE UL transmissions.

2.2.1.1 LTE Infrastructure

These measurements were supported by existing LTE infrastructure in Public Safety Communications Research Division (PSCRD), primarily consisting of a virtual evolved packet core (EPC) that performs several functions. The virtual EPC has all of the same nodes as a larger, separate core network, including: mobility management entity (MME) (the main LTE signaling node), serving gateway (SGW) (for forwarding and routing user data packets), and packet gateway (PGW) (for internet protocol (IP) routing of data). A separate home subscriber server (HSS) is used for provisioning and authenticating the UEs. Each of the loading and DUT UEs were individually provisioned for service in the HSS. All traffic from the DUT and UTG UEs use the same priority. All UEs defaulted to quality of service class

Table 2.1: Summary of testbed components.

Anechoic Chamber/ Radiated Path		
Name	Item	Primary Purpose
UE1	User equipment	DUT UE
UE2	User equipment	Optional UE used to load the network
Absorber	Wall of RF absorber	Decrease the recorded influence of UE2
eNB Antenna	Horn antenna	Couple UEs to eNB
VST Antenna	Horn antenna	Couple VST to UE1
RF Test Circuit		
Name	Item	Primary Purpose
FA1	Fixed attenuator	Shift the level of cell signal to/from the DUT UE
SUM	Splitter/Combiner	Sum/split the cell signals
HC1	Hybrid coupler	Shift the phase of the cell uplink signal into the diversity RX port of the eNB
HC2	Hybrid coupler	Shift phase of downlink cell signal into diversity RX port of UTG
FA2	Fixed attenuator	Adjust downlink signal level of the cell
DC	Directional coupler	Couple a small portion of the DUT UE signal for sampling by the VSA
RF-S	RF switch	Toggle between an RF load (for noise reference measurements) and the input signal
VA	Variable attenuator	Adjust the path loss between the DUT UE and the eNB
LTE		
Name	Item	Primary Purpose
VSA	Vector spectrum analyzer	Captures UE1 uplink for verification
eNB	Evolved node B	Manages the radio access network
UTG	UE traffic generator	Loads the eNB with emulated UE traffic
Control Network		
Name	Item	Primary Purpose
e-hub	Ethernet hub	Connects control PC to eNB Controller and UTG host
Control PC	Control computer	Synchronizes testbed components
eNB Controller	Control computer	Configures the eNB
UTG Host	Control computer	Configures the UTG
u-hub	USB Hub	Connects the UEs to control computer
IQ Acquisition		
Name	Item	Primary Purpose
VST	Vector signal transceiver	Records IQ
RAID Server	Fast storage device	Stores the recorded IQ

identifier (QCI) 9 and remained at the same priority throughout the LTE network.

2.2.1.2 LTE eNB

The eNB manages the radio access network (RAN), scheduling of resource allocations, and handover decisions on the LTE network. The eNB selected for these measurements was a COTS eNB with a single radio-head configured to host one cell. This eNB was loaded with firmware from the manufacturer that was compliant with all major features of the 3rd-Generation Partnership Project (3GPP) Release 13. The eNB was a macro-cell LTE Band 66 product. The eNB was configured with software provided by the manufacturer, beginning from a factory default condition with factors of interest assigned to test values. To aid in automating the measurements, configuration files were pre-made based on the experimental design described in [1]. These files were created in vendor software, then saved as extensible markup language (XML). These files were then loaded to the eNB as required, rebooting the eNB with each configuration change.

2.2.1.3 LTE UE Traffic Generator

The UTG is telecommunications test equipment that is designed to load the eNB with the desired number of UEs and data traffic. The UTG simulates a variable number of UEs with configurable RSRPs and data rates, causing the uplink traffic pattern and physical resource block (PRB) allocation to reflect a realistic system with multiple users. It also creates a diagnostic log file, documenting certain LTE physical layer properties on a 0.5 second time span. The UTG has the capability to run the designed scenario via Command Line Interface (CLI) automation. To match the DUT UE and UTG UEs specifications, all of the simulated loading UEs were configured to be Category-4 as defined in 3GPP [3].

2.2.1.4 Vector Signal Analyzer

The signal analyzer records spectrograms that are used as the basis for the physical measurement of the DUT UE UL emissions. This spectrogram also gives the power distribution binned into time aligned single transmission time interval (TTI) (1 ms resolution) and binned frequency aligned to the LTE UL PRBs. The VSA captures a continuous stream of these data for several seconds or more. This is achieved in practice by real-time analysis of IQ data. The ideal test instrument for this purpose would align the spectrogram data by demodulating the UL waveform and synchronizing to symbols in the LTE waveform. Unfortunately, the NASCTN test team did not have an instrument available that could both support this function and acquire continuously for several seconds. Therefore, the team collected unsynchronized samples and oversampled the spectrogram time resolution. Time alignment and downsampling techniques to arrive at spectrogram of interest are detailed in [1], section 4.2. The key specification of the instrument's spectrogram acquisition is in the time-domain oversampling where a time resolution at least a factor of 10 smaller than the 1 millisecond (ms) TTI is required. This is necessary, because the alignment and subsequent downsampling need to exclude samples that straddle the boundary between TTIs. The instrument was set to sample at 53 μ s resolution, which is equivalent to 19 samples per ms. The VSA was set to a center frequency of 1770 MHz with a span dependent on the allocation of the eNB, either 4 MHz, 9 MHz, or 19MHz for the 5 MHz, 10 MHz, and 20 MHz allocations respectively. The span was smaller than the allocation to avoid recording a 1 MHz guard band. The reduced frequency span of the VSA does not affect the recorded IQ from the VST, see below.

2.2.1.5 DUT UEs - Devices and Traffic

The LTE waveform captures were performed with two COTS LTE UE devices that were released to the United States (US) market in 2018. Both devices were of the same model, but differing serial numbers, and contained a software image provided by a major commercial carrier. The devices were "unlocked" such that they were not locked to a commercial network and could be used on the NBIT laboratory network. In 3GPP, UEs are grouped based on their hardware and software capabilities in both uplink and downlink. Each UE category has a higher throughput than the previous one, and the UE may be able to support higher modulation, greater numbers of antennas or both. Both of the DUT UEs supported Band 66 (AWS-3). To optimize test throughput the UE's nonvolatile random-access memory (NVRAM) were configured to prevent handover attempts and searches for other cells near the test environment. This

forces the DUT UEs to stay locked on the Band 66 cell of interest. An application designed for generating and sending IP traffic configured and controlled the uplink traffic of the DUT UEs. A developer bridge was inserted between the application on the DUT UE and the control PC. The connection from the control PC was independent of the wireless LTE connection. The measurement configuration dictated the IP application setup, including traffic type (set to UDP) and data rate to a server running on the control PC. The control PC stored a log of the connection for troubleshooting purposes.

2.2.1.6 USRD Monitoring Software

Most major manufacturers of LTE chipsets provide some type of user equipment self-reported diagnostics (USRD) tool for accessing information directly from the chipset within a COTS UE. There are also some third-party vendors who market a similar product and open-source software packages that function on devices with root access. In any case, the USRD tool provides a variety of information from the current state and behavior of the UE. This software tool can be used to troubleshoot system issues, debug new features, or collect metrics on performance. To get this information, the software forces the UE into a mode where it will echo the LTE protocol stack messages to an output port (e.g., USB) on the UE. Due to the high number of messages, events, and status indicators available in the LTE protocol stack, a filter is used to only collect pertinent messages during acquisition. The type of USRD software used here is different from other applications that can be installed on top of a UE's operating system. Some applications may be able to provide the same or similar information as the USRD software, but they may consume more of the UE's computing resources. In rare cases, this could impact the UE's performance or ability to maintain a desired data rate during a measurement.

2.2.1.7 Vector Signal Transceiver

The vector signal transceiver was configured with appropriate settings to capture IQ recordings for an LTE signal centered at 1770 MHz, with a bandwidth of 30 MHz using a sampling rate of 61.44 MS/s. The reference power was level set to -25 dBm and all IQ recordings were relative to this level. In order to avoid recording the local oscillator (LO) at the center frequency in the band of interest, an LO offset of -21 MHz was applied from the center frequency. The IQ recordings were captured for a total of 5 s, and due to the size of the data files, were streamed directly to a RAID drive. Once the IQ recordings have been captured and collated with the DUT logs and VSA captures, downsampling and alignment were performed in much the same way as described in [1], Section 4.2 for the vector signal analyzer data handling.

2.3 Testbed Radiated Path

The radiated portion of the testbed was realized in an anechoic chamber (5 m x 10 m x 5 m) that under nominal RF absorbing tile configuration has a 3 m x 3 m x 3 m quiet zone and exceeds the requirements set forth by ANSI C63.4 [4] for site voltage standing wave ratio (SVSWR) and IEC 61000-4-3 [5] for field uniformity. A schematic view from the top of the setup is shown in Figure 2.2. The VST antenna (blue) is connected to a VST which records the outputs of UE1 and nominally UE2. The placement and orientation of this antenna was chosen such that the experiment:

- satisfies the far-field distance approximation,
- maximizes dynamic range in the measurement of the UL signal from UE1,
- aligns boresight and is co-polarized with the maximal radiation output from UE1 and UE2 as measured in [6]
- minimizes absorber wall scattering and diffraction effects on the UE2 signal structure.

The eNB antenna (red), also a dual-ridge horn antenna, acted as the eNB broadcast and reception antenna (see Figure 2.2), as well as the VSA recording antenna. It was aligned such that there was a line of sight path component to UE1 and to UE2 in the absence of the absorber wall. Note that with the absorber wall the eNB antenna to UE2 boresight path was obstructed. Furthermore, the link between the VST and eNB antenna was minimized to the extent possible, such that DL energy into the VST antenna was negligible due to path loss (47.8 ± 0.4 dB) and frequency offset (400 MHz). Other radiated experiment configurations may prove to be valid as well. One could conceive a setup with a

single antenna and standard RF circuitry to fulfill both functions of the eNB and VST antenna. In this work, two antennas were used to further separate DL signal contributions to the VST recordings and to improve on the dynamic range of the UL recordings.

This work makes use of an absorber wall between the two UEs to simulate the presence of two AWS-3 users at disparate distances. The anechoic chamber size limited the free space path loss differential between the two test UEs such that the absorber wall proved to be necessary. The wall was 2.4 m wide, 0.6 m deep, and 2.4 m tall and constructed of walkway absorber with planar, non-pyramidal surfaces.

The link budgets and specific details on antenna characteristics are presented in Appendix A.

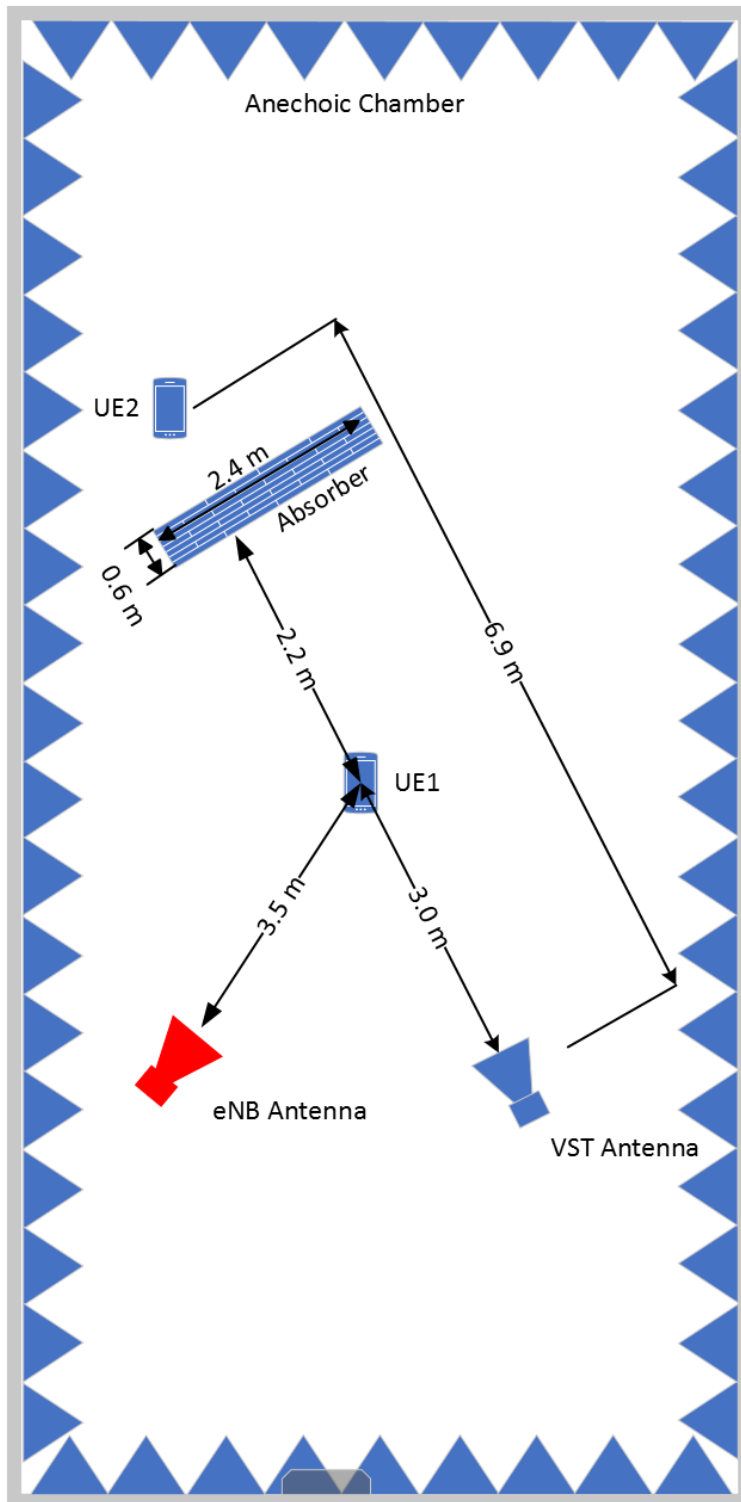


Figure 2.2: Schematic diagram of the laboratory capture. The eNB antenna (red) had a line-of-sight view to UE1 and a glancing/non line-of-sight view to UE2. The VST antenna (blue) was geometrically aligned with the DUT UEs. Note: The path-loss verification step used horn antennas and subsequently dipole antennas at the UE locations to derive link budgets.

Chapter 3

Test Implementation

3.1 LTE Configuration

In an LTE system, the UE uses the power control equation to calculate its power output level (for examples see pages 15-57 of [7]). The parameters for this calculation are collected from the eNB configuration broadcast, the RF condition of the UE, the UE hardware capabilities and the amount of data requested for data transmission. Ignoring the fact that a UE can be limited by the LTE Policy and Charging Control, we configured our LTE parameters to match stable and useful configurations of interest. By matching these configurations, we were able to measure the transmission power of the DUT UE under the influence of varying factors.

3.1.1 Factors

Once the static environment of the LTE system is established, several factors were varied to observe their influence on the UL emissions from the DUT UE. The first factor investigated was the power control mechanism of the eNB, and was alternated between open and closed loop. In addition, the allocation size, or channel bandwidth, of the uplink was varied between 5 MHz, 10 MHz and 20 MHz. The eNB configuration for resource blanking was also selected from no resource blanking, blanking of the upper 6 resource blocks, blanking of the upper 10 resource blocks, and blanking of the central 10% of the allocation. This factor was investigated on the premise that assets particularly sensitive to adjacent-band LTE emissions may become significantly resilient when an extra guard band is implemented. Finally, three factors not determined by eNB configuration were also investigated. The data rate of the DUT UE was varied, taking on values of 0.5, 1, 5, and 20 megabits per second (Mbit/s). The number of UEs attached, excluding the DUT UE, was alternated between the values of 3, 5, and 15. The last factor explored was the presence of a second radiating phone in the anechoic chamber. The complete set of parameters is shown in Table 4.1.

3.1.2 eNB Configuration

In these tests, a commercially available macro cell eNB was used. Default values were selected for all of the eNB's input parameters except for a few parameters affecting UE power transmission. The eNB was configured to have a static fractional power control value of 0.8, an uplink power target of -85 dBm/PRB and a reference signal power (RSP) of -11.4 dBm. All eNB parameters not explicitly mentioned were set to a vendor provided default.

3.1.3 UE Configuration

The DUT for this experiment was a commonly used Category-4 COTS UE. A Category-4 UE is defined as a single antenna transmitter handset with the capability of using up to a 16QAM modulation in the UL direction. All UE configuration parameters on the UE were set to the default factory values. The UE was placed in a location to target a RSRP from -85 to -95 dBm. This value was chosen to be such that the UE would broadcast a significant power, but not be at its maximum total power of 23 dBm.

3.1.4 UTG Configuration

An UTG was used to generate network traffic emulating the loading that additional UEs would create in the eNB's cell. The UTG created additional valid data that consumes a fraction of the cell resources without the complexity that

using additional COTS UEs would create. We were able to emulate UEs that provide a desirable RSRP that is easily specified via the proprietary control software of the UTG. The configuration of the UTG emulated the placement of UEs at a radius of 2000 meters from the eNB to create the desired RSRP of -94 dBm, similar to the desired signal-to-interference-plus-noise ratio (SINR) of the DUT that was selected. The loading UEs synthesized by our commercial traffic generator were identically configured to have a data rate of 500 kilobits per second (kbit/s). The number of UEs and the associated traffic were selected to create a realistic 10%, 20%, 40% occupancy of available resources at the eNB's cell.

3.1.5 Use Cases

The anticipated use of these IQ recordings of UE UL is in the application of spectrum-sharing studies that require realistic LTE traffic as an out-of-band activity, such as the study of a receiver operating in an adjacent band to a commercial LTE carrier. By providing the captures at a high-dynamic-range, researchers can introduce the signals at power levels that are of relevance to a particular system and physical condition of interest. The use cases for this project were selected based on a broad range of needs for high dynamic range IQ recordings that could be used to simulate adjacent band emitters. Various allocations were chosen to match allocation bandwidths that might be seen in the field. These eNB allocations were matched with a power control mode of closed loop power control (CLPC) or open loop power control (OLPC), DUT data rate, eNB loading as created by the UTG, and the presence of a second UE. In total there were 56 test cases that were selected by considering the levels of the eNB configuration, loading and bandwidth.

3.2 Testbed Automation

To capture UE UL IQ recordings under the test conditions, a test-automation and test-network solution was built. Test automation is required due to the length of the tests, complexity of individual system states, and broad test space that needed to be set and recorded. Test inputs were provided as a comma separated value (CSV) file describing the different system states with a full list available in Section 4.3. Outputs from the test system included diagnostic logs from the UE, trace files from the VSA, and the IQ files recorded as the output of the testbed. Details on the logs and data verification method can be found in Chapter 5. The testbed network is shown in Figure 3.1. To physically connect the equipment to a control computer acting as a host for the test-automation, the testbed is networked using either USB or wired LAN connections between the control computer and the major components of the system. LAN communications connect the eNB hardware and UTG host computer to the Control PC. This allows the Control PC to transfer configuration files in XML format to the eNB backhaul. The link also allows the UTG host computer to talk to the UTG hardware through a command line interface (CLI). Other hardware such as the VSA, the path loss (PL) attenuator, the RF switch, and the UEs interfaced with the Control PC via USB hubs. This hardware uses Microsoft .NET framework (.NET)*, CLI or a standard commands for programmable instruments (SCPI) to communicate with the devices. The VST chassis that is used to capture IQ recordings is the only instrument that does not share a network connection with the remainder of the test network, due to internal networking policy, and minimal connections are made with the testbed. A clock signal and hardware trigger pulse both originating from the VSA are the only connections. Custom LabVIEW* software on the VST is used to loop through the acquisitions, and await the hardware trigger.

A combination of Python* and National Instruments (NI) LabVIEW were used in order to automate various components within the testbed.

3.2.1 Python Automation

Manual programming of the eNB is typically done via a proprietary interface that contains safety checks that will not upload disallowed states to the equipment memory. In order to automate this software interface and circumvent direct

*Certain commercial products or company names are identified here to describe our study adequately. Such identification is not intended to imply recommendation or endorsement by the National Institute of Standards and Technology, nor is it intended to imply that the products or names identified are necessarily the best available for the purpose.

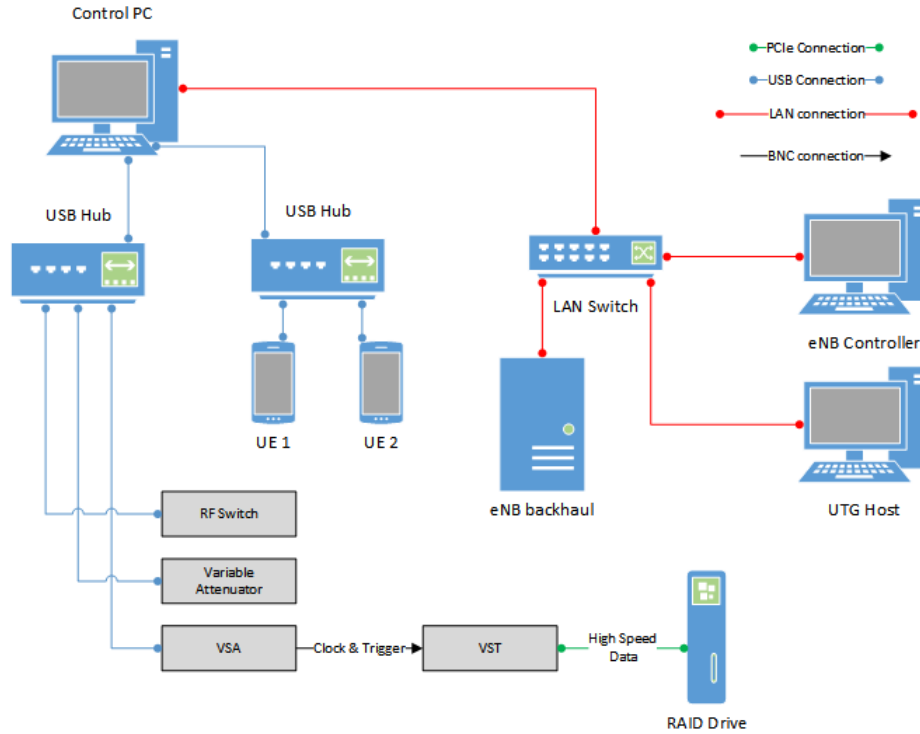


Figure 3.1: Data and control connections within the testbed network.

programming of the electrically erasable programmable read-only memory (EEPROM) of the eNB, a Python Windows graphical user interface (GUI) automation library was used. This Python automation library finds Windows handles by title and sends keystrokes to those specific Windows handles to load a complete set of configuration parameters defined within a pre-built XML file. Upon uploading a new configuration file, the eNB system undergoes a full power cycle and a full memory reload. Automation of the UTG occurred via a transmission control protocol (TCP) server on the UTG host, open and awaiting specific encoded communications from the control computer. A command was issued to this socket to open the proprietary UTG software and upon the software opening that same socket was used to stream a script of CLI arguments that has been pre-compiled and placed on to the control computer. The UE was automated via a terminal connection made through Android Debug Bridge (ADB) software facilitated by a USB connection to the device. Once within the UE terminal, an application designed for generating and sending IP traffic is initiated with various CLI arguments to create LTE traffic that is routed to a server on the control computer via the test-network. The iPerf* software was used with the user datagram protocol (UDP) argument to ensure that the traffic created was UDP. Therefore the iPerf server on the control computer was not required, but acts as another layer of diagnostic. The RF path was configured using .NET* libraries for setting RF attenuation and switch states allowing the path to be switched from a matched load to an active path from the eNB antenna in the anechoic chamber to the eNB with a configurable RF attenuation. The attenuation for this particular test set was static and remained fixed throughout the entire acquisition. Finally a VSA was used to capture spectrograms of the incoming signal on the eNB conducted path, and conventional SCPI commands were issued to the VSA to set the state, acquire and fetch the IQ recordings.

3.2.2 LabVIEW Automation

In addition to these main Python components, a standalone NI VST chassis was connected to the testbed through its clock signal, an external trigger, and a separate dedicated RF feed from the anechoic chamber. The VST captured high-speed IQ recordings, and the software for this data acquisition was written in LabVIEW. The control software is

in the form of a typical producer-consumer structure, or parallel loops that either produce or consume data at different rates, and passes through multiple states as the software is run. For instance, on software startup or change of input parameters the VST passes through a state that configures the RF hardware so that, upon issuing an acquire command, the hardware was immediately available. The software was written to enter an awaiting-trigger state and acquire a fixed number of IQ recordings outputting the data files in the same file hierarchy as that defined by the main log collection. Though the VST software included a TCP socket, there is no communication connection between the primary testbed and the VST equipment. Therefore, the IQ recordings are logged with a timestamp and required subsequent collation. The standalone VST user interface (UI) can be seen in Figure 3.2.

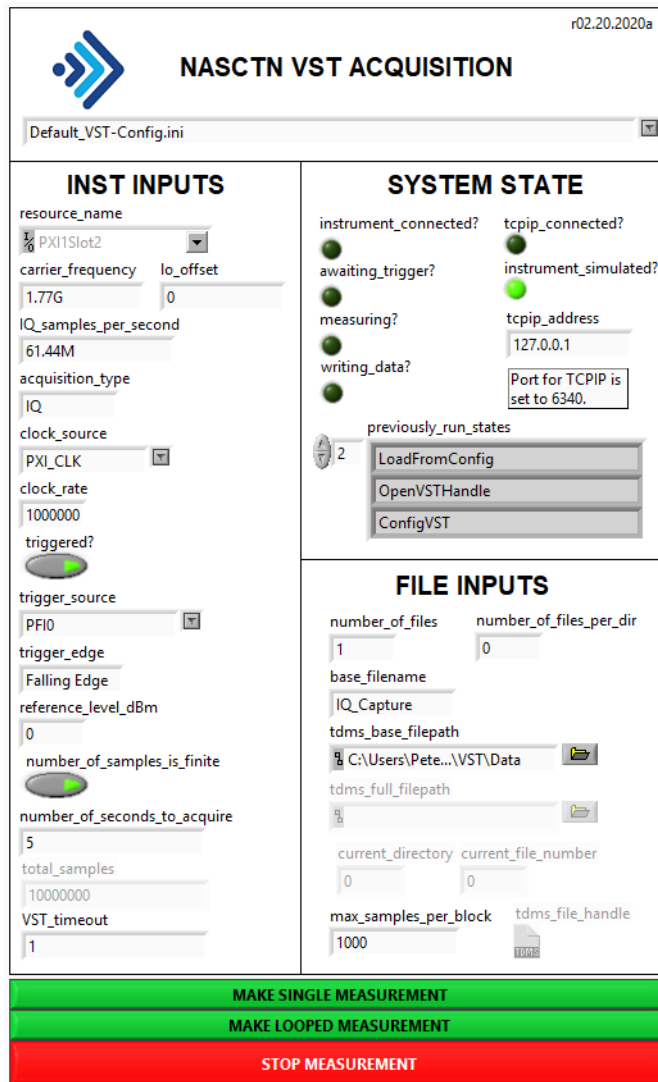


Figure 3.2: VST IQ recording-capture software user interface. Functionality focused on test configuration, instrument, and file inputs, as well as observing the real-time test system state for debugging.

Chapter 4

Test Execution

4.1 Test Sequence

A high-level overview of the test sequence is seen in Figure 4.1. The test sequence iterates through all test cases in the defined order, read from a CSV file input, to the testbed. The test matrix can be seen in Figure 4.1. eNB configuration, additional UE traffic provided by the UTG, primary UE data rate, and the presence of a second UE within the chamber are all configurations which must be set prior to performing the data acquisition. In each test case, a configuration was applied to the hardware in the test setup, and data were acquired and recorded. A single test is defined as a single iteration of the main test loop, or the execution of the test sequence from the start of loading of configuration files to the decision point in determining if all cases have finished. In order to more efficiently use test time, the necessity for an eNB reboot/reconfiguration is determined based on the previous state of the system. An important practical aspect of this measurement campaign was the overall test execution time. The testbed automation improves throughput by using multi-threaded concurrency. The benefits were most significant when configuring the slowest equipment simultaneously. In this implementation, changing the eNB configuration and a reboot of the UTG were the slowest operations, so they were performed concurrently. The set up and the measurement of the matched load for calibration by the VSA was also executed concurrently with the initial UE setup.

4.2 Testbed-Log Collection

Data from several sources were captured and saved to provide a combination of diagnostic information and IQ recordings of the DUT UE UL transmissions. The collected data consisted of power control, UL broadcast, and byte status register information from the DUT UE. This information was extracted and organized by the system frame, subframe and relative timestamp. This produced a set of diagnostic information identified within the nearest millisecond. These log files also produced a complete record of active PRBs that we used to identify the frequency of active sub carriers in the IQ recordings from the VST, and the binned power from the VSA spectrograms. We used a cross-correlation to synchronize the time of acquisition between the UE, the VSA and the VST, as detailed in Chapter 4 of [1].

4.2.1 Data Flow and Storage

While multiple components of the system generated data, the bulk of the data was collated on a network-accessible drive at the time of capture. In particular, the UTG log files, UE diagnostic log files, and VSA traces were all gathered from their respective locations, down-sampled as required, and stored by timestamp with an experimental description. However, due to the size and rate of the data generated by the IQ recordings, as well as the local necessity that the controller remain on a different network from the remainder of the system, the IQ recording data flow is separate from the bulk of the log files. The IQ recordings are initially stored into a buffer as they are captured on the VST instrument itself and real-time streamed in to a RAID storage device that is connected via a multisystem extension interface (MXI) cable and controller. The IQ recordings are stored in technical data management streaming (TDMS) format with header information that describes the state of the instrument and a timestamp indicating when the capture was taken. Because the VST control chassis was on a different network from the rest of the instrumentation, the data were captured and then collated with the remainder of the log files after the experiment completed.

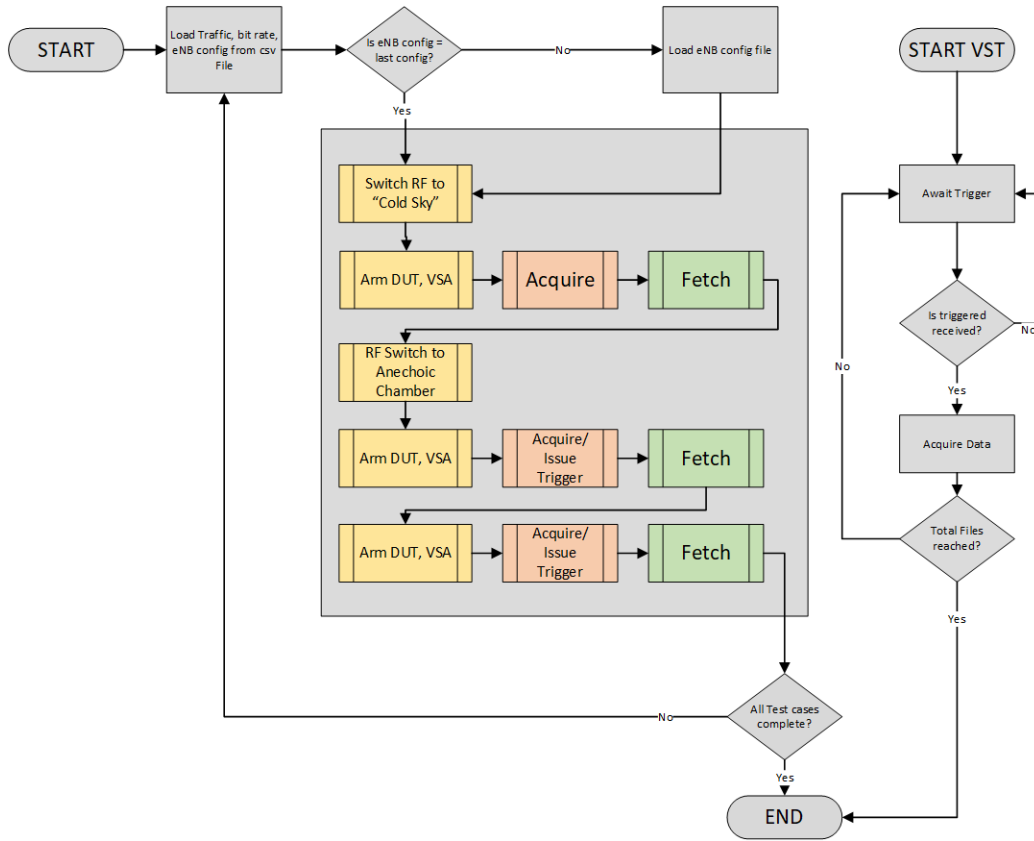


Figure 4.1: High-level test sequence specification.

4.3 Test Matrix

Test #	Scheduler			Power Control		P_0		α	UTG				DUT UE			DUT UE 2	
	Awareness	Allocation	RB mask	PUSCH	PUCCH	PUSCH	PUCCH		#UEs	UL Rate	Traffic Type	UE RSRP	Target RSRP	UL Rate	Traffic Type	UL Rate	Traffic Type
1	Unaware	20 MHz	None	CLPC	CLPC	-85	-117	0.8	15	500kbps	UDP	-95	-95	500 kbps	UDP	None	UDP
2	Unaware	20 MHz	None	CLPC	CLPC	-85	-117	0.8	15	500kbps	UDP	-95	-95	1 Mbps	UDP	None	UDP
3	Unaware	20 MHz	None	CLPC	CLPC	-85	-117	0.8	15	500kbps	UDP	-95	-95	5 Mbps	UDP	None	UDP
4	Unaware	20 MHz	None	CLPC	CLPC	-85	-117	0.8	15	500kbps	UDP	-95	-95	10 Mbps	UDP	None	UDP
5	Unaware	20 MHz	None	CLPC	CLPC	-85	-117	0.8	3	500kbps	UDP	-95	-95	500 kbps	UDP	None	UDP
6	Unaware	20 MHz	None	CLPC	CLPC	-85	-117	0.8	3	500kbps	UDP	-95	-95	1 Mbps	UDP	None	UDP
7	Unaware	20 MHz	None	CLPC	CLPC	-85	-117	0.8	3	500kbps	UDP	-95	-95	5 Mbps	UDP	None	UDP
8	Unaware	20 MHz	None	CLPC	CLPC	-85	-117	0.8	3	500kbps	UDP	-95	-95	10 Mbps	UDP	None	UDP
9	Unaware	20 MHz	Upper 6	CLPC	CLPC	-85	-117	0.8	3	500kbps	UDP	-95	-95	500 kbps	UDP	None	UDP
10	Unaware	20 MHz	Upper 6	CLPC	CLPC	-85	-117	0.8	3	500kbps	UDP	-95	-95	1 Mbps	UDP	None	UDP
11	Unaware	20 MHz	Upper 6	CLPC	CLPC	-85	-117	0.8	3	500kbps	UDP	-95	-95	5 Mbps	UDP	None	UDP
12	Unaware	20 MHz	Upper 6	CLPC	CLPC	-85	-117	0.8	3	500kbps	UDP	-95	-95	10 Mbps	UDP	None	UDP
13	Unaware	20 MHz	Upper 10	CLPC	CLPC	-85	-117	0.8	3	500kbps	UDP	-95	-95	500 kbps	UDP	None	UDP
14	Unaware	20 MHz	Upper 10	CLPC	CLPC	-85	-117	0.8	3	500kbps	UDP	-95	-95	1 Mbps	UDP	None	UDP
15	Unaware	20 MHz	Upper 10	CLPC	CLPC	-85	-117	0.8	3	500kbps	UDP	-95	-95	5 Mbps	UDP	None	UDP
16	Unaware	20 MHz	Upper 10	CLPC	CLPC	-85	-117	0.8	3	500kbps	UDP	-95	-95	10 Mbps	UDP	None	UDP
17	Unaware	10 MHz	None	CLPC	CLPC	-85	-117	0.8	15	500kbps	UDP	-95	-95	1 Mbps	UDP	None	UDP
18	Unaware	10 MHz	None	CLPC	CLPC	-85	-117	0.8	15	500kbps	UDP	-95	-95	5 Mbps	UDP	None	UDP
19	Unaware	10 MHz	None	CLPC	CLPC	-85	-117	0.8	3	500kbps	UDP	-95	-95	500 kbps	UDP	None	UDP
20	Unaware	10 MHz	None	CLPC	CLPC	-85	-117	0.8	3	500kbps	UDP	-95	-95	1 Mbps	UDP	None	UDP
21	Unaware	10 MHz	None	CLPC	CLPC	-85	-117	0.8	3	500kbps	UDP	-95	-95	5 Mbps	UDP	None	UDP
22	Unaware	5 MHz	None	CLPC	CLPC	-85	-117	0.8	3	500kbps	UDP	-95	-95	500 kbps	UDP	None	UDP
23	Unaware	5 MHz	None	CLPC	CLPC	-85	-117	0.8	3	500kbps	UDP	-95	-95	1 Mbps	UDP	None	UDP
24	Unaware	20 MHz	None	OLPC	OLPC	-85	-117	0.8	15	500kbps	UDP	-95	-95	500 kbps	UDP	None	UDP
25	Unaware	20 MHz	None	OLPC	OLPC	-85	-117	0.8	7	500kbps	UDP	-95	-95	500 kbps	UDP	None	UDP
26	Unaware	20 MHz	None	OLPC	OLPC	-85	-117	0.8	3	500kbps	UDP	-95	-95	500 kbps	UDP	None	UDP
27	Unaware	20 MHz	None	CLPC	CLPC	-85	-117	0.8	7	500kbps	UDP	-95	-95	500 kbps	UDP	None	UDP
28	Unaware	20 MHz	None	CLPC	CLPC	-85	-117	0.8	7	500kbps	UDP	-95	-95	1 Mbps	UDP	None	UDP
29	Unaware	20 MHz	None	CLPC	CLPC	-85	-117	0.8	7	500kbps	UDP	-95	-95	5 Mbps	UDP	None	UDP
30	Unaware	20 MHz	None	CLPC	CLPC	-85	-117	0.8	7	500kbps	UDP	-95	-95	10 Mbps	UDP	None	UDP
31	Unaware	20 MHz	Center 10	CLPC	CLPC	-85	-117	0.8	3	500kbps	UDP	-95	-95	500 kbps	UDP	None	UDP
32	Unaware	20 MHz	Center 10	CLPC	CLPC	-85	-117	0.8	3	500kbps	UDP	-95	-95	1 Mbps	UDP	None	UDP
33	Unaware	20 MHz	Center 10	CLPC	CLPC	-85	-117	0.8	3	500kbps	UDP	-95	-95	5 Mbps	UDP	None	UDP
34	Unaware	20 MHz	Center 10	CLPC	CLPC	-85	-117	0.8	3	500kbps	UDP	-95	-95	10 Mbps	UDP	None	UDP
35	Unaware	10 MHz	None	OLPC	OLPC	-85	-117	0.8	15	500kbps	UDP	-95	-95	500 kbps	UDP	None	UDP
36	Unaware	10 MHz	None	OLPC	OLPC	-85	-117	0.8	7	500kbps	UDP	-95	-95	500 kbps	UDP	None	UDP
37	Unaware	10 MHz	None	OLPC	OLPC	-85	-117	0.8	3	500kbps	UDP	-95	-95	500 kbps	UDP	None	UDP
38	Unaware	10 MHz	None	CLPC	CLPC	-85	-117	0.8	15	500kbps	UDP	-95	-95	500 kbps	UDP	None	UDP
39	Unaware	10 MHz	None	CLPC	CLPC	-85	-117	0.8	7	500kbps	UDP	-95	-95	500 kbps	UDP	None	UDP
40	Unaware	10 MHz	None	CLPC	CLPC	-85	-117	0.8	7	500kbps	UDP	-95	-95	1 Mbps	UDP	None	UDP
41	Unaware	10 MHz	None	CLPC	CLPC	-85	-117	0.8	7	500kbps	UDP	-95	-95	5 Mbps	UDP	None	UDP
42	Unaware	10 MHz	Center 6	CLPC	CLPC	-85	-117	0.8	3	500kbps	UDP	-95	-95	500 kbps	UDP	None	UDP
43	Unaware	10 MHz	Center 6	CLPC	CLPC	-85	-117	0.8	3	500kbps	UDP	-95	-95	1 Mbps	UDP	None	UDP
44	Unaware	10 MHz	Center 6	CLPC	CLPC	-85	-117	0.8	3	500kbps	UDP	-95	-95	5 Mbps	UDP	None	UDP
45	Unaware	5 MHz	None	OLPC	OLPC	-85	-117	0.8	7	500kbps	UDP	-95	-95	500 kbps	UDP	None	UDP
46	Unaware	5 MHz	None	OLPC	OLPC	-85	-117	0.8	3	500kbps	UDP	-95	-95	500 kbps	UDP	None	UDP
47	Unaware	5 MHz	None	CLPC	CLPC	-85	-117	0.8	7	500kbps	UDP	-95	-95	500 kbps	UDP	None	UDP
48	Unaware	5 MHz	None	CLPC	CLPC	-85	-117	0.8	7	500kbps	UDP	-95	-95	1 Mbps	UDP	None	UDP
49	Unaware	20 MHz	None	CLPC	CLPC	-85	-117	0.8	15	500kbps	UDP	-95	-95	1 Mbps	UDP	500kbps	UDP
50	Unaware	20 MHz	None	CLPC	CLPC	-85	-117	0.8	3	500kbps	UDP	-95	-95	1 Mbps	UDP	500kbps	UDP
51	Unaware	20 MHz	None	OLPC	OLPC	-85	-117	0.8	3	500kbps	UDP	-95	-95	500 kbps	UDP	500kbps	UDP
52	Unaware	20 MHz	None	CLPC	CLPC	-85	-117	0.8	3	500kbps	UDP	-95	-95	500 kbps	UDP	500kbps	UDP
53	Unaware	10 MHz	None	OLPC	OLPC	-85	-117	0.8	3	500kbps	UDP	-95	-95	500 kbps	UDP	500kbps	UDP
54	Unaware	10 MHz	None	CLPC	CLPC	-85	-117	0.8	3	500kbps	UDP	-95	-95	500 kbps	UDP	500kbps	UDP
55	Unaware	5 MHz	None	CLPC	CLPC	-85	-117	0.8	3	500kbps	UDP	-95	-95	500 kbps	UDP	500kbps	UDP
56	Unaware	10 MHz	Upper 4	CLPC	CLPC	-85	-117	0.8	3	500kbps	UDP	-95	-95	5 Mbps	UDP	None	UDP

Table 4.1: Test Configurations.

Chapter 5

Test Verification and Data Synchronization

Each data acquisition went through an extensive verification process beginning by confirming the state of the testbed at acquisition time and ending with a comparison of frequency and time dependent power measurements. This verification process ensures that the test executed to completion, the test parameters were correct, and that the IQ recordings correspond to the UE diagnostic information. The testbed state was confirmed through a series of scripts and human review that identified the configuration of interest in the settings files for the eNB and the UTG. The configuration of the eNB is saved from the control computer before an experiment, and downloaded from the eNB in a separate step and compared to the intended setting. For the UTG, a series of command-line imperatives are sent from the control computer to the UTG and the corresponding confirmation log file is saved. This operations log file is reviewed to ensure the intended distribution of emulated loading UEs is correct. The final and most important step of data verification comes from the simultaneous time alignment of three independent measurements of the UE electromagnetic emissions.

5.1 Data Parsing & Processing

5.1.1 Diagnostic Data (USRD)

For each subframe of the link, the UE provides a series of diagnostic reports. Multiple values are of interest during the verification process. First the system frame and system subframe number create a ms-by-ms time basis that is used to coordinate the various outputs of the UE and other recording components. The total transmitted power per TTI, the number of physical resource blocks, and the starting resource block reported from the UE are used to create a synthetic spectrogram mask that has a 1 ms/15 kHz resolution in time/frequency. This spectrogram, along with an initial timestamp, is used as a basis for the overall system clock time. Any spectrogram or IQ recording of interest is transformed to match the time resolution, and then a cross correlation of the two is performed, aligning the data sets at the maximum. For full details see Section 5.1.4.

5.1.2 VSA Data

The spectrogram contains at least 10 samples during the 1 ms TTI. This is necessary, because the alignment and down-sampling needs to remove samples that straddle the boundary between TTIs. The test team sampled at a resolution based on the allocation of the uplink channel, as seen in Table 5.1.

Table 5.1: VSA acquisition bandwidth per allocation.

LTE Allocation	Time Resolution	Analysis Bandwidth
20 MHz	53.33 μ s	19 MHz
10 MHz	53.33 μ s	9 MHz
5 MHz	53.33 μ s	4 MHz

5.1.3 IQ Recordings

The IQ recordings were captured and saved as TDMS files that contained headers that defined the state of the VST instrument at the time of the acquisition with the IQ data stored as unsigned 16 bit integers. To process these IQ recordings, the TDMS file header was omitted and the remaining data split into their binary components and then interleaved. The amplitude values of the IQ recordings were then processed using a Fast Fourier Transform (FFT) at 15 kHz, creating a spectrogram with the frequency resolution of a single resource block and the time resolution of TTIs. This process follows the one presented in [1] Section 4.2.2, with the sampling rate of 61.44 MS/s. This allowed the same process that is used for the alignment of the VSA trace data to be repeated with the IQ recordings. This IQ recording data was then time-aligned both with the diagnostic logs from the UE as well as the VSA spectrogram, thereby confirming that the IQ represented the same data as captured by the diagnostic software from the emitter and the VSA on a separate RF path.

5.1.4 Time Alignment

The alignment of the USRD data, VSA data and VST IQ recordings follows the flow described in Chapter 4 of [1] and summarized here. A spectrogram was created from the USRD information. Then a downsampled spectrogram is created from the VSA data. Finally, the VST IQ is used to create a third spectrogram. The time-alignment process is applied to each pair of spectrograms in sequence. This results in three spectrogram time series with a universal start time and an elapsed time. The time alignment process is based on a cross correlation of the spectrogram from the USRD with the other measured spectrograms. In Figure 5.1, an example of the process is shown for two repetitive captures of the test configuration 1 in Table 4.1. The approximate time is known from the control computer. However, precise alignment to the communications system time, based on the eNB generated frame and subframe number, requires refinement and in our case is based on the cross-correlation. The time at which the maximum value occurs determines an offset for the measured spectrogram. After each spectrogram is aligned they are compared. In Figure 5.2, a segment of each of the three spectrograms for 0.5 s of acquisition time is shown. This methodology of redundant captures provides the advantages of the UE diagnostic information, including modulation coding scheme (MCS) index, total power per TTI and PRB grant size, RSRP and UE measured DL path loss being informed by real-time measurements of power and IQ recordings with independent measures of path loss, all synchronized to the system subframe. This presents the unique chance to correlate system messages with electromagnetic measurements providing a bridge between emulated systems and field measurements.

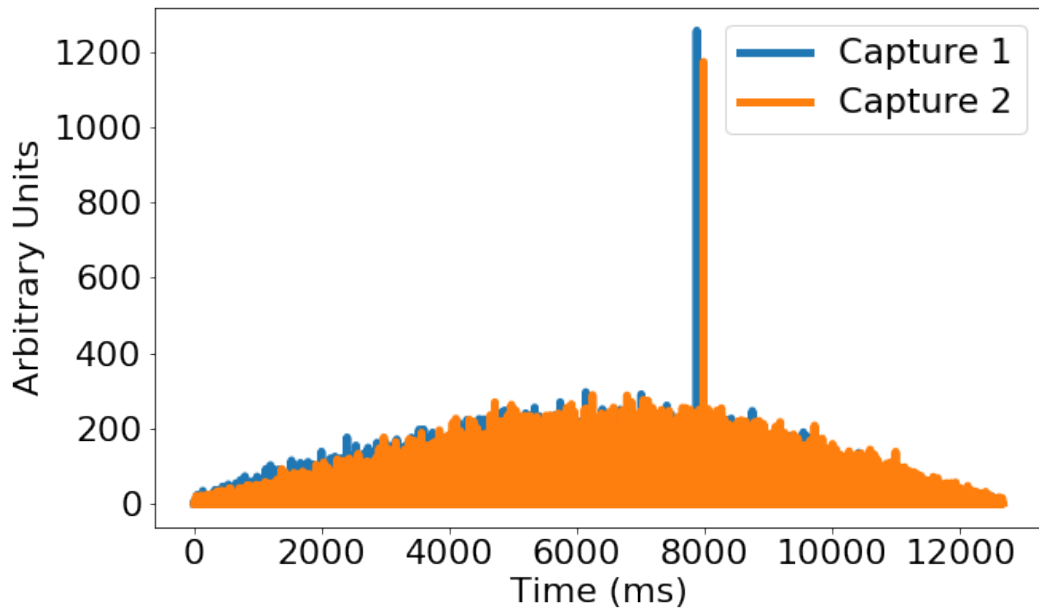


Figure 5.1: Cross correlation of the UE synthetic spectrogram and IQ recording generated spectrogram for the testbed successive captures as shown as capture 1 and capture 2. The time at which the maximum value occurs indicates an offset for the measured spectrogram (in ms) from the system time.

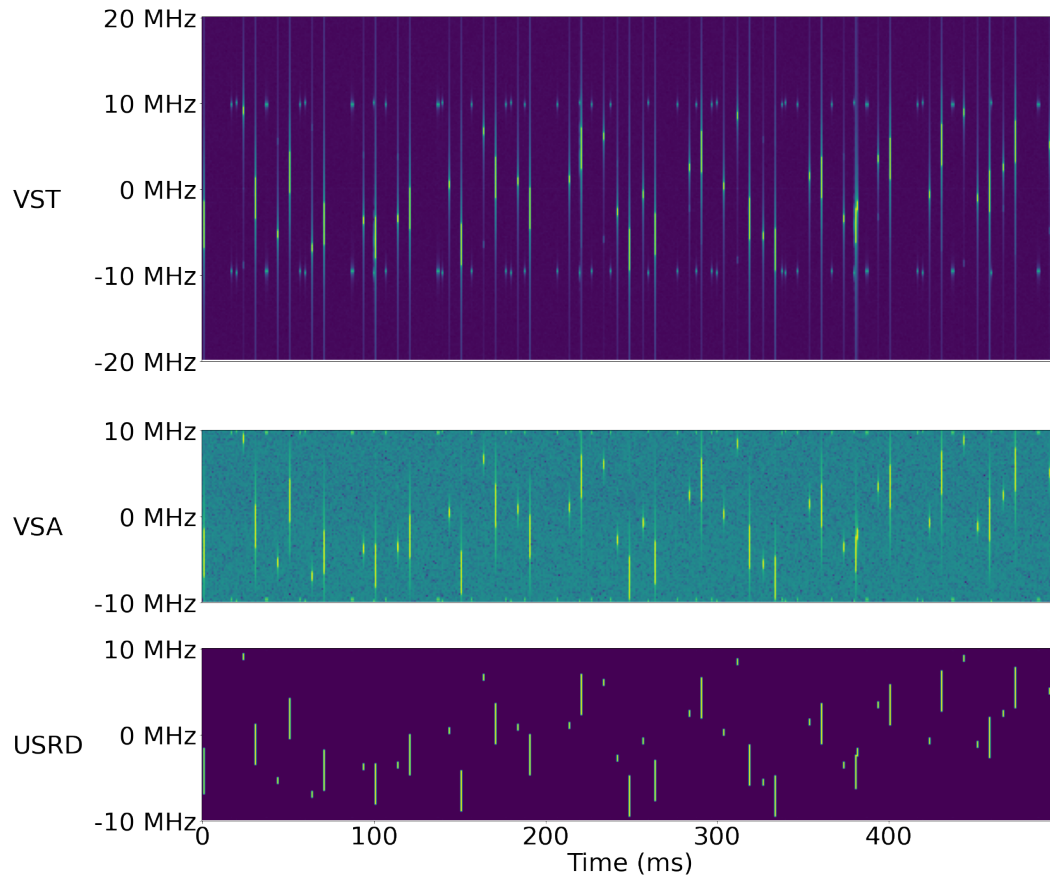


Figure 5.2: Aligned spectrograms of IQ from the VST, VSA , and UE generated spectrograms from USRD.

Chapter 6

Conclusion

In conclusion, IQ recordings of LTE UE UL under realistic network conditions are cataloged for use in receiver susceptibility measurements. These IQ captures can be aggregated, amplified, attenuated, frequency shifted, or filtered to suit the needs of researchers investigating the effect of LTE-based systems on victim receivers of any type. This methodology emphasizes a single UE's radiated behavior representing a system in which a single UE (UE1) is dominant and does not represent an aggregate interference signal. To extend the process to more than two UEs radiating at comparable powers, extensions of this work would be required. The UE IQ recordings are acquired from a UE radiating into an anechoic chamber while it is connected to a loaded eNB, with predefined settings of interest. The IQ data are recorded using a VST in VSA mode on a radiated path that selectively acquires the emission of the UE at a low RF path loss.

Appendix A

Calibration and Verification Measurements

This appendix is designed to document specific measurements of the paths of critical interest in the LTE cell covered in Chapter 2.3. The verification and calibration of the experimental setup requires measurement of the radiated path loss between components of the LTE cell, conducted measurement of the connectorized components, and cable verification. We also confirm all of these measurements using the reported power from a commercial UE. The end connected to a short-circuit (left) and the time-domain reflectometry from that data where time is converted to distance (right). In the time domain, the reflection from the short-circuit at the end of the cable is seen as the large peak with reflection from adapters shown as smaller peaks to the left of the main peak.

A.1 Over-the-Air Link Budget Measurements

In Figure A.1, four key paths determine the path losses between the eNB, the UEs, and the VST. The losses were measured with a four-port vector network analyzer (VNA). The VNA was calibrated at the end of each of the cables just before the input to the respective horn antenna with an electronic calibration unit [8]. Horn antennas were chosen to couple signal to the VST and eNB to maximize directionality for alignment and rejection of spurious noise. Additionally, horn antennas were also used to stand in for the UEs in the experimental setup for purposes of measuring the path losses. The antennas were set up using a taut string and tape measure for coarse height adjustment and alignment. In order to make fine adjustments to the height and angular position of the antennas, the transmission between the UE antennas and the VST antenna were measured and maximized with the VNA. The eNB antenna was optimized toward the UE1 antenna in the same manner. All calibrations were confirmed with omni directional antennas in the UEs positions, to better simulate UE antenna performance, and verified with UE self-reported received power. In addition, the VNA calibration was checked by measuring a thru connector across each pair of cables and verifying unity transmission within the specifications of the connector. The path losses were measured with only the two antennas of interest connected, aligned on boresight, and the other cables terminated with 50 Ohm loads. The measurement between the VST and UE2 antennas had the UE1 antenna removed.

To ensure the far-field condition, we used the length of a typical UE (0.16 m) as an upper bound for its antenna aperture D , and the lower-bound wavelength λ at 1770 MHz of 0.17 m. Then, the Fraunhofer distance, d , which sets the lower bound of the far-field assumption, defined as [9]

$$d = \frac{2D^2}{\lambda}, \quad (\text{A.1})$$

is computed to be 0.3 m.

Therefore, because the antennas were separated by more than ten times the Fraunhofer distance, the emissions were considered in the far-field regime.

The path-loss measurement results between the VST and UE1 antennas for both the uplink and downlink frequencies of the AWS-3 band are shown in Figure A.2. The UE1 antenna tripod was moved 10 cm between repeats either laterally, closer, or further from the VST antenna, then back to the original position. The distance of 10 cm was chosen

Table A.1: Radiated path loss measurement accounting for uncertainty due to antenna placement and frequency averaging.

Path	Uplink Path Loss (dB)	Downlink Path Loss (dB)
UE1 - eNB	32.9 ± 0.2	34.2 ± 0.1
UE2 - eNB	42.9 ± 0.2	48.0 ± 1.0
UE1 - VST	27.5 ± 0.2	28.0 ± 0.2
UE2 - VST	55.0 ± 3.0	52.0 ± 3.0

to account for uncertainty in the location of the phase center of the horn antenna and as an overestimate of any human placement error. Also, the polarization of the UE1 antenna was rotated 5° to account for polarization error in repeat placement of the antenna. Several measurements were performed before the experimental campaign took place. A recheck of the measurement was performed after the experimental campaign and is also shown in the plot. All of these antenna movements and the recheck are referred to in Figure A.2 as the measurement iteration.

The same repeat measurements for each pair of antennas in the chamber were performed (where the UE antennas were moved to determine the variability), and the results are summarized in Table A.1. As can be seen in figure A.2, the movement of the UE1 antenna had a similar spread in the measured path loss as the variability over frequency averaging. Therefore, the mean value of the loss and the uncertainty are calculated over all the frequency point measured for the band of interest. The mean value and its uncertainty are reported in the table.

However, the UE2 antenna behind the absorber wall was much more sensitive to movement. The sensitivity is shown in figure A.3 where the same repeatability measurement procedure as outlined above was performed with the UE2 horn antenna and the VST antenna. Once again, the error bars represent the one sigma standard deviation of the frequency averaging. The spread due to position variation of the antenna is dominant over the frequency spread. This position sensitivity is due to the UE2 horn antenna's proximity to the absorber wall. Absorbers, while designed to absorb energy, can still have substantial residual reflection and scattering coefficients. The uncertainty associated with these measurement is shown in Table A.1. The reproducibility of the UE2 placement is a consideration depending on the uncertainty desired on the overall measurement.

The plots only show the S-parameter squared, but to calculate the average loss at either the uplink or downlink frequencies the impedance mismatch must be accounted for by,

$$L_{path} = \frac{\langle |S_{21}| \rangle_f^2}{1 - \langle |S_{11}| \rangle_f^2}, \quad (\text{A.2})$$

where the measurement is assumed between ports 1 and 2 of the VNA, and the loss is represented by L_{path} . The impedance mismatch and the of the VST antenna on port 2 is not considered since it is a constant of the experimental setup and taken as part of the loss mechanism. The gain of the UE1 antenna is accounted for in later assessments, while the gain of the VST antenna is also considered part of the system. The measured loss values from (A.2) for the UL and DL frequencies of AWS-3 are shown in Table A.1 for each pair of antennas measured.

In the experimental configuration, an absorber wall was used to simulate UE2 being at a greater distance. The effect of the wall is shown in Figure A.4. The absorber also selectively decreases the amount of uplink radiation from the UE2 position arriving at the VST. The orientation of the wall created a radiated path loss differences of 9 dB offset for the communication to the eNB with UE2, and an additional 28 dB path loss of the UE2 at the VST.

Table A.2: Conducted path loss measurements.

Path	Uplink Loss (dB)	Downlink Loss (dB)
Cable Loss (VST)	7.5 ± 0.2	7.7 ± 0.2
Cable Loss (eNB)	5.2 ± 0.2	5.3 ± 0.2
Testbed Circuit	42.0 ± 0.2	42.0 ± 0.2

A.2 Conducted Path Link Budget Measurement

There are three conducted elements to the test setup for which we evaluated path loss: the cabling between the VST antenna and the VST input connector; the cabling between the eNB antenna and the testbed circuit output connector; and the losses through the eNB testbed circuit.

All of the conducted loss measurements used a calibration reference plane at the end of two test cables. Then, two thru adapters were measured and corrected for, allowing a calibration reference plane at the inputs to the test antennas. The uplink and downlink loss characteristics of the cabling in the AWS-3 band are detailed in Table A.2. We estimate the uncertainties in the cable loss results by introducing bends into the cables between repeat measurements. This simulated the effects of cable movement that occur between measurement runs during setup and calibration.

Additionally, the loss budget required measurement of the loss through the testbed circuit. A diagram of the circuit that connects the eNB to the test chamber is shown in Figure A.5. The circuit is described in detail in a previous NASCTN report [1]. In the figure, each of the circuit components are named and identified in Table 2.1. For the purpose of understanding the loss through the circuit, we terminated the unused cables with 50 Ohm loads and altered the setting of the variable attenuator identified as VA in Figure A.5. Then, the calibrated VNA was used to measure the loss between the ports shown with red arrows in Figure A.5.

A.3 Cable Verification

The first step in the setup process was to verify the quality of the cabling used. The electrical connections to the antennas in the experiment used 18 GHz type-N cables. There were three 20 m cables connecting the VST, UE1, and UE2 antennas to the bulkhead connector on the interior of the anechoic chamber wall. A 3 m cable connected the VNA to the same bulkhead on the outside of the chamber. The eNB antenna had a 15 m cable inside the chamber, and a 3 m cable on the outside. The quality of the cables was verified utilizing time-domain reflectometry measurements with the VNA to ensure no defects in the cable due to kinks, impedance mismatches, or any other type of internal damage [10]. Additionally, we checked for leakage between terminated cables and found no signal above the noise floor of the VNA.

A.4 Total System Losses and Uncertainty

The total system loss we expect from the eNB to UE1, L_{tot} , can be calculated in linear units as,

$$L_{tot} = L_{path}L_{cable(eNB)}L_{circuit}/G, \quad (A.3)$$

where G is the gain of the horn antenna representing the UE, L_{path} is the radiated loss between the reference planes of the VNA measurements (including the two horn antenna gains), $L_{cable(eNB)}$ is the loss of the eNB cable, and $L_{circuit}$ is the loss of the testbed circuit. Equation A.3 is valid for the loss from the eNB. For the loss to the VST from UE1, (A.3) is modified as,

$$L_{tot} = L_{path}L_{cable(VST)}/G, \quad (A.4)$$

where $L_{cable(VST)}$ is the loss of the VST cable.

The antenna gain for the UE1 horn antenna was examined in a previous report [6]. The UE2 horn is the same model

as the UE1 and shares the same nominal specifications, although a slightly different gain value as measured by the manufacturer. The antenna gains are 10.4 dBi and 10.3 dBi respectively. We estimate the uncertainty in gain from the coarse frequency measurements by the manufacturer combined with interpolation uncertainty for the frequencies used in these measurements. This estimate was presented in [6] and assumes a smoothly varying gain as a function of frequency. We determined the uncertainty in the gain to be 0.9 dB.

The uncertainty on the value in (A.3) is given by [11],

$$\sigma L_{\text{tot}} = L_{\text{tot}} \sqrt{\left(\frac{\sigma L_{\text{path}}}{L_{\text{path}}}\right)^2 + \left(\frac{\sigma G}{G}\right)^2 + \left(\frac{\sigma L_{\text{circuit}}}{L_{\text{circuit}}}\right)^2 + \left(\frac{\sigma L_{\text{cable(eNB)}}}{L_{\text{cable(eNB)}}}\right)^2}. \quad (\text{A.5})$$

The terms under the radical are the relative uncertainties of the given quantities in linear units. All of the measurements and derived quantities from the measurements were carried out with linear units and converted to dB at the end. A summary of the component losses measured and the resulting uncertainties are shown in Table A.3.

Table A.3: Summary of system losses and associated uncertainties.

Description	Variable	Uplink Value (dB)	Downlink Value (dB)
Radiated Path Loss (VST Ant to UE1)	L_{path}	27.5 ± 0.1	28.0 ± 0.2
Radiated Path Loss (eNB Ant to UE1)	L_{path}	32.9 ± 0.2	34.2 ± 0.1
Radiated Path Loss (VST Ant to UE2)	L_{path}	55.0 ± 3.0	52.0 ± 3.0
Radiated Path Loss (eNB Ant to UE2)	L_{path}	42.9 ± 0.2	48.0 ± 1.0
Cable Loss (VST Ant)	L_{cable}	7.5 ± 0.2	7.7 ± 0.2
Cable Loss (eNB Ant)	L_{cable}	5.2 ± 0.2	5.3 ± 0.2
Testbed Circuit Loss	L_{circuit}	42.0 ± 0.2	42.0 ± 0.2
Antenna Gain (UE1)	G	10.4 ± 0.9	8.0 ± 1.0
Antenna Gain (UE2)	G	10.3 ± 0.9	8.0 ± 1.0
Total Loss (VST to UE1)	L_{tot}	45.0 ± 2.0	44.0 ± 2.0
Total Loss (eNB to UE1)	L_{tot}	91.0 ± 2.0	92.0 ± 2.0
Total Loss (VST to UE2)	L_{tot}	73.0 ± 2.0	70.0 ± 3.0
Total Loss (eNB to UE2)	L_{tot}	100.0 ± 2.0	106.0 ± 3.0

In conclusion, the use of an absorber wall and an extra sampling antenna allowed a direct measurement of the uplink emissions from a DUT UE at a relatively low path loss (45 dB) while maintaining a realistic path loss to the eNB of 91 dB. Additionally, a second network-loading UE can be added with a path loss of 100 dB to the eNB while having its characteristic uplink emissions selectively decreased at the measurement plane of a VST by 28 dB compared to the DUT UE.

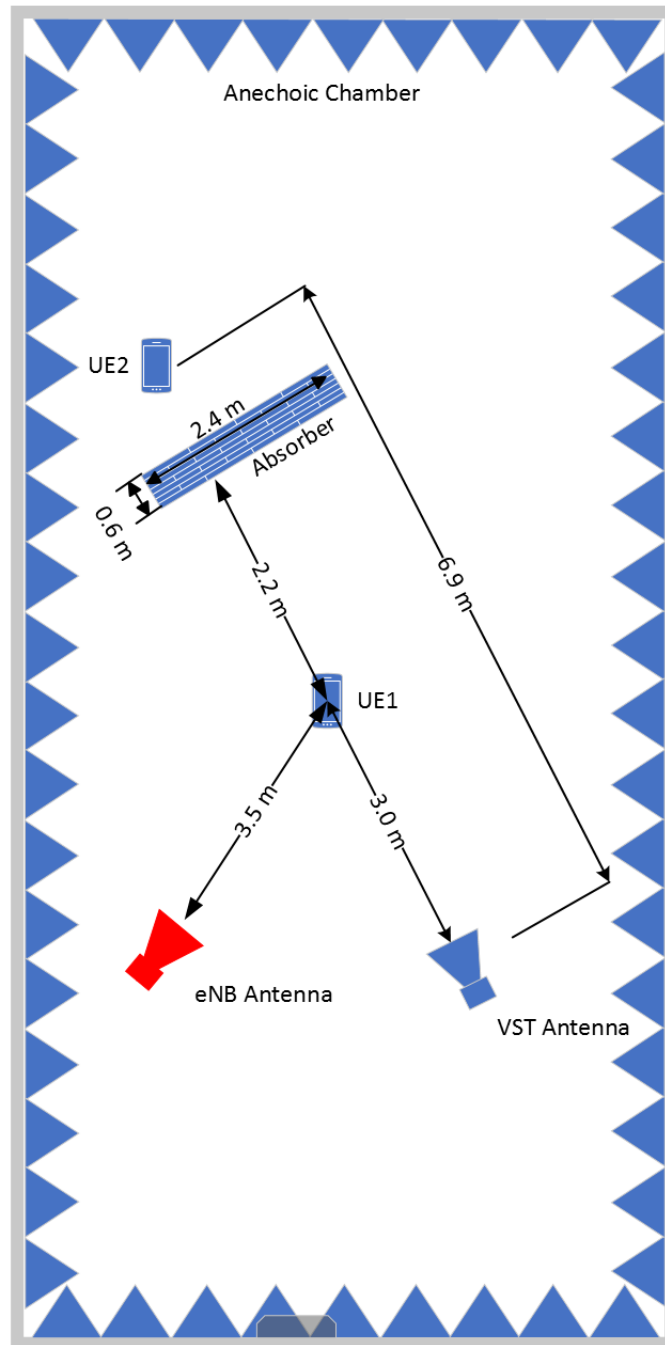


Figure A.1: Overview of Anechoic Chamber Setup.

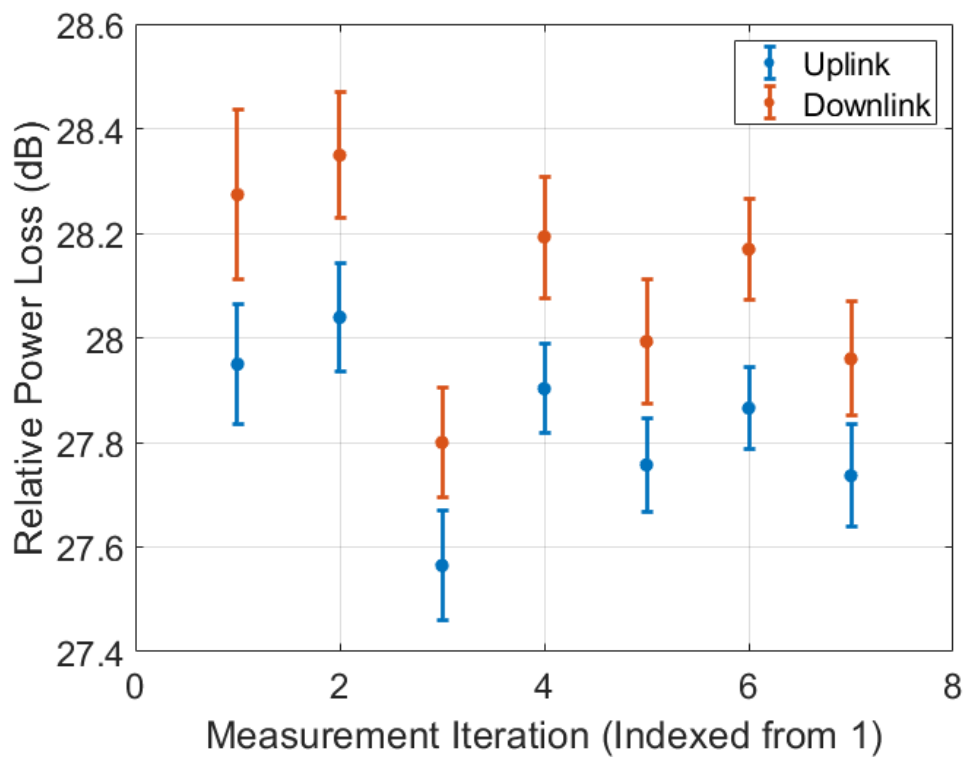


Figure A.2: Plot of the relative power loss between the VST and UE1 horn antennas for uplink (blue) and downlink (red) frequencies vs the corresponding movement of the UE1 antenna. The error bars represent one standard deviation relative error across the frequencies averaged. The measurement iterations correspond to: 1. Initial alignment of antennas, 2. Movement laterally 10 cm from initial alignment, 3. Movement laterally in other direction 10 cm, 4. Movement forward from initial alignment 10 cm, 5. Movement backward from initial alignment 10 cm, 6. Change of polarization 5° , 7. Remeasure at nominally initial alignment after experimental run.

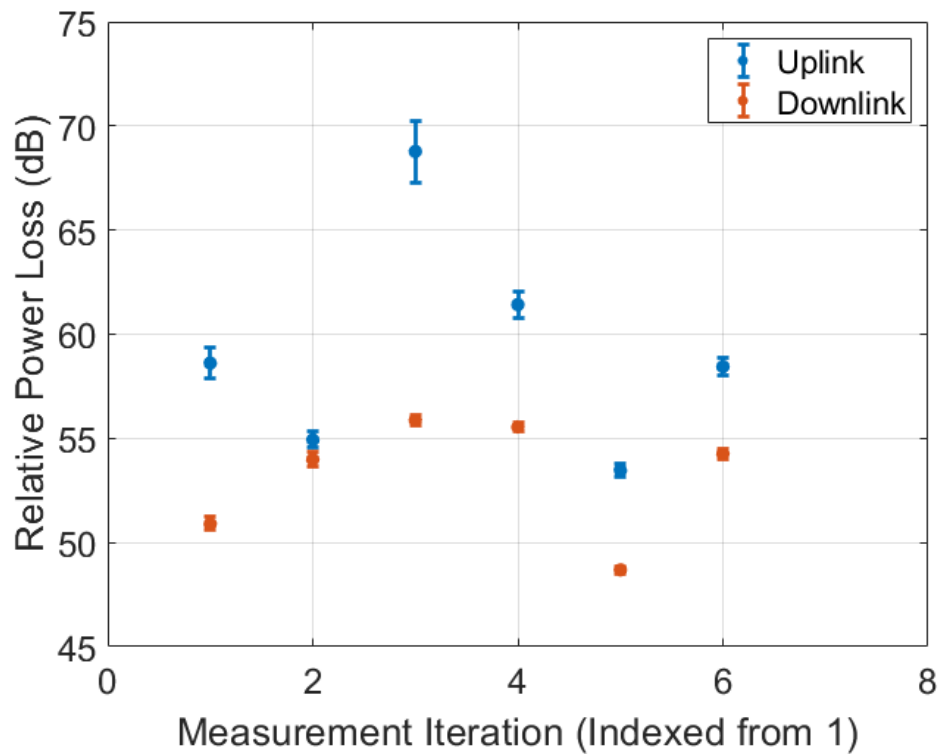


Figure A.3: Plot of the relative power loss between the VST and UE2 horn antennas for uplink (blue) and downlink (red) frequencies vs the corresponding movement of the UE1 antenna. The error bars represent one standard deviation relative error across the frequencies averaged. The measurement iterations correspond to: 1. Initial alignment of antennas, 2. Movement laterally 10 cm from initial alignment, 3. Movement laterally in other direction 10 cm, 4. Movement forward from initial alignment 10 cm, 5. Movement backward from initial alignment 10 cm, 6. Change of polarization 5° . In this case, the placement error of the antenna is the dominant source of uncertainty.

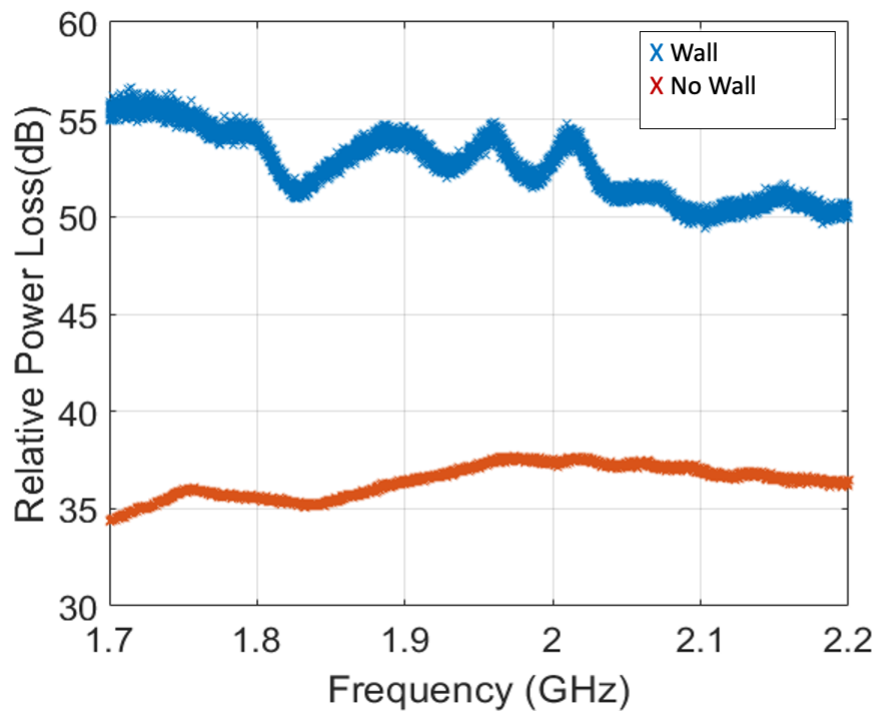


Figure A.4: Plot of the relative power loss between the VST antenna and the UE2 antenna.

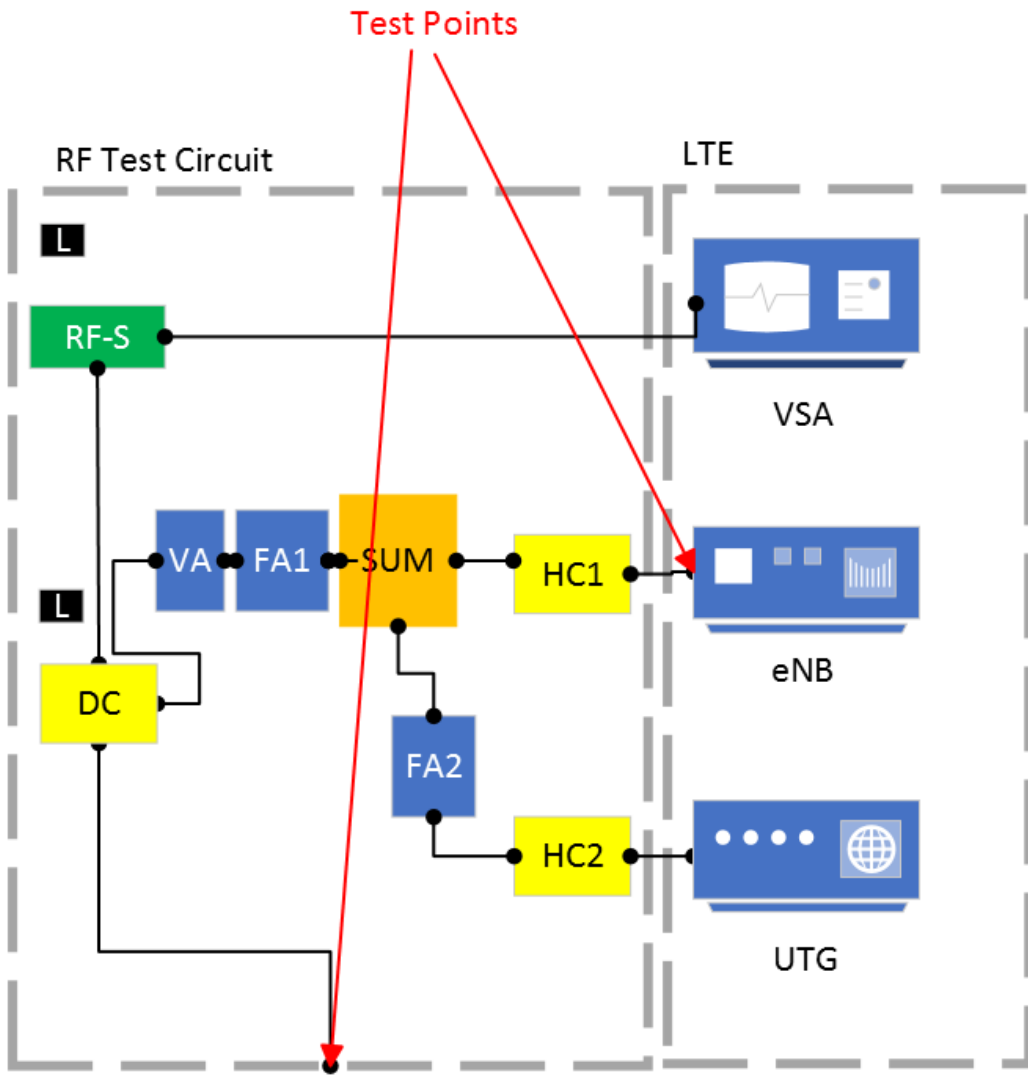


Figure A.5: Electrical schematic of the NASCTN LTE Testbed.

Appendix B

Graphical Overview of IQ Recordings

Each of the following plots represents the first 140 ms of a 5 s capture (one of the two repeats), with the parameters outlined in Chapter 3. These plots contain, a spectrogram with millisecond time resolution; the average of this spectrogram as a function of time for each millisecond of the capture, and the maximum of the capture for each frequency bin for the 140 ms sample, these values are relative to the reference power level of -25 dBm. In addition, a table summarizing the capture's factors and their value is shown at the bottom of the graphic.

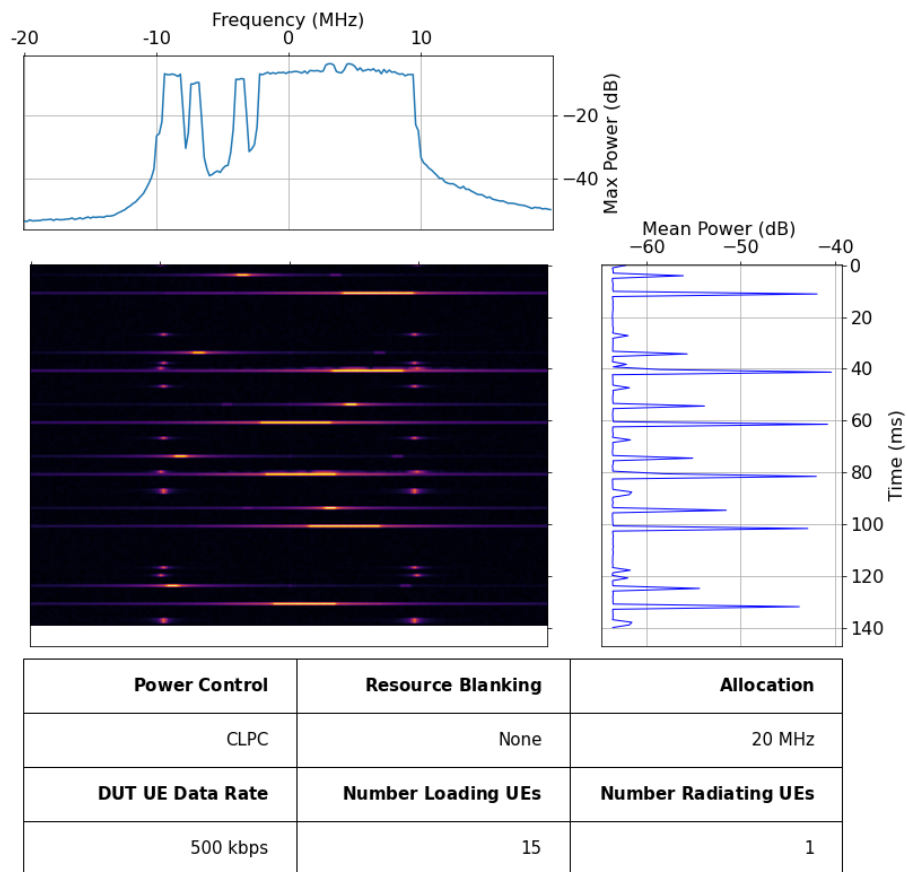


Figure B.1: 140 milliseconds of IQ Recording 1 of Configuration Number 1.

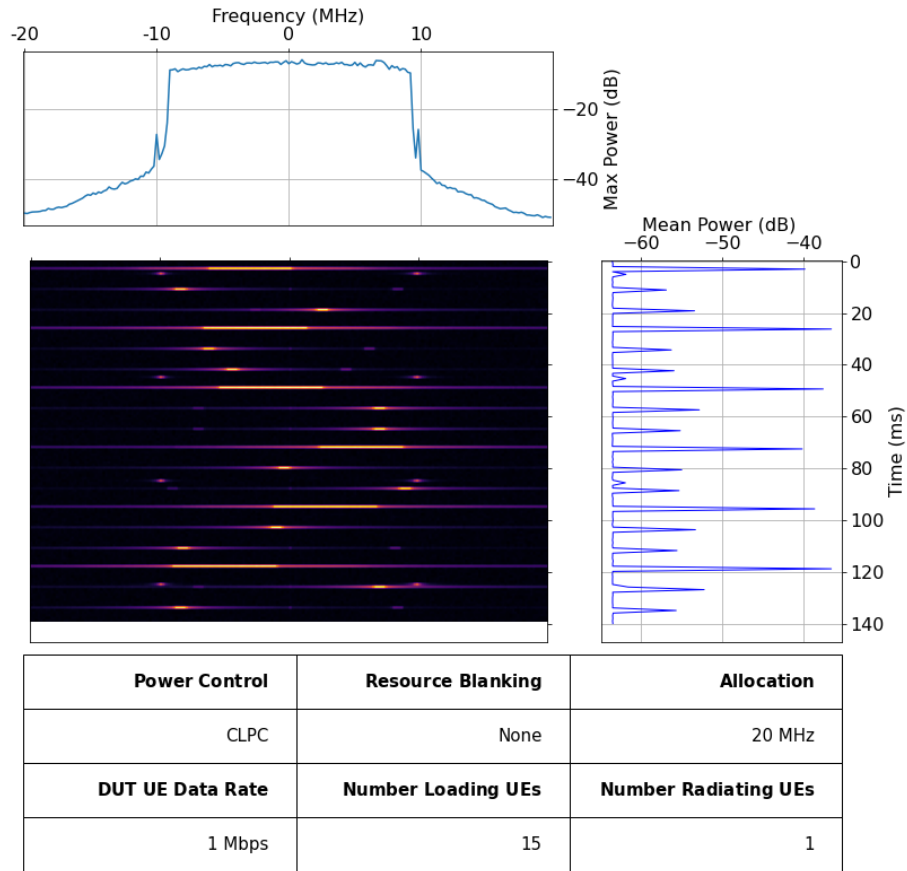


Figure B.2: 140 milliseconds of IQ Recording 1 of Configuration Number 2.

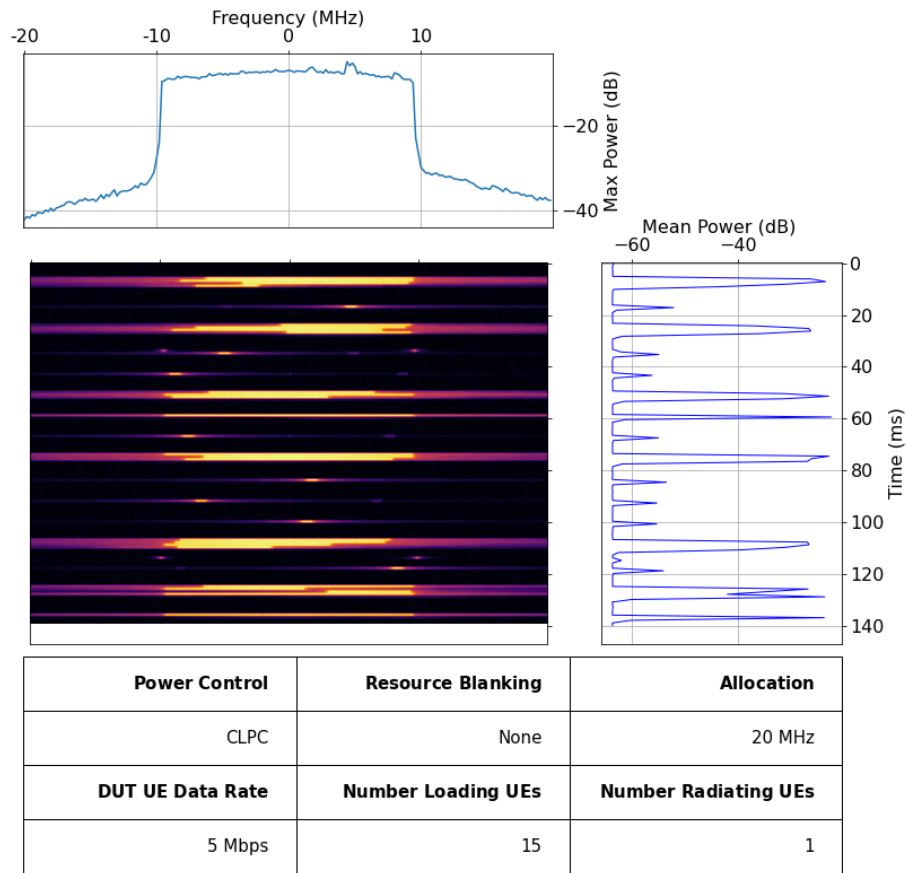


Figure B.3: 140 milliseconds of IQ Recording 1 of Configuration Number 3.

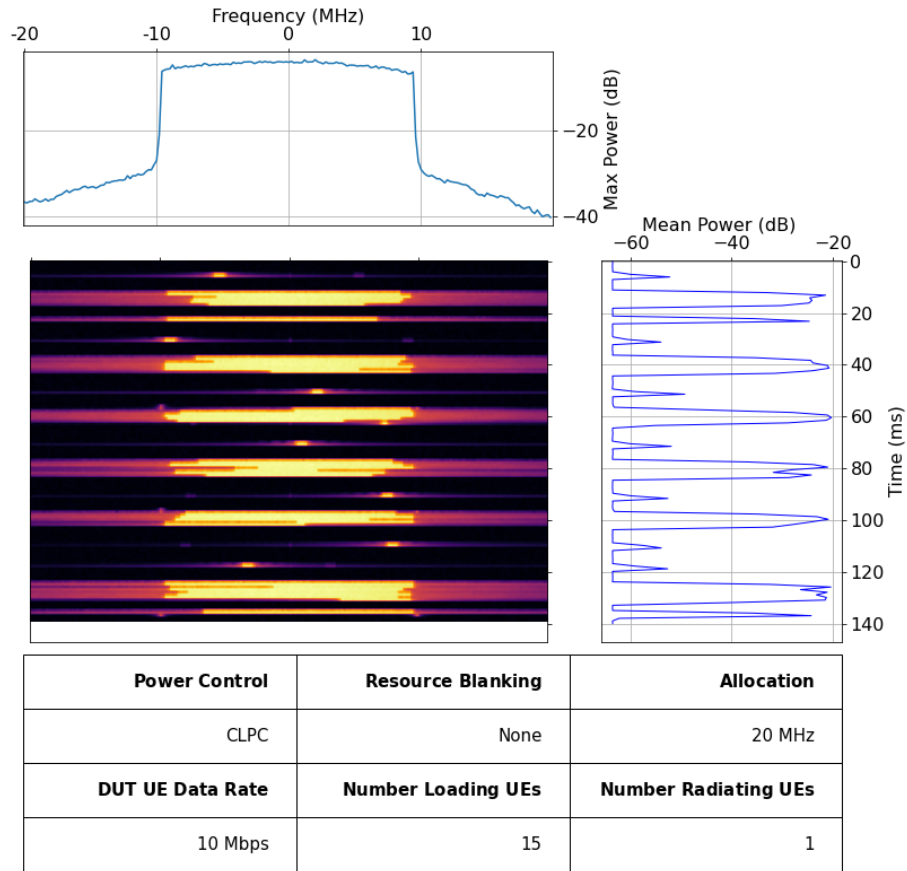


Figure B.4: 140 milliseconds of IQ Recording 1 of Configuration Number 4.

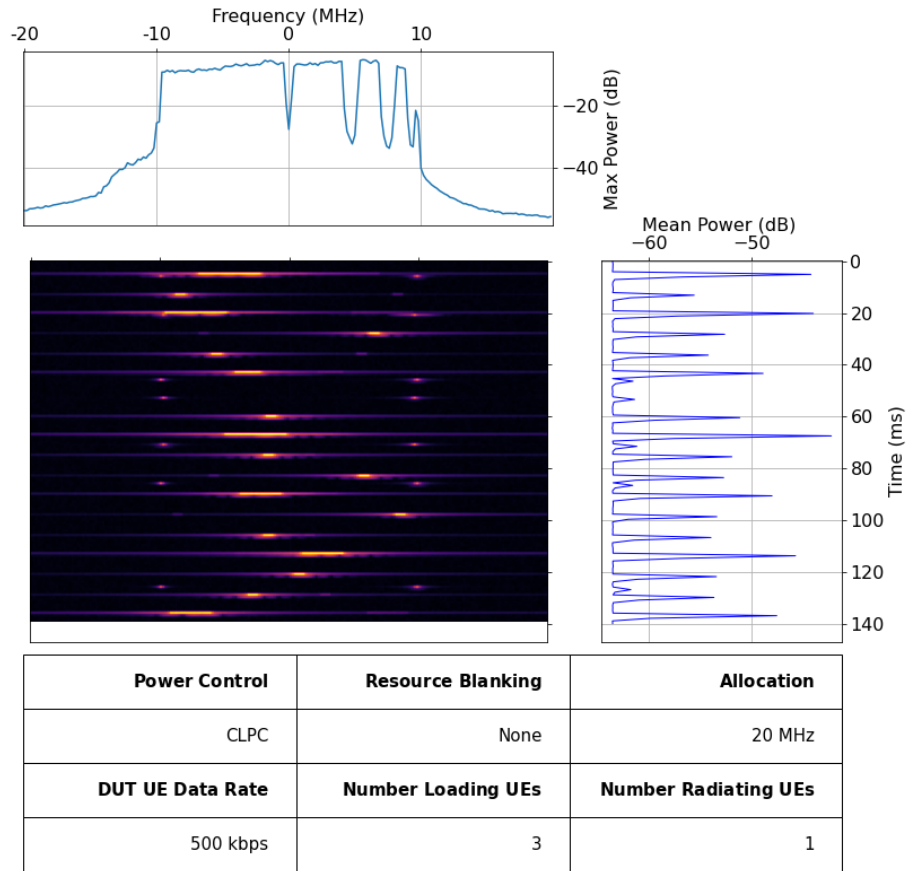


Figure B.5: 140 milliseconds of IQ Recording 1 of Configuration Number 5.

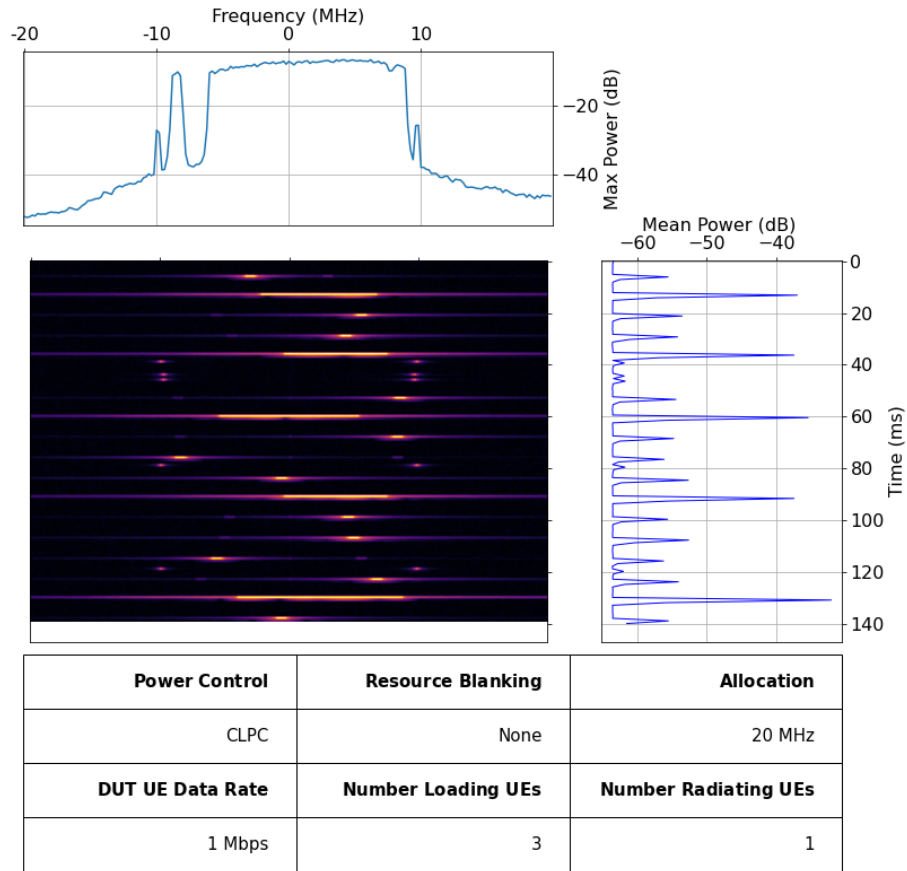


Figure B.6: 140 milliseconds of IQ Recording 1 of Configuration Number 6.

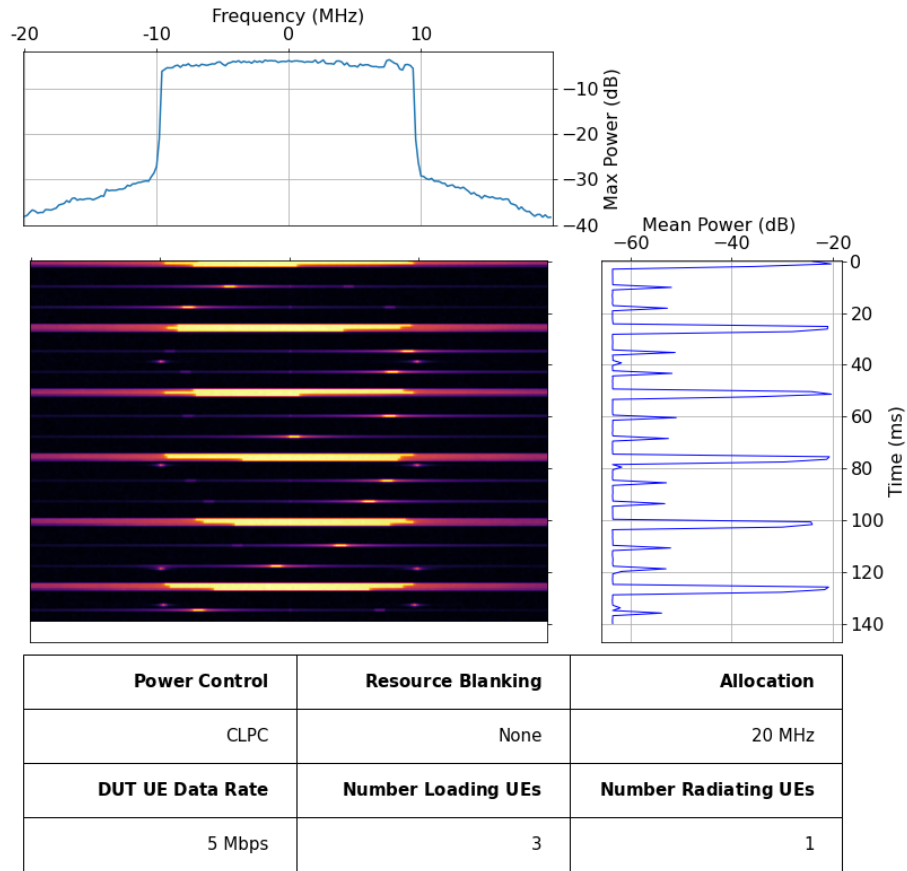


Figure B.7: 140 milliseconds of IQ Recording 1 of Configuration Number 7.

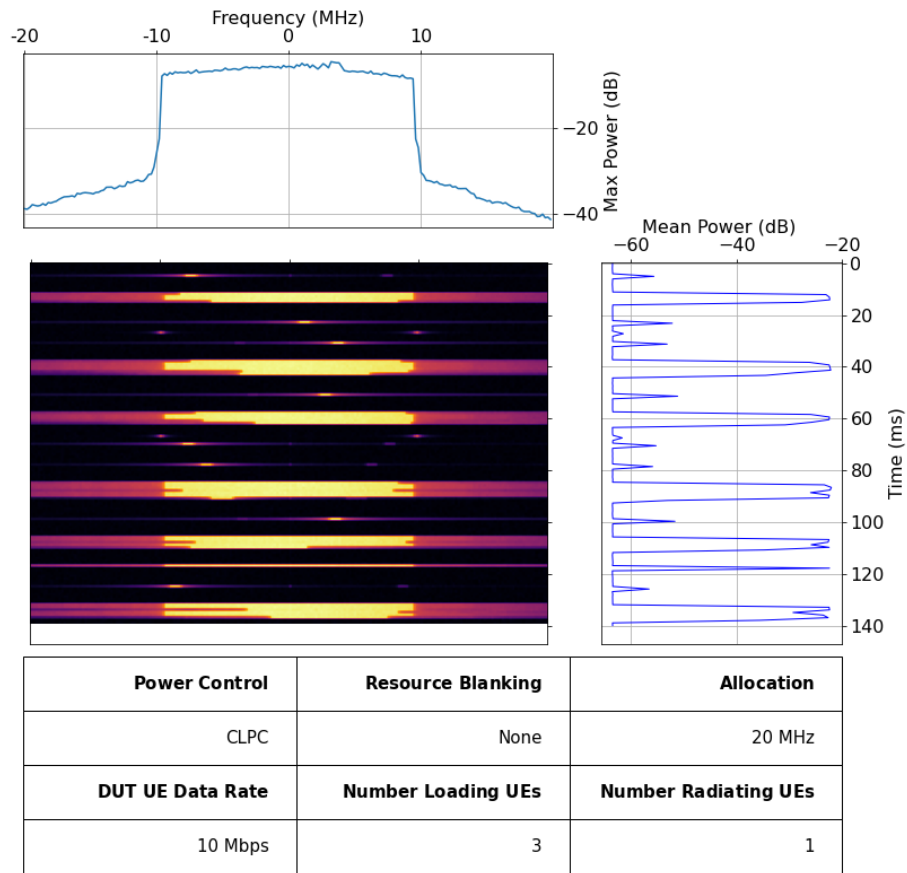


Figure B.8: 140 milliseconds of IQ Recording 1 of Configuration Number 8.

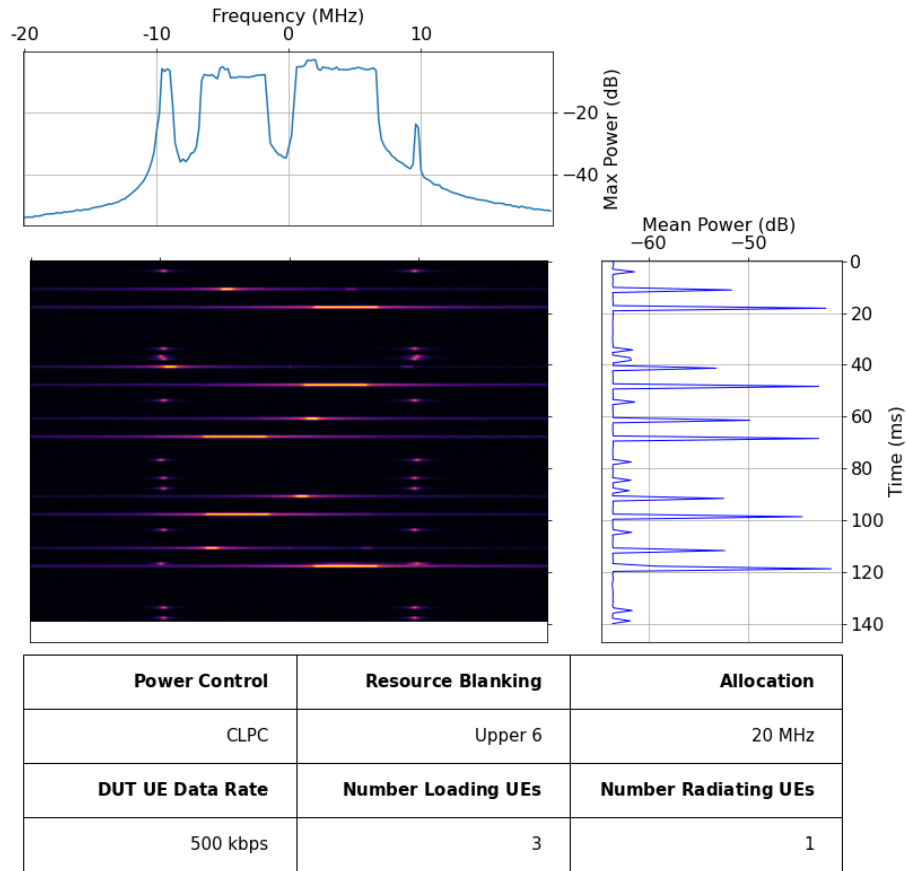


Figure B.9: 140 milliseconds of IQ Recording 1 of Configuration Number 9.

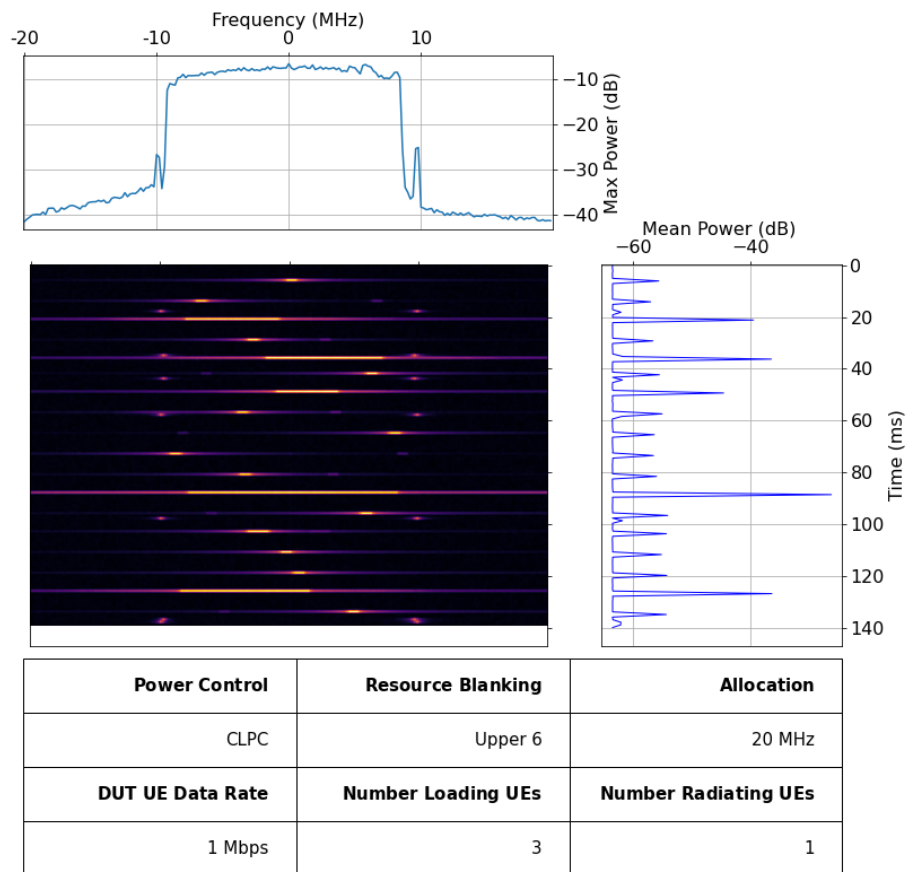


Figure B.10: 140 milliseconds of IQ Recording 1 of Configuration Number 10.

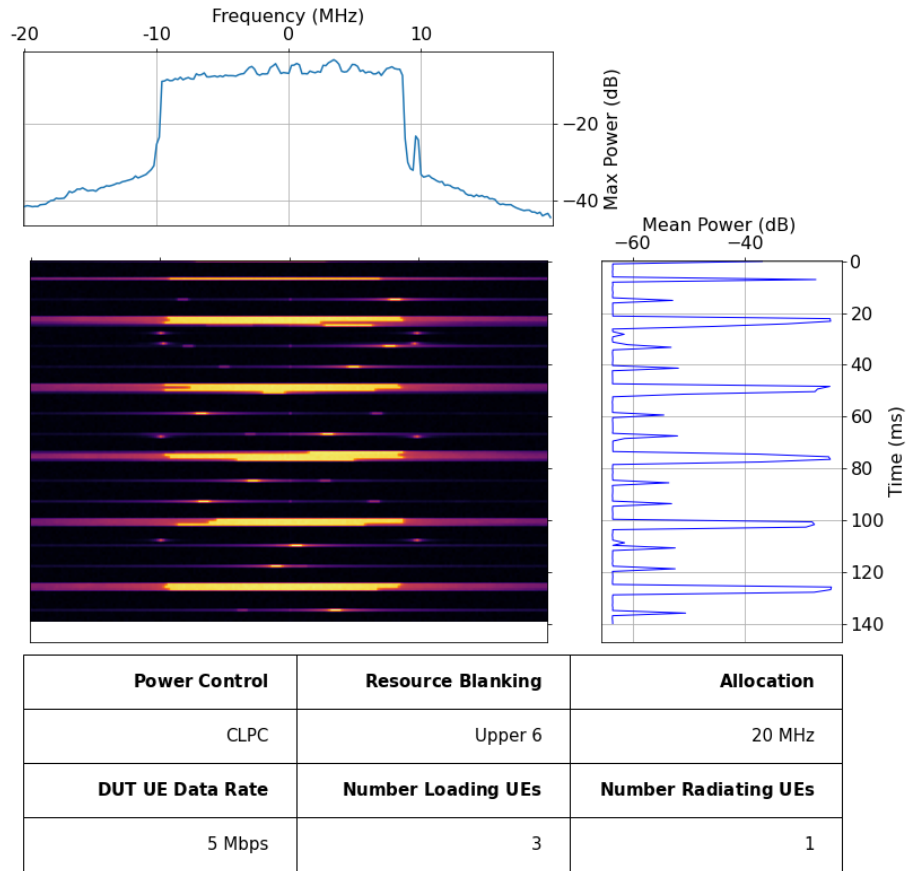


Figure B.11: 140 milliseconds of IQ Recording 1 of Configuration Number 11.

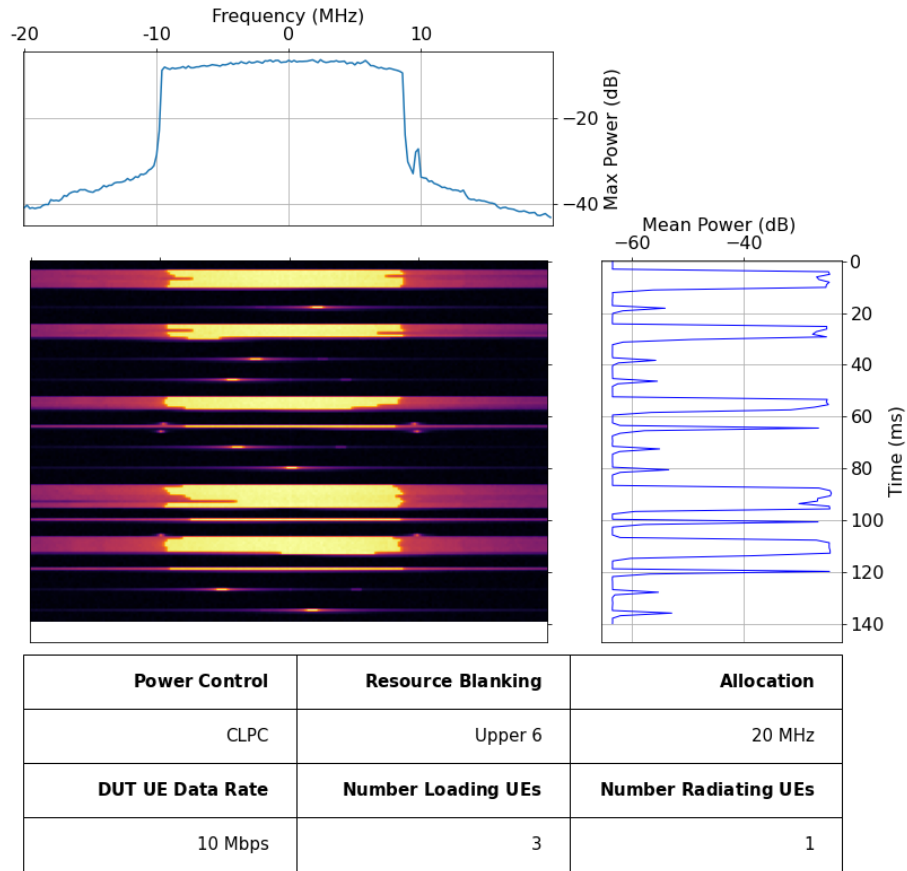


Figure B.12: 140 milliseconds of IQ Recording 1 of Configuration Number 12.

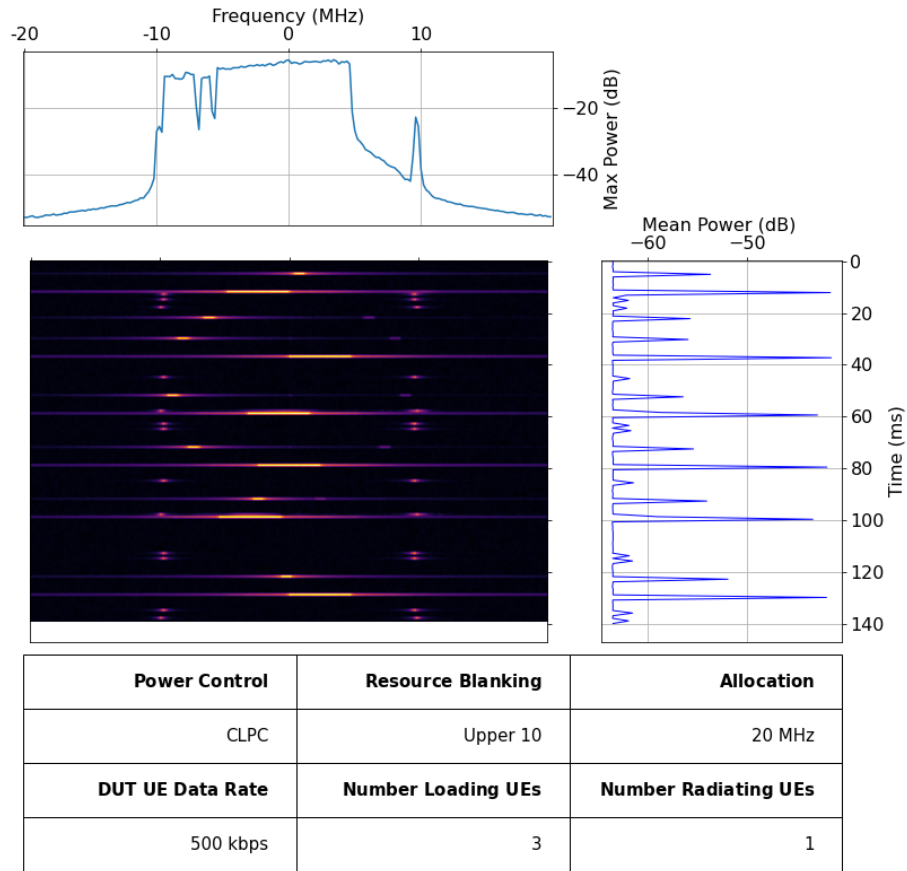


Figure B.13: 140 milliseconds of IQ Recording 1 of Configuration Number 13.

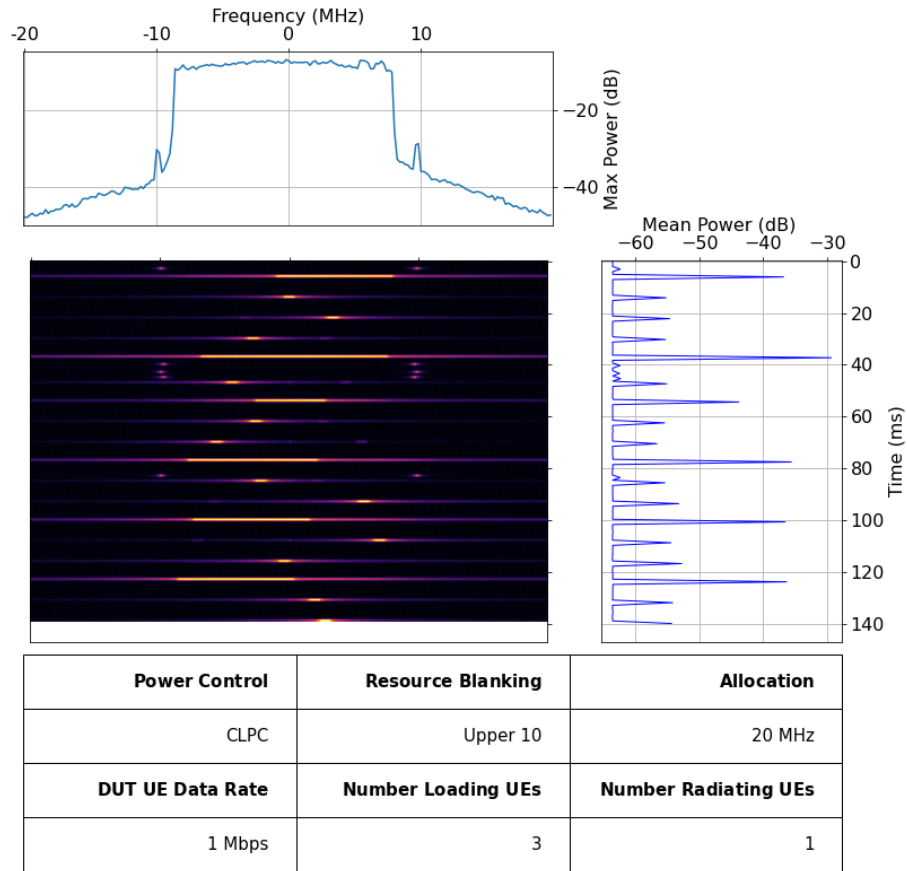


Figure B.14: 140 milliseconds of IQ Recording 1 of Configuration Number 14.

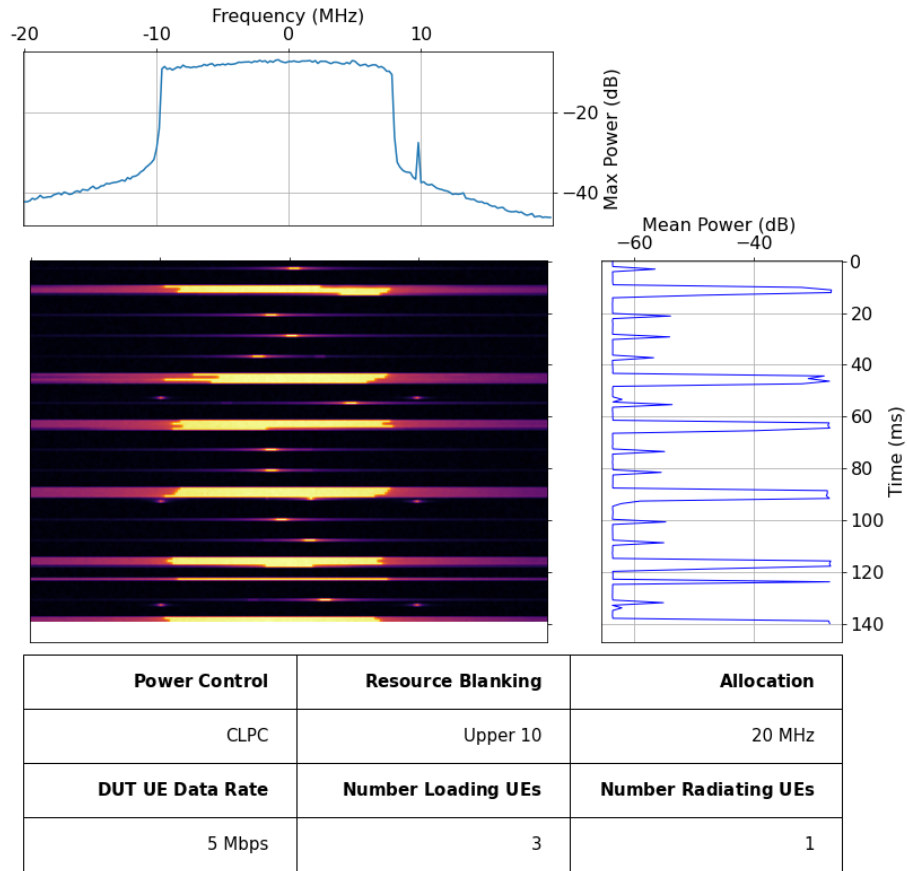


Figure B.15: 140 milliseconds of IQ Recording 1 of Configuration Number 15.

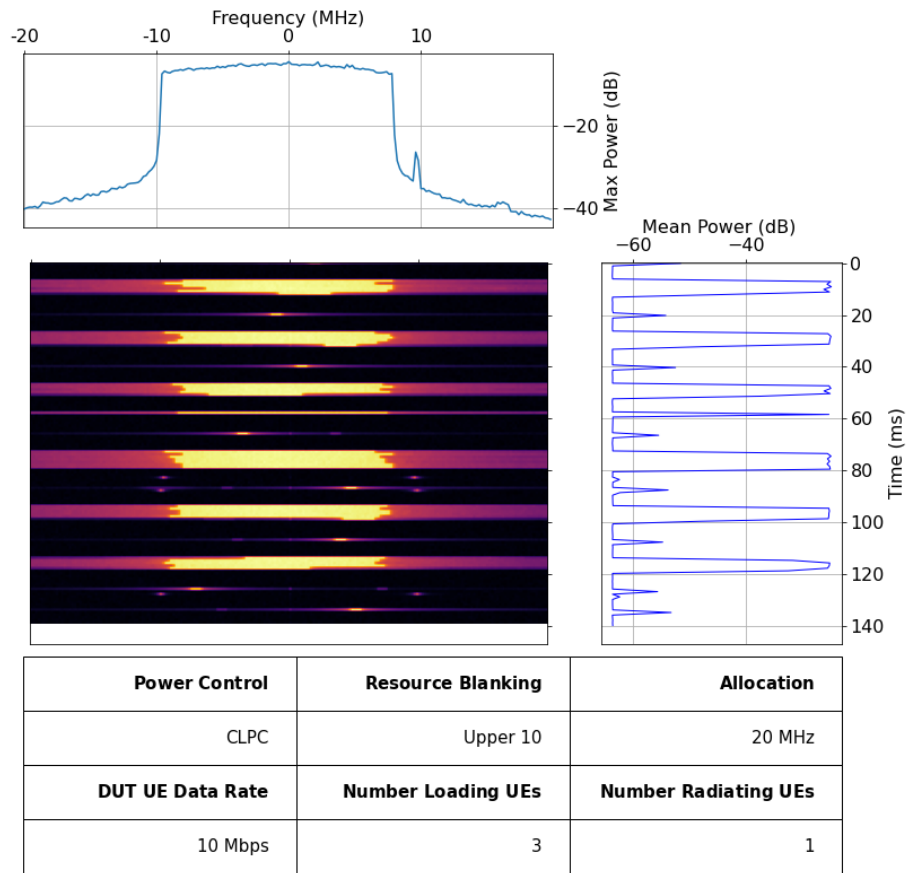


Figure B.16: 140 milliseconds of IQ Recording 1 of Configuration Number 16.

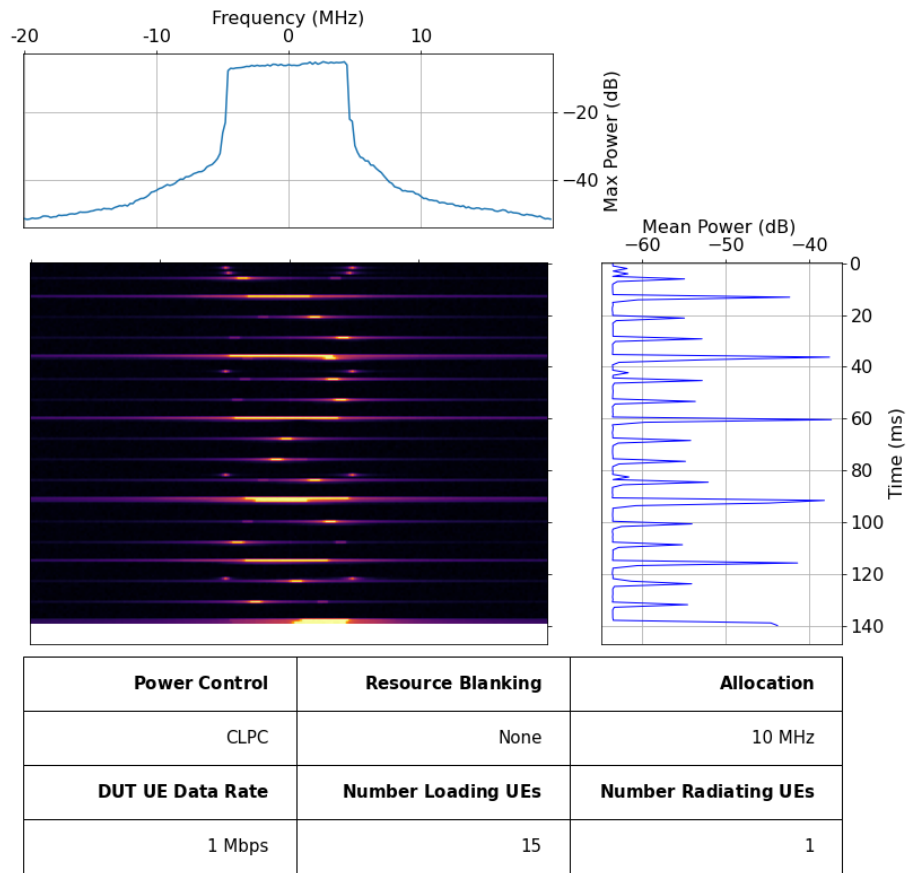


Figure B.17: 140 milliseconds of IQ Recording 1 of Configuration Number 17.

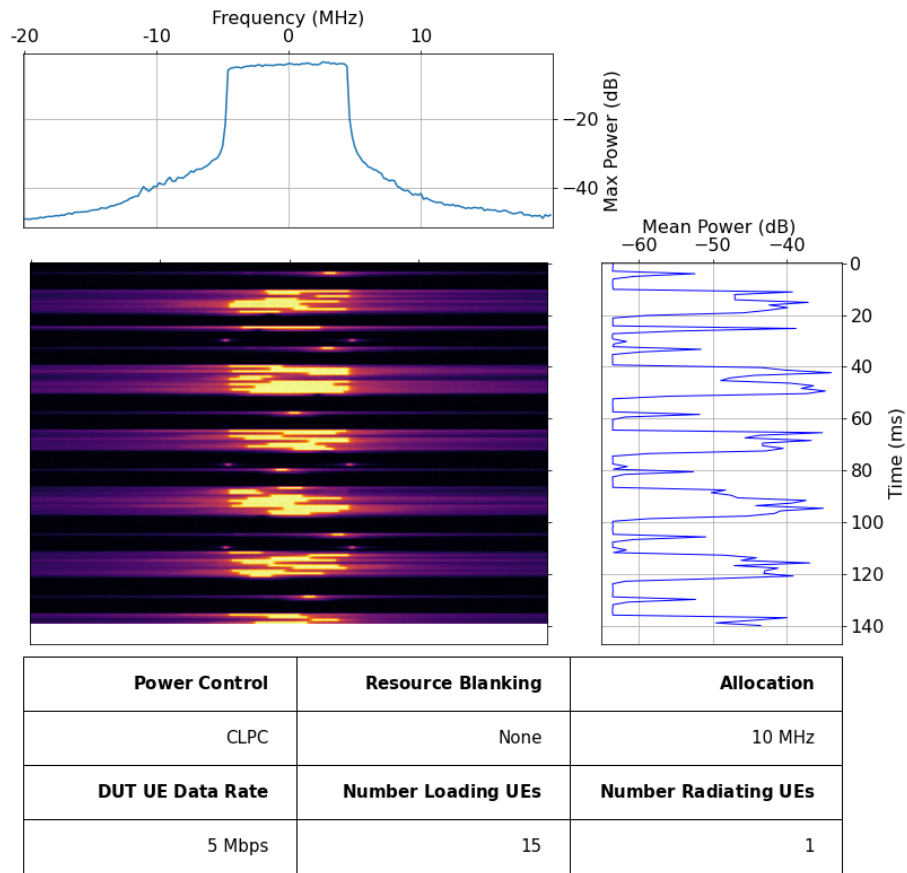


Figure B.18: 140 milliseconds of IQ Recording 1 of Configuration Number 18.

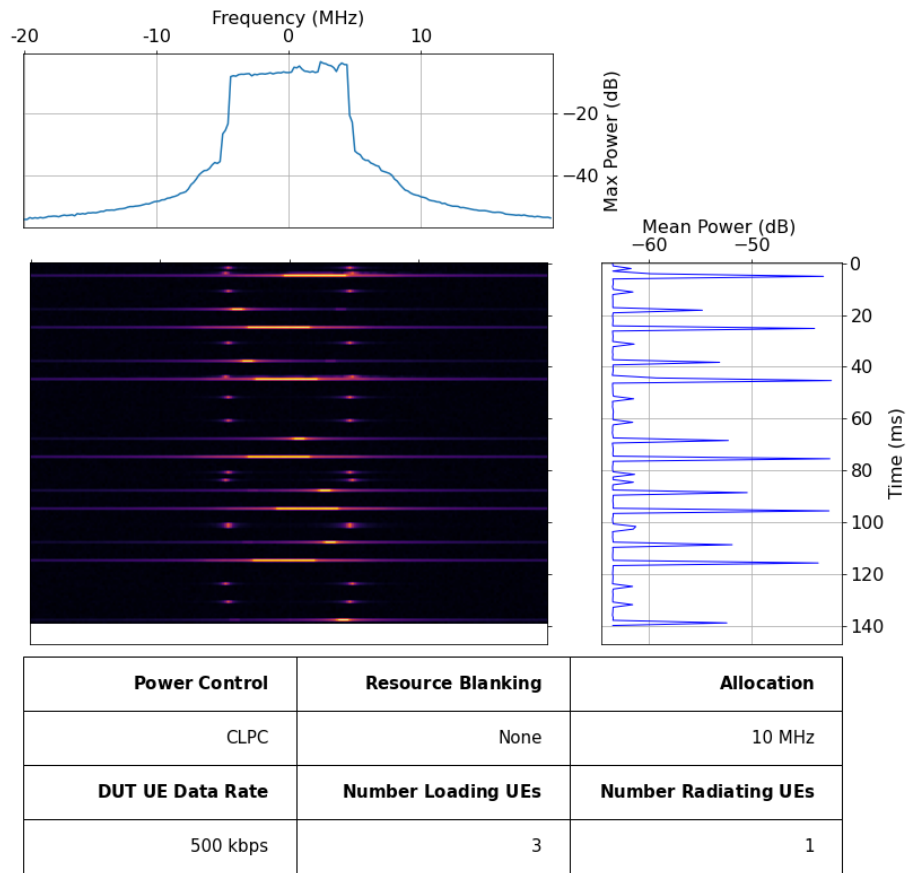


Figure B.19: 140 milliseconds of IQ Recording 1 of Configuration Number 19.

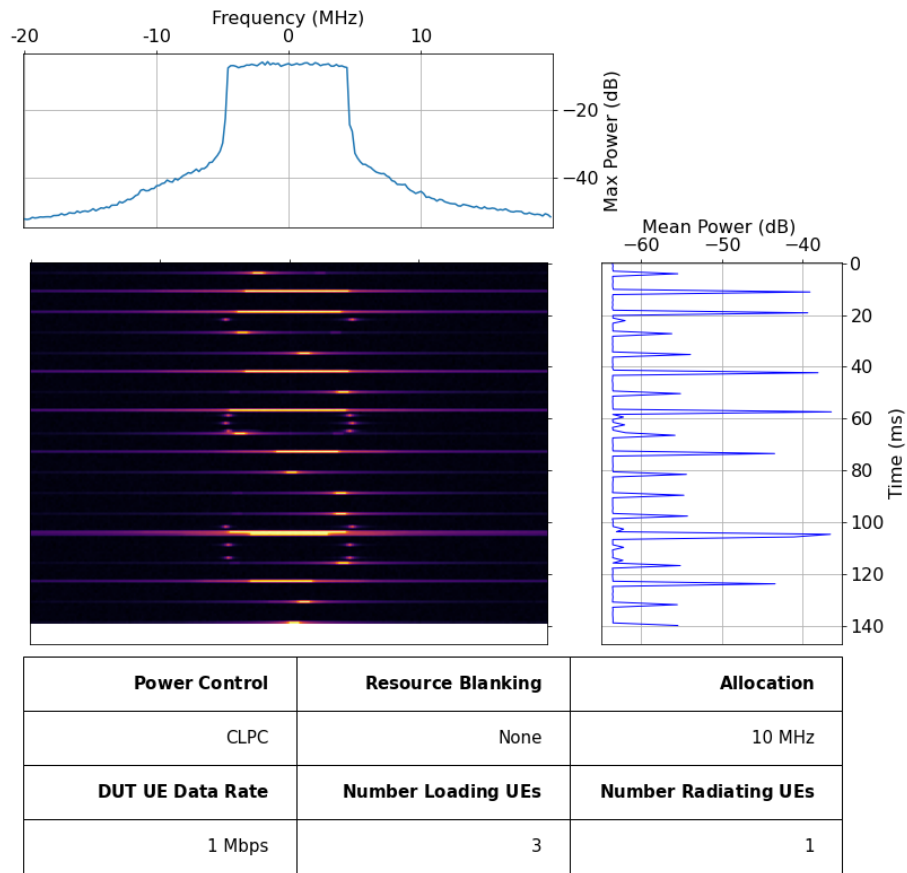


Figure B.20: 140 milliseconds of IQ Recording 1 of Configuration Number 20.

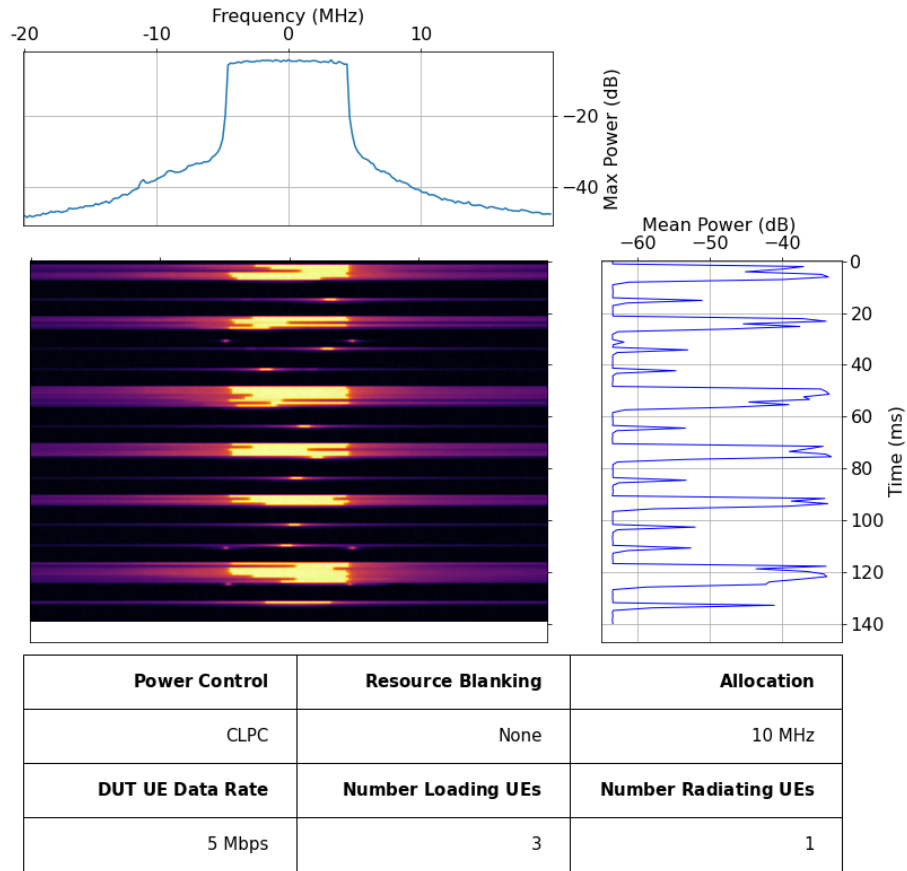


Figure B.21: 140 milliseconds of IQ Recording 1 of Configuration Number 21.

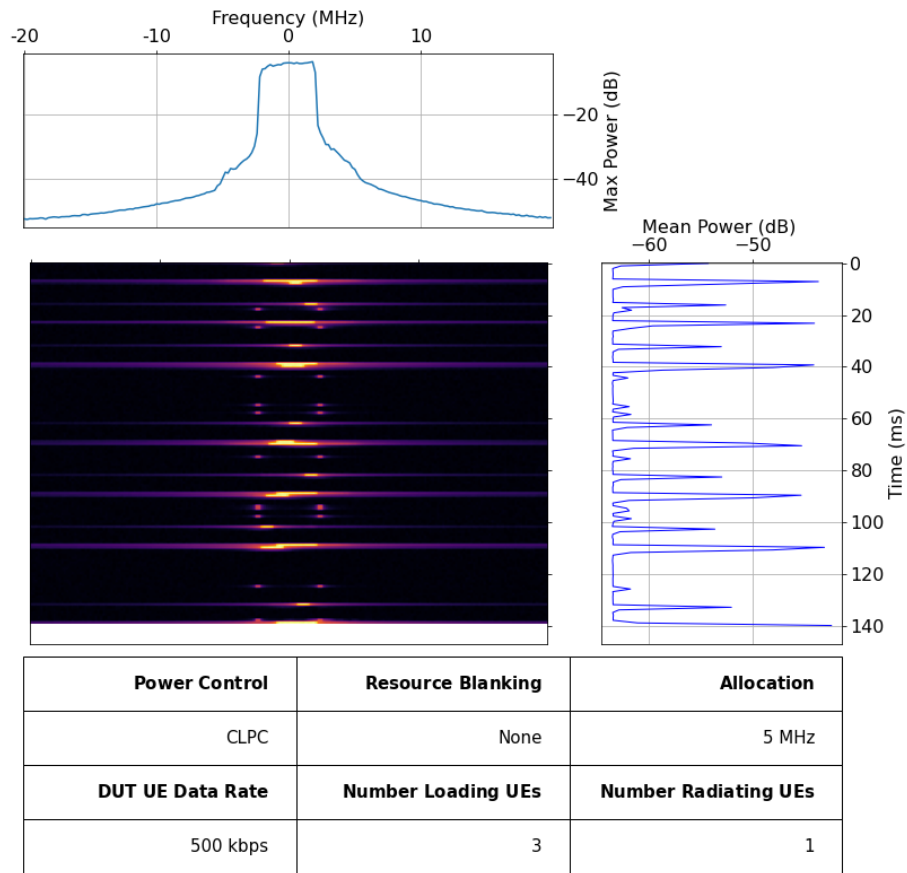


Figure B.22: 140 milliseconds of IQ Recording 1 of Configuration Number 22.

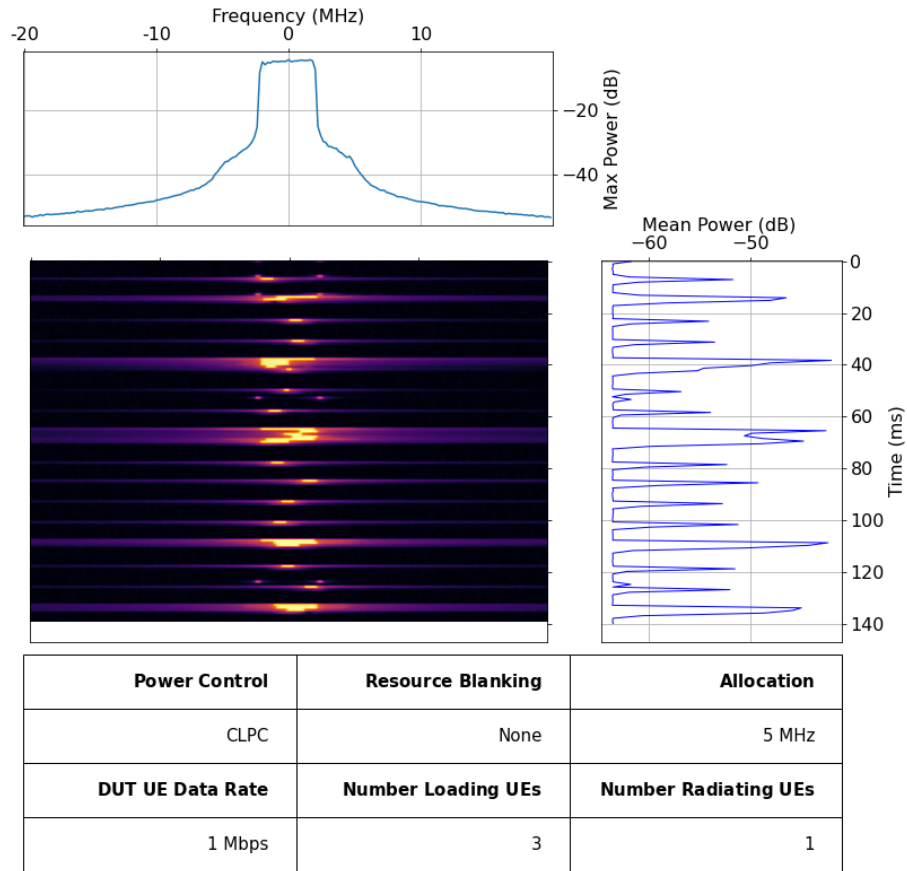


Figure B.23: 140 milliseconds of IQ Recording 1 of Configuration Number 23.

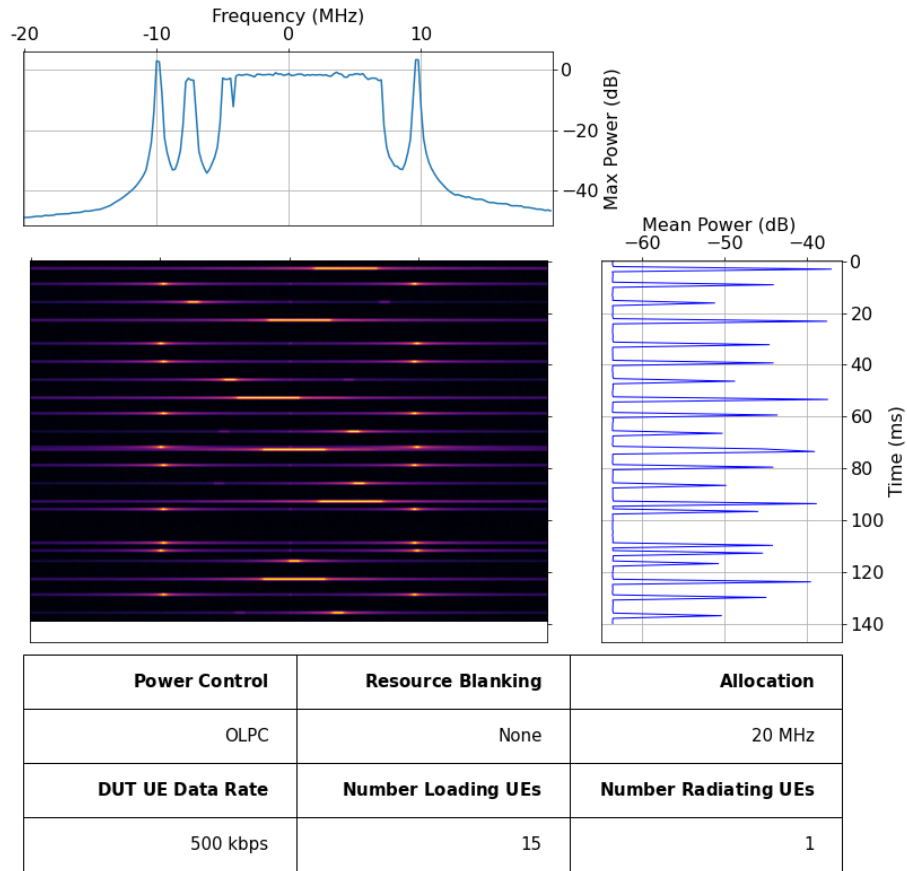


Figure B.24: 140 milliseconds of IQ Recording 1 of Configuration Number 24.

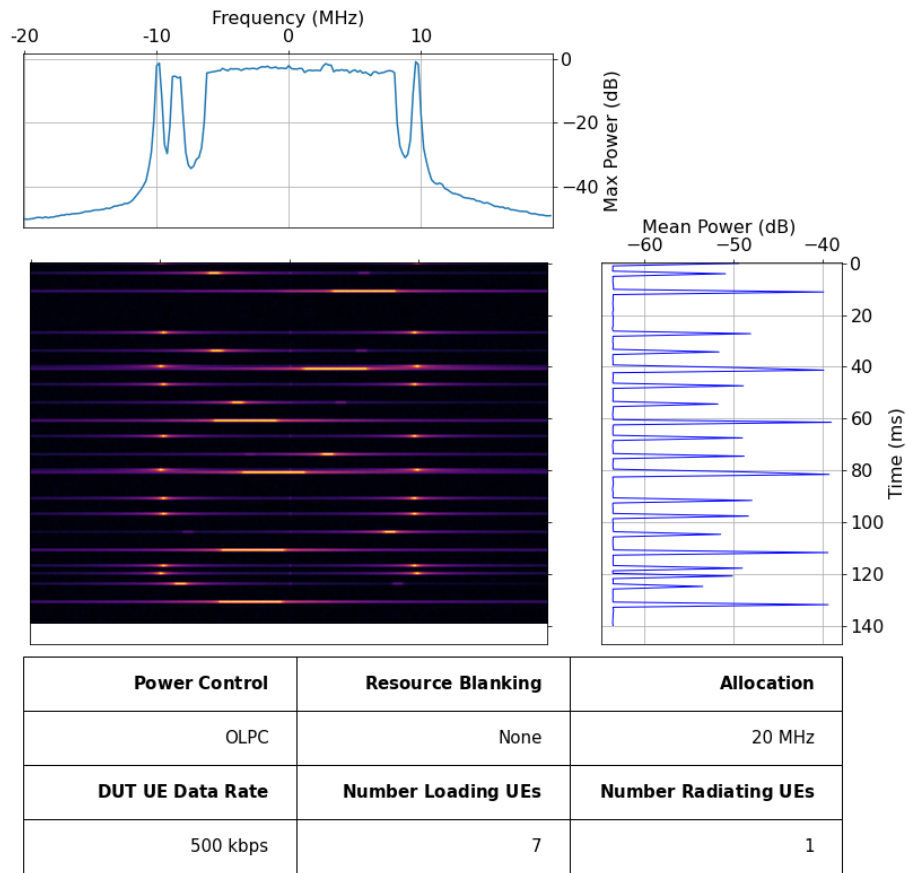


Figure B.25: 140 milliseconds of IQ Recording 1 of Configuration Number 25.

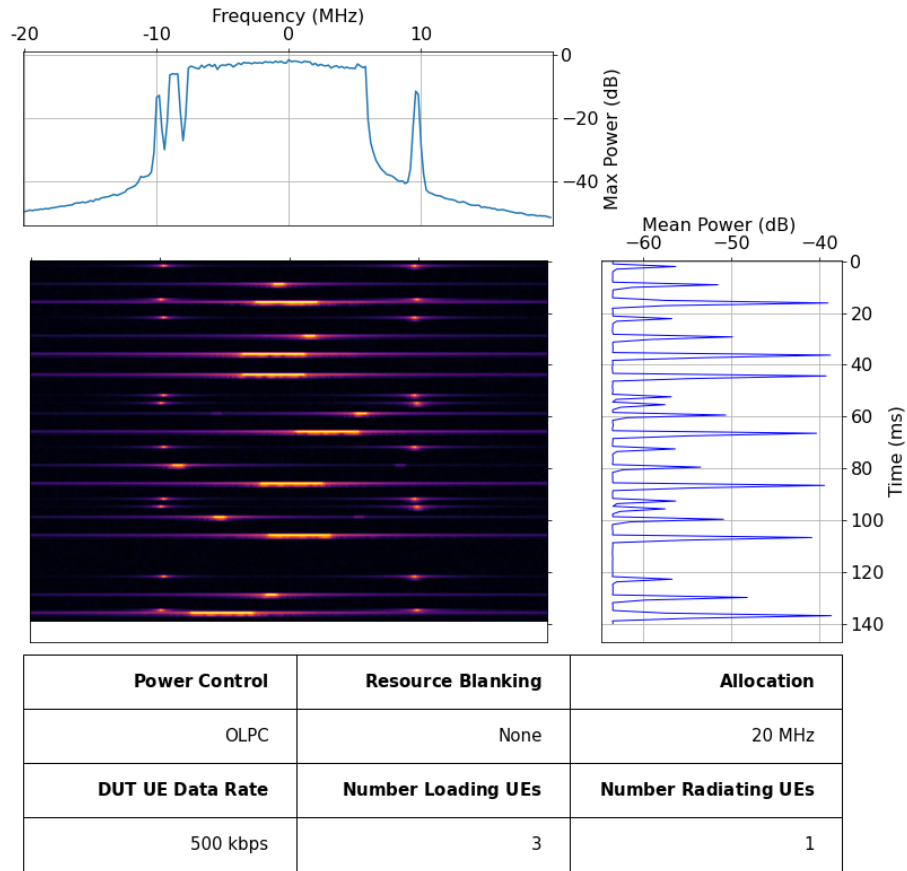


Figure B.26: 140 milliseconds of IQ Recording 1 of Configuration Number 26.

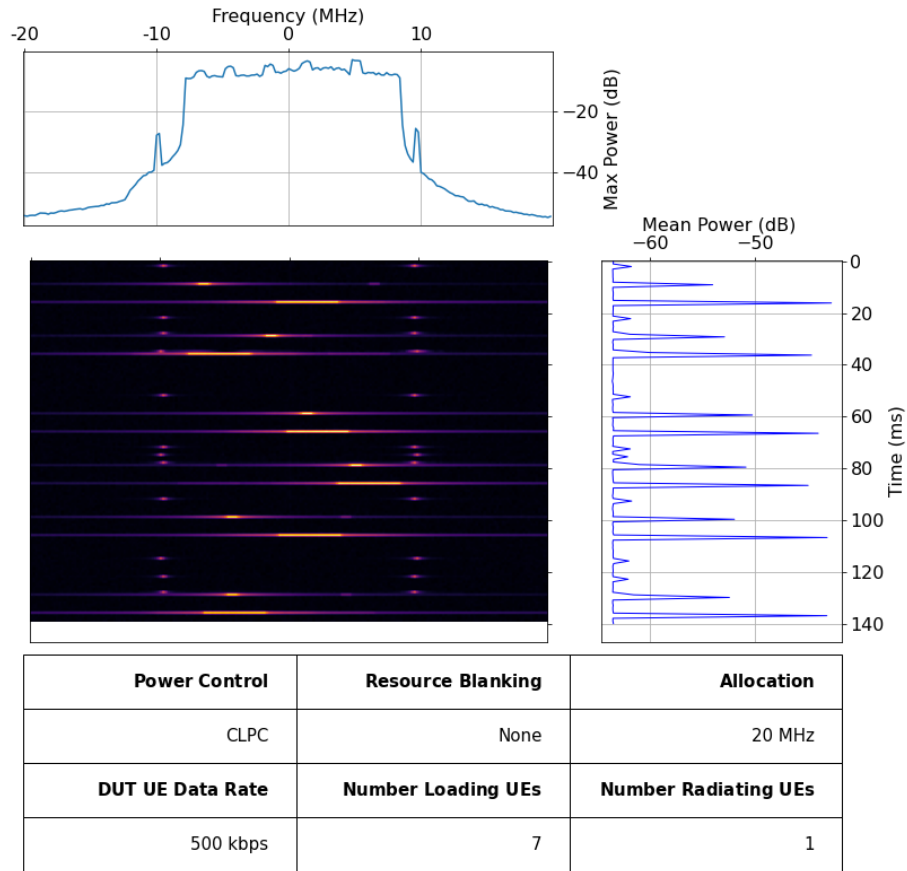


Figure B.27: 140 milliseconds of IQ Recording 1 of Configuration Number 27.

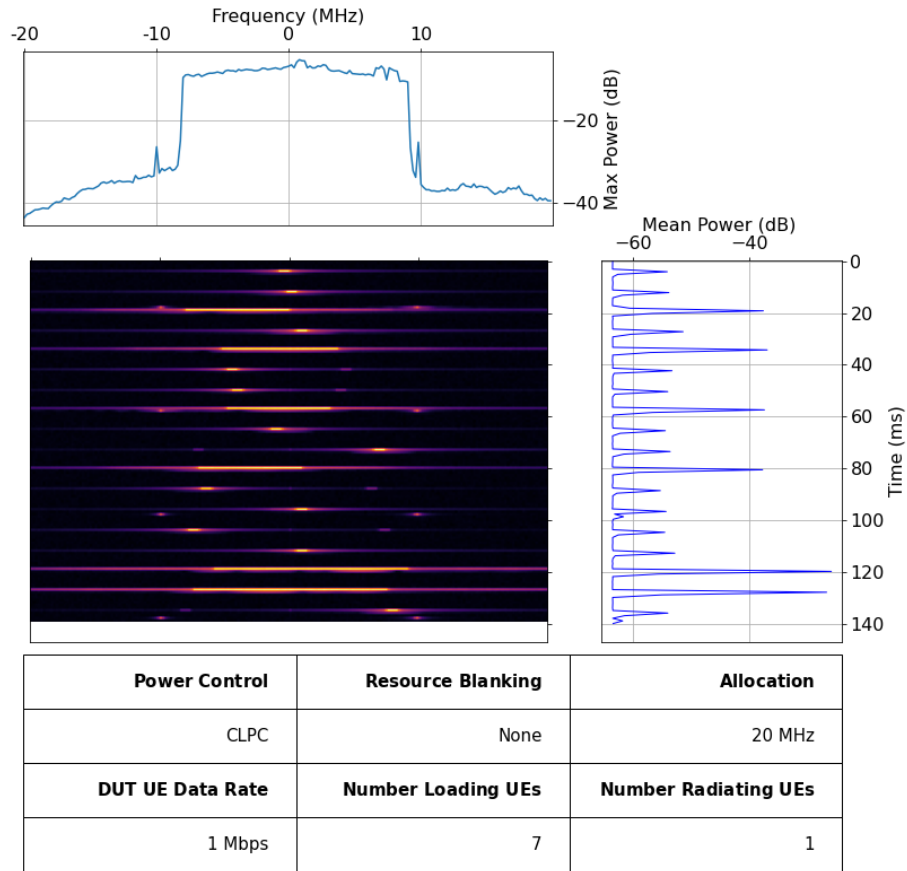


Figure B.28: 140 milliseconds of IQ Recording 1 of Configuration Number 28.

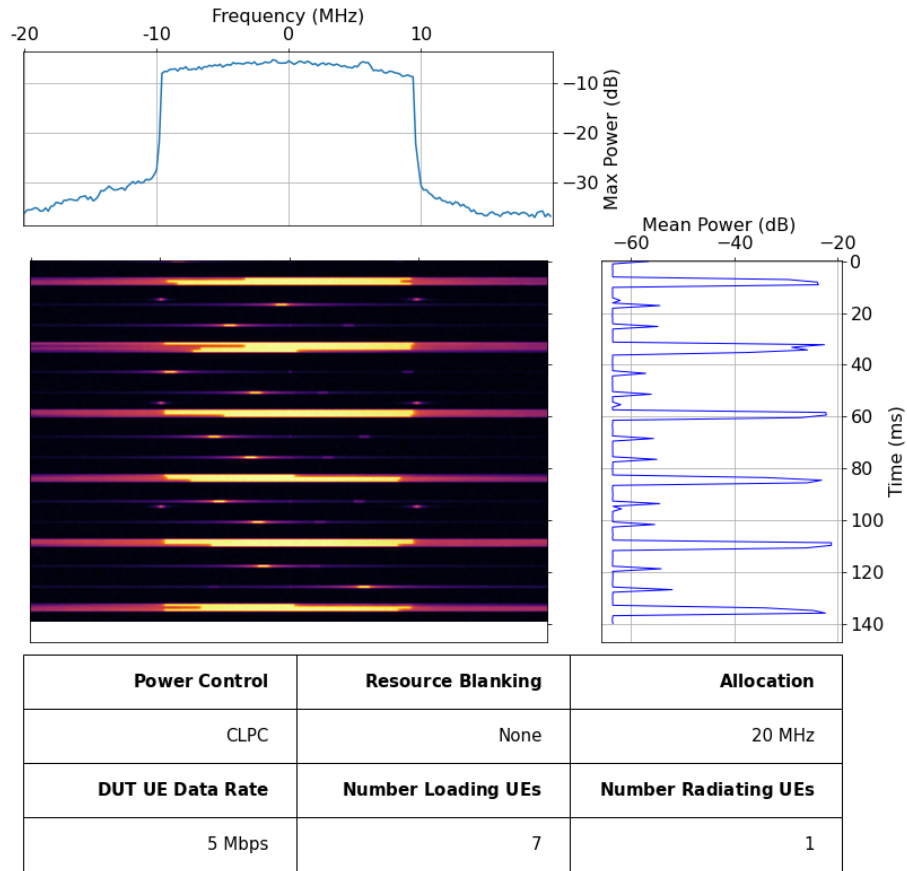


Figure B.29: 140 milliseconds of IQ Recording 1 of Configuration Number 29.

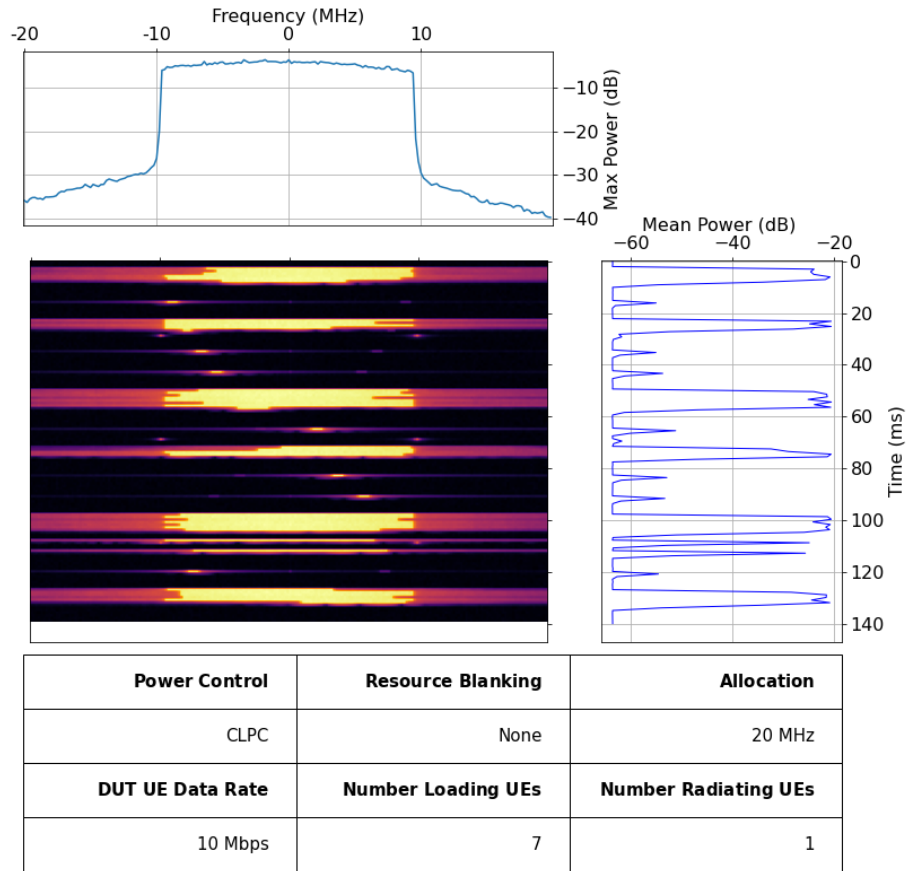


Figure B.30: 140 milliseconds of IQ Recording 1 of Configuration Number 30.

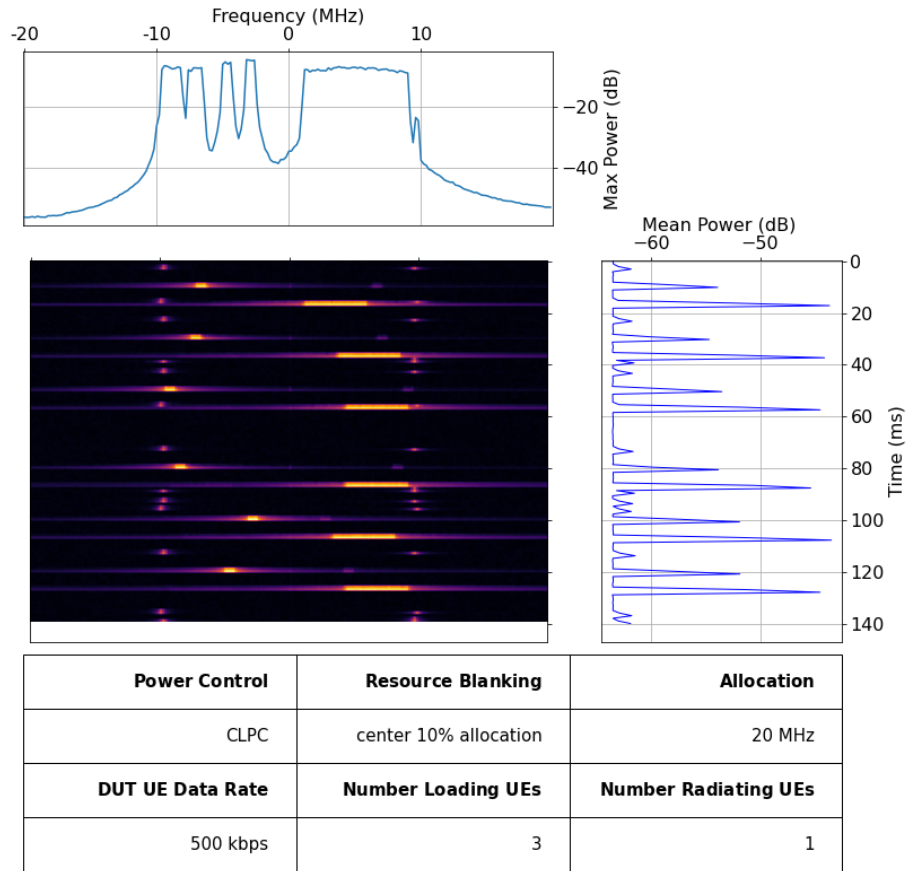


Figure B.31: 140 milliseconds of IQ Recording 1 of Configuration Number 31.

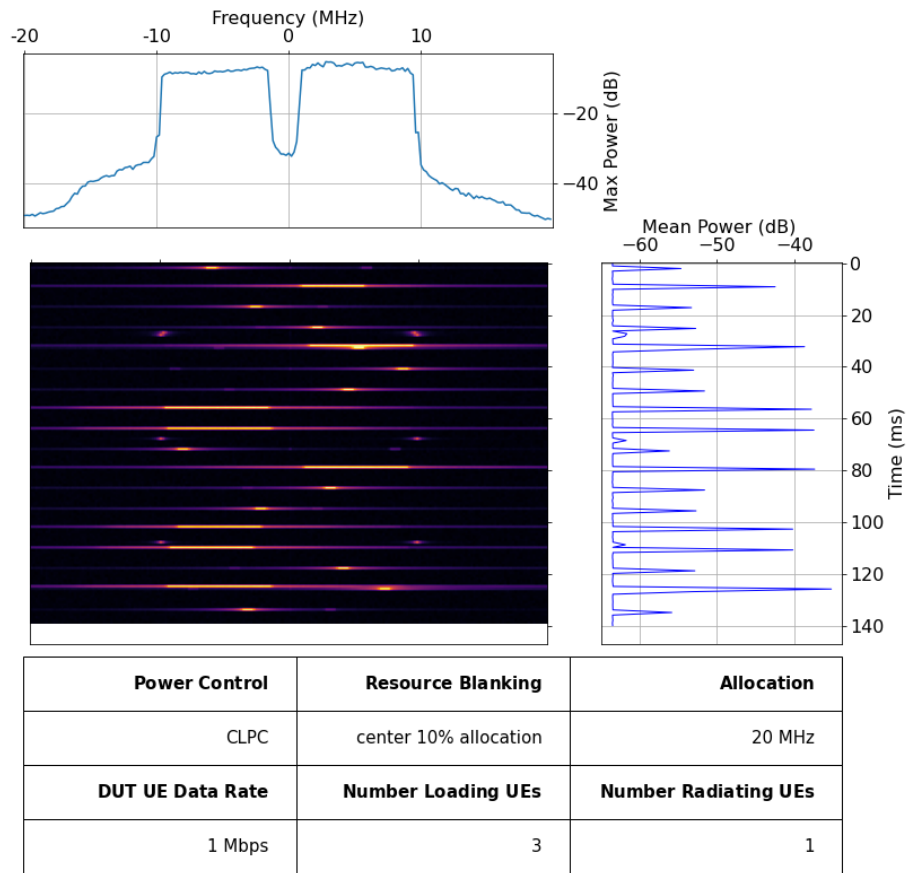


Figure B.32: 140 milliseconds of IQ Recording 1 of Configuration Number 32.

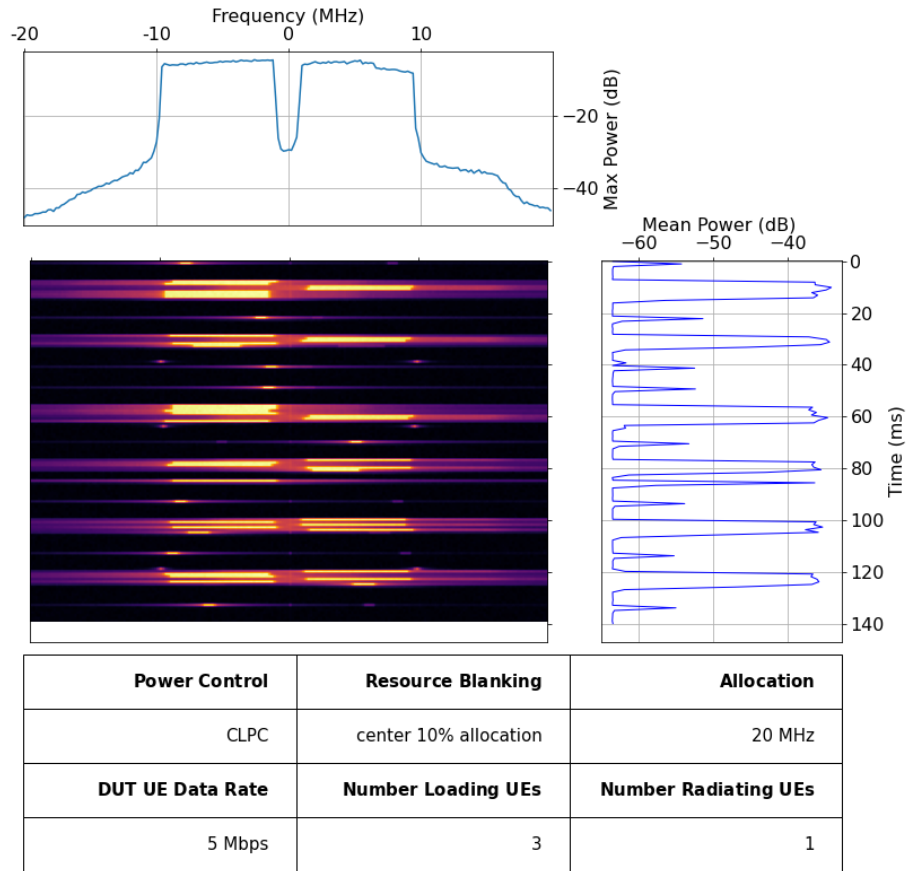


Figure B.33: 140 milliseconds of IQ Recording 1 of Configuration Number 33.

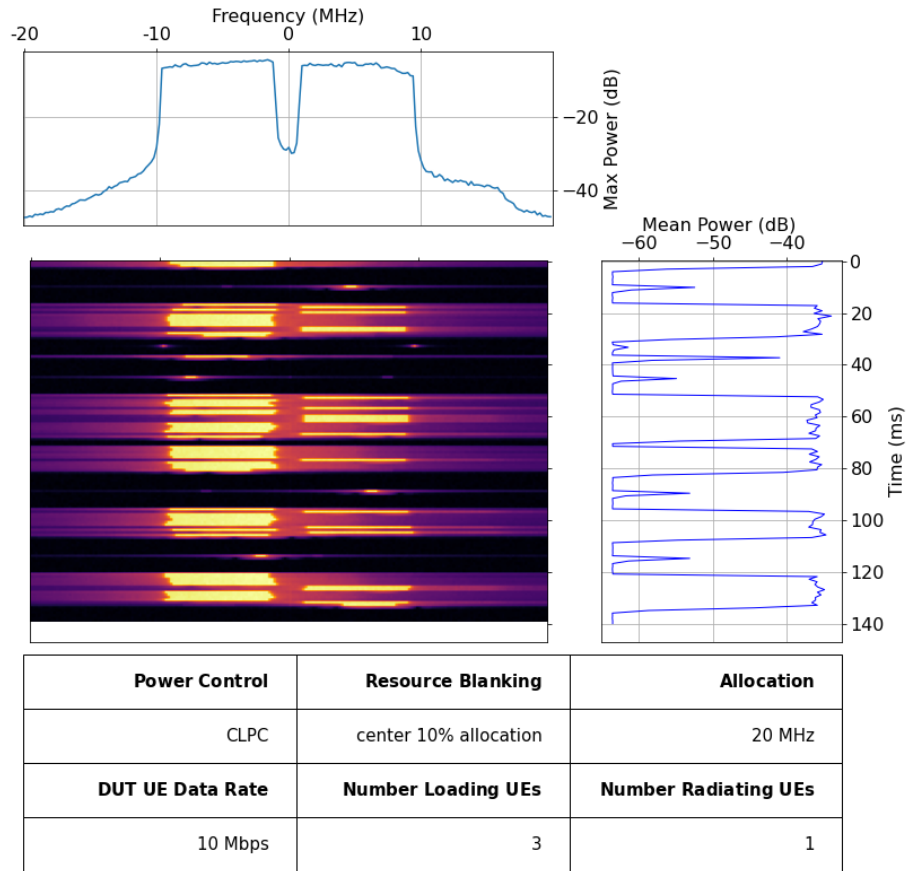


Figure B.34: 140 milliseconds of IQ Recording 1 of Configuration Number 34.

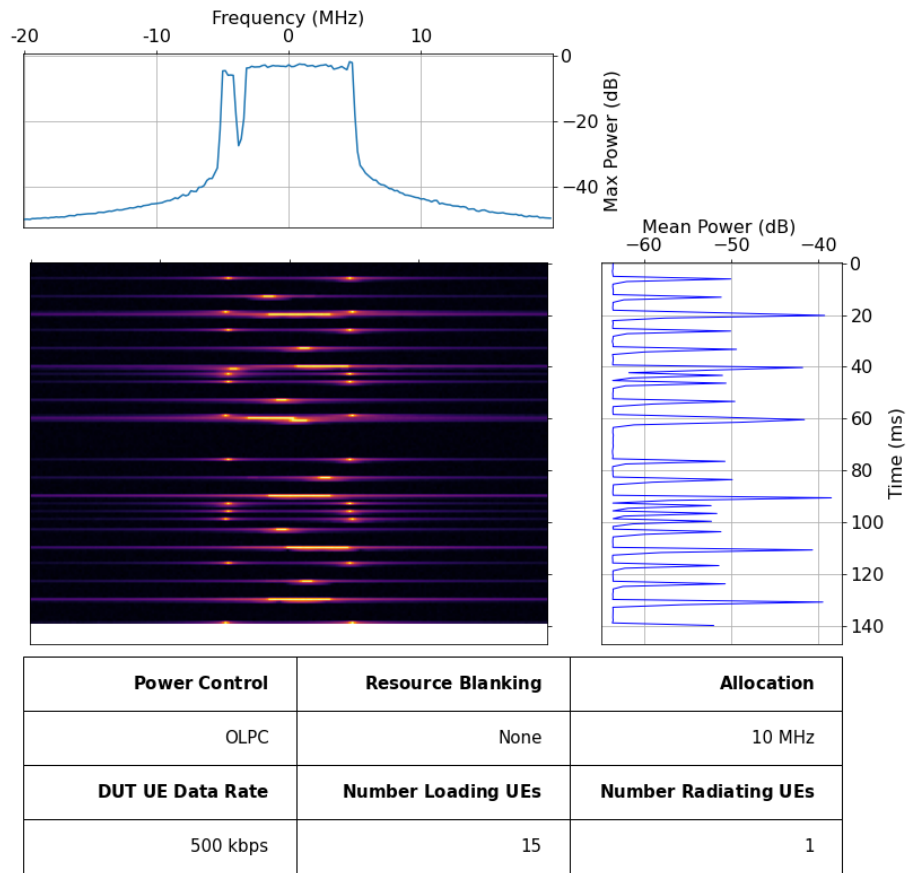


Figure B.35: 140 milliseconds of IQ Recording 1 of Configuration Number 35.

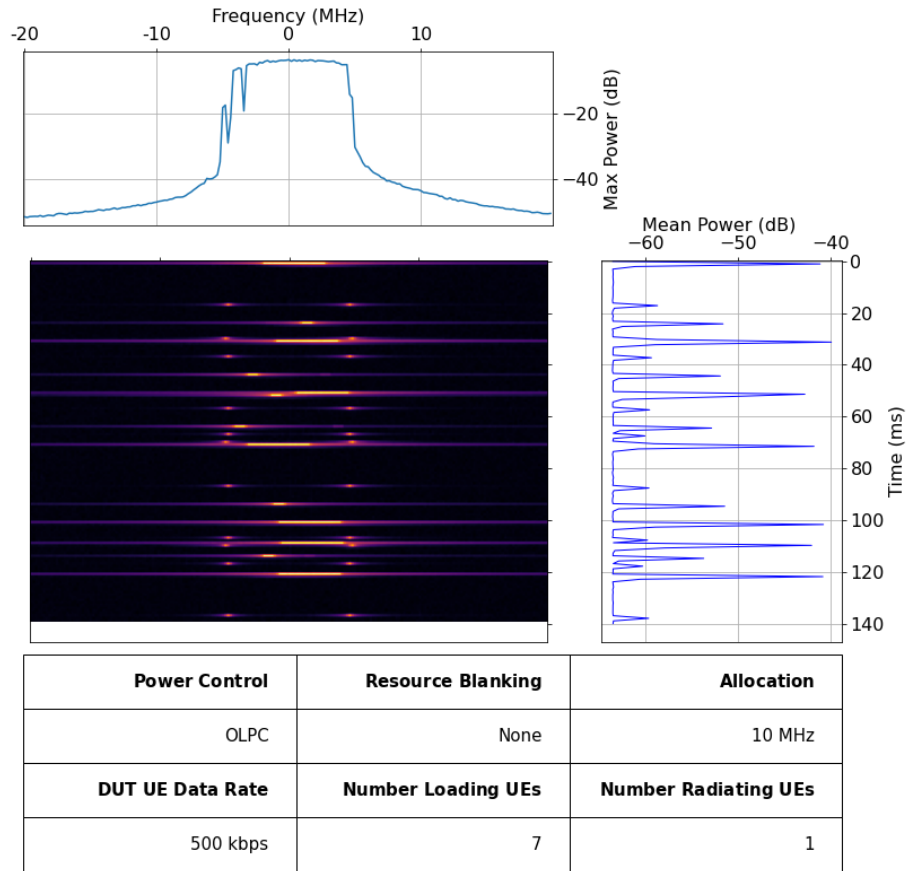


Figure B.36: 140 milliseconds of IQ Recording 1 of Configuration Number 36.

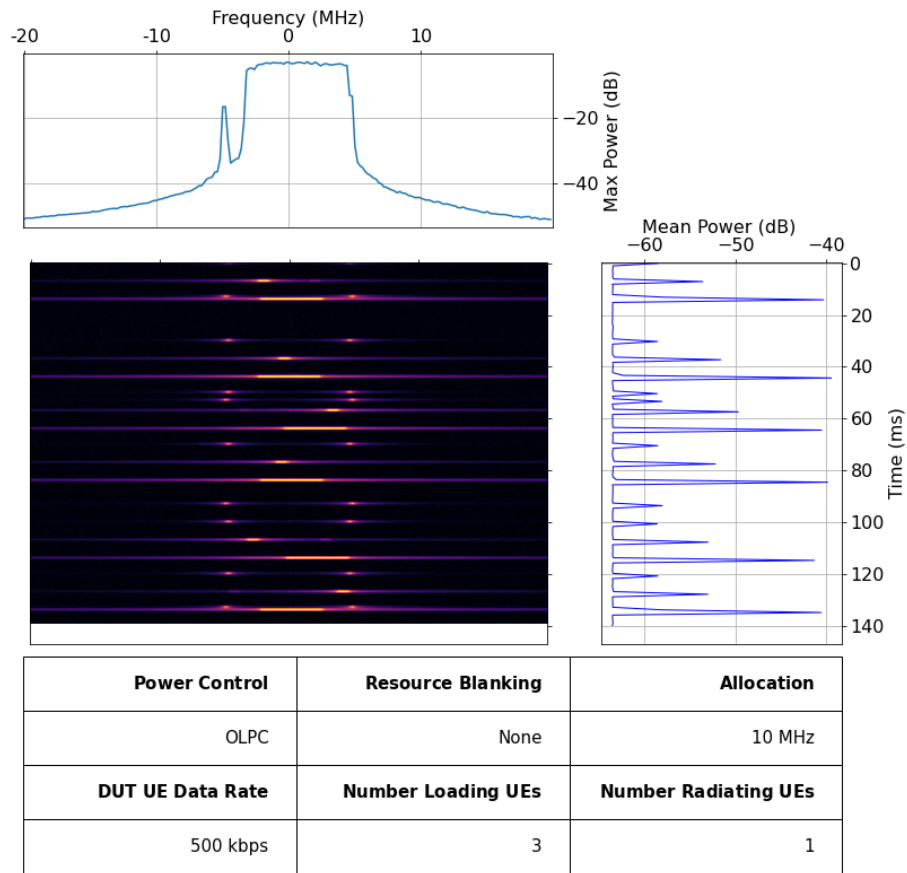


Figure B.37: 140 milliseconds of IQ Recording 1 of Configuration Number 37.

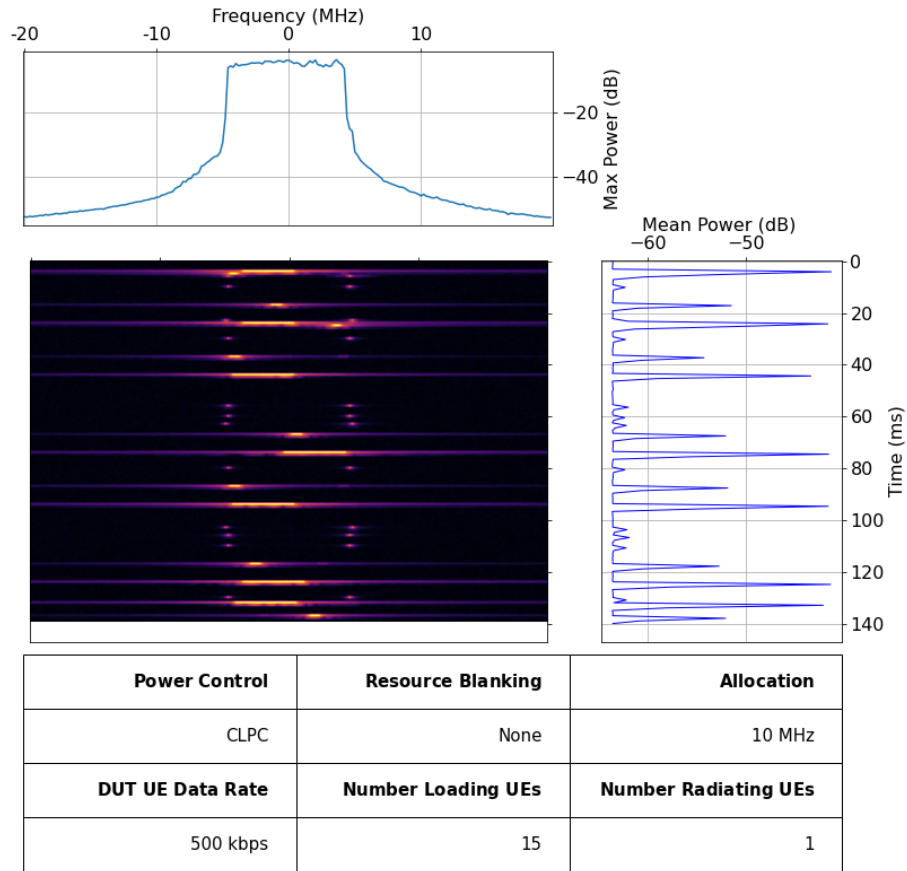


Figure B.38: 140 milliseconds of IQ Recording 1 of Configuration Number 38.

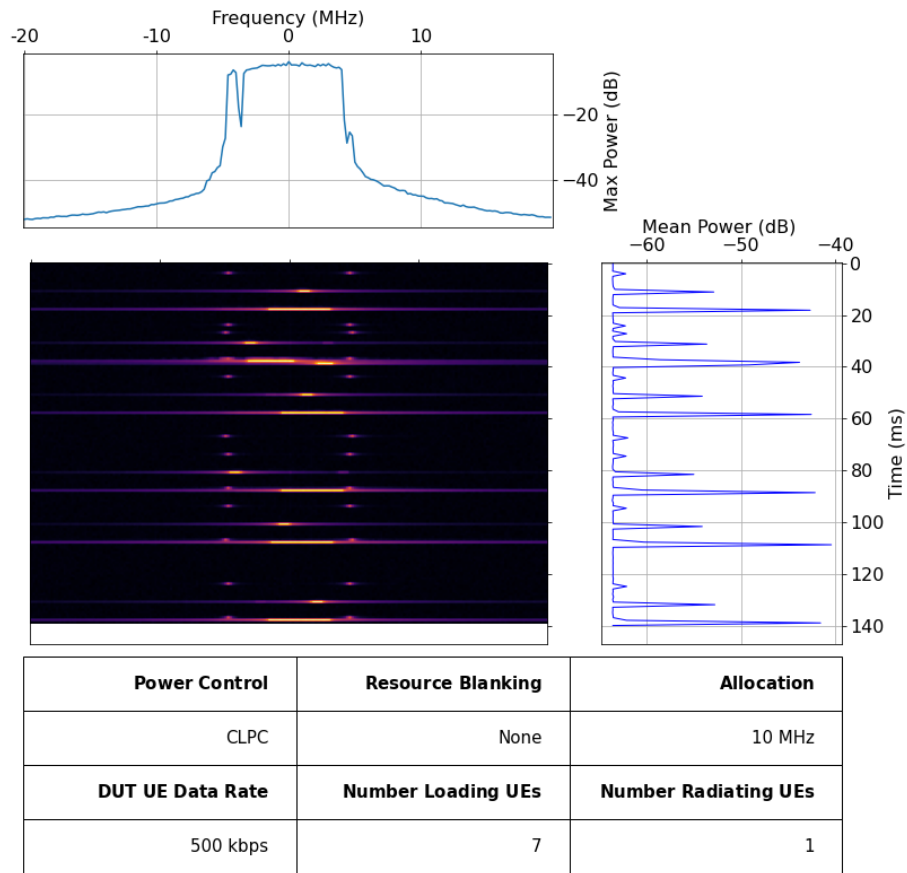


Figure B.39: 140 milliseconds of IQ Recording 1 of Configuration Number 39.

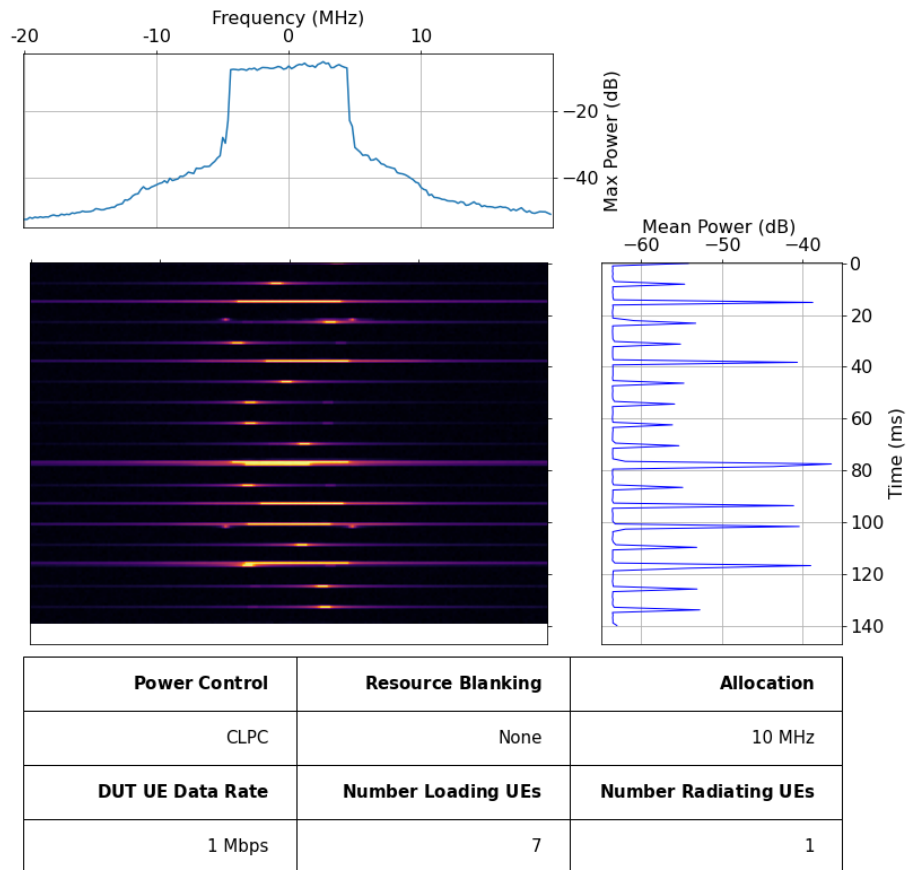


Figure B.40: 140 milliseconds of IQ Recording 1 of Configuration Number 40.

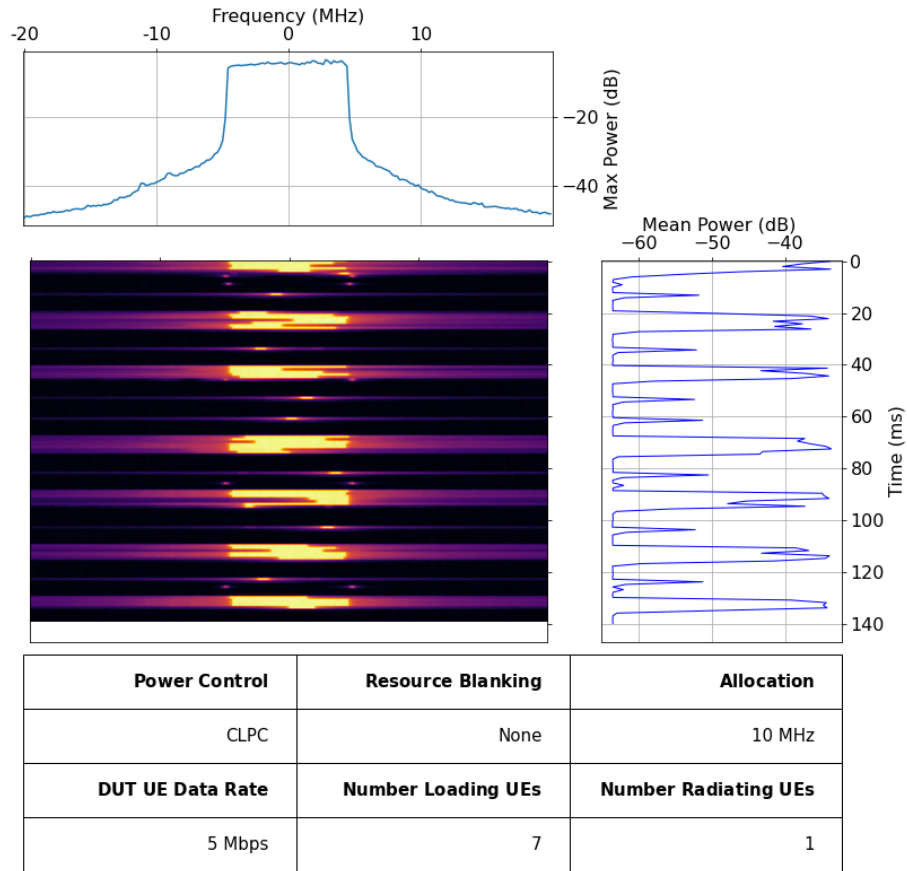


Figure B.41: 140 milliseconds of IQ Recording 1 of Configuration Number 41.

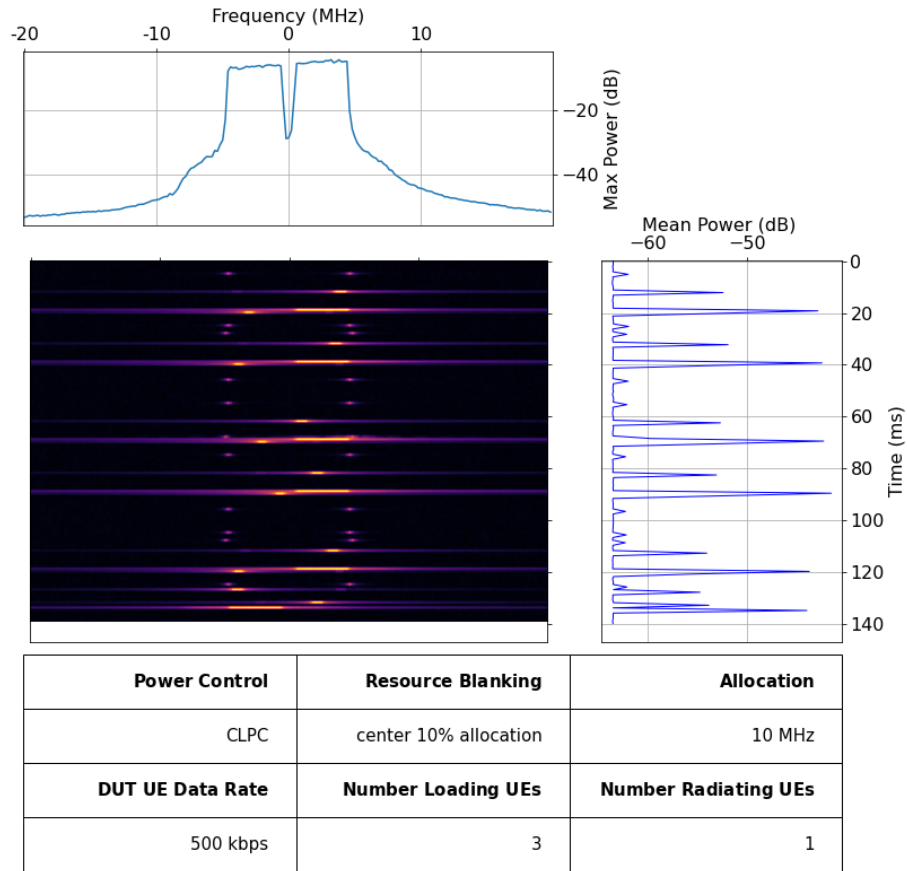


Figure B.42: 140 milliseconds of IQ Recording 1 of Configuration Number 42.

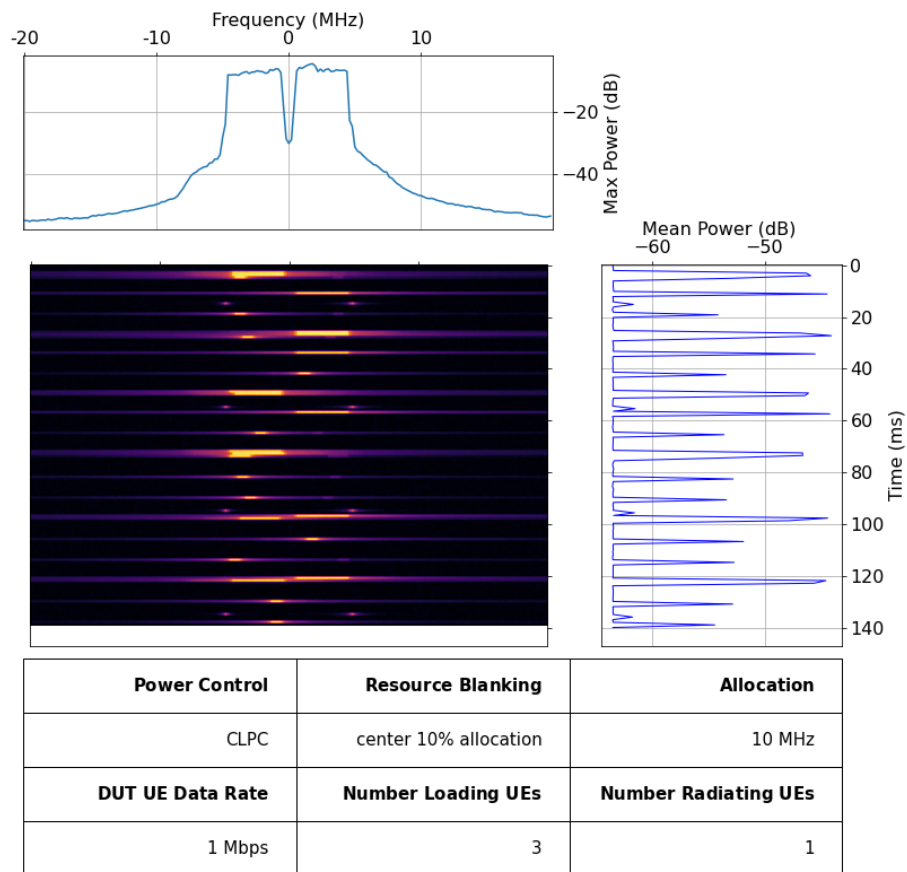


Figure B.43: 140 milliseconds of IQ Recording 1 of Configuration Number 43.

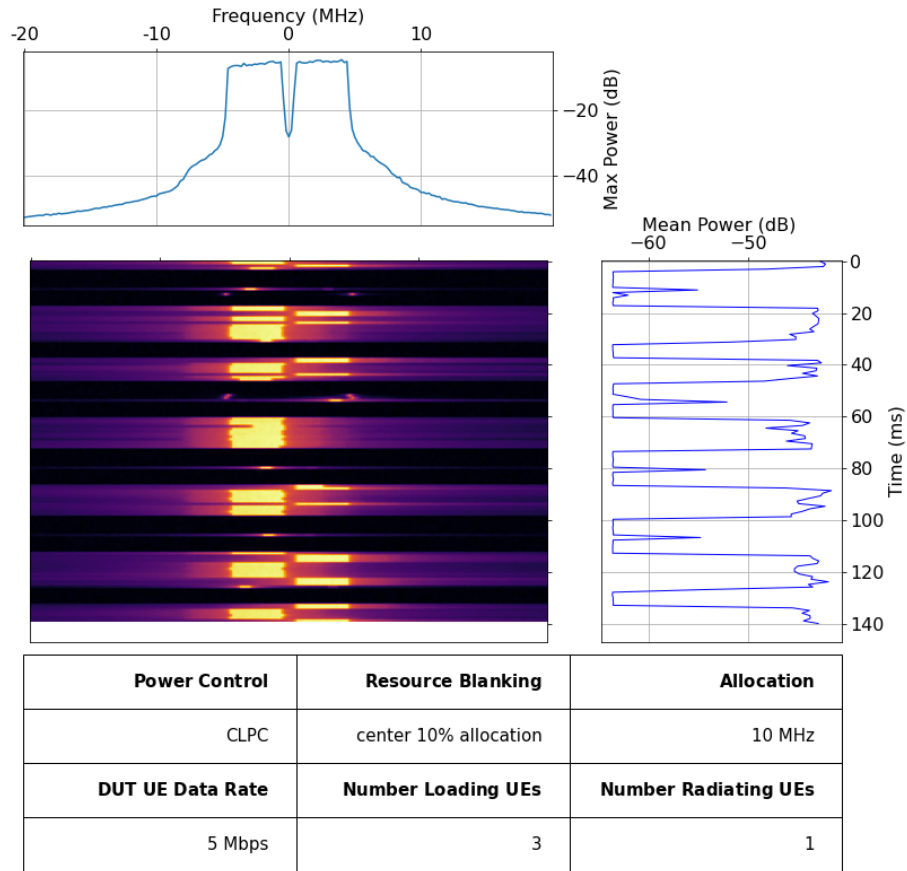


Figure B.44: 140 milliseconds of IQ Recording 1 of Configuration Number 44.

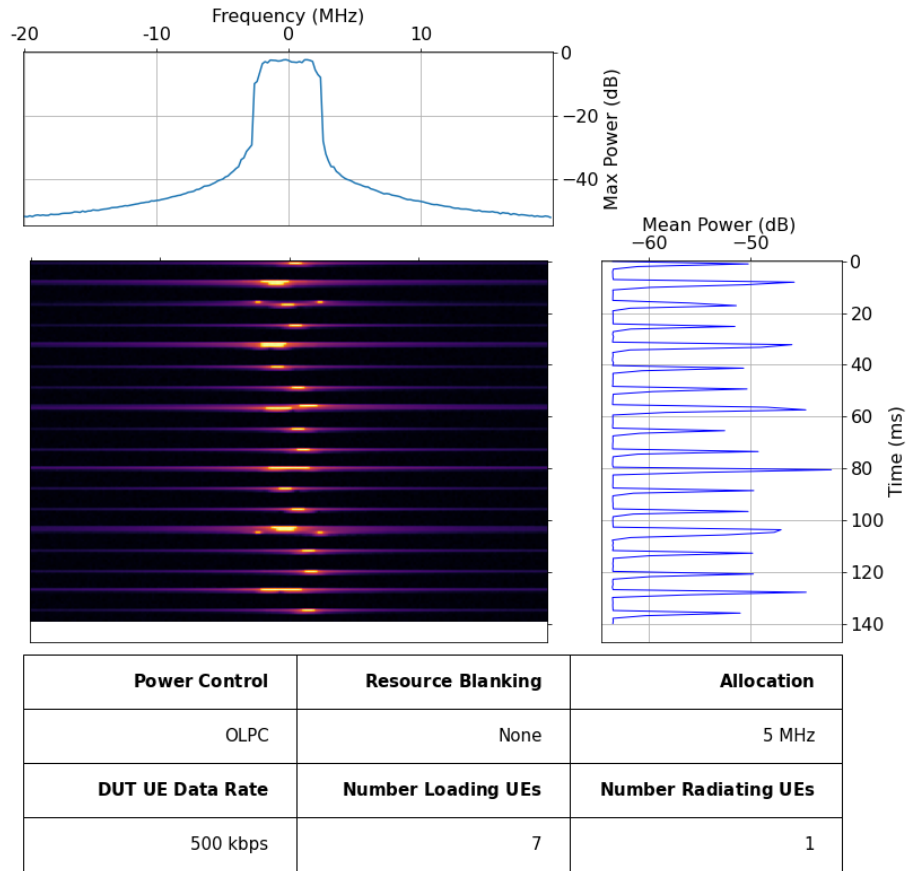


Figure B.45: 140 milliseconds of IQ Recording 1 of Configuration Number 45.

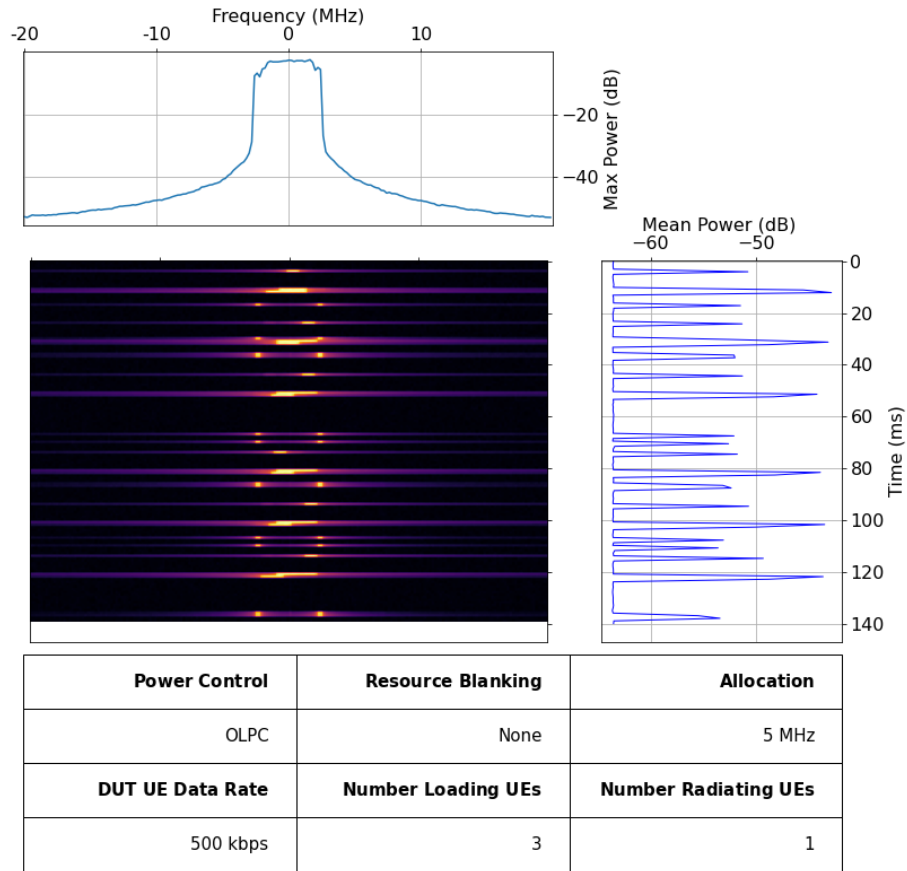


Figure B.46: 140 milliseconds of IQ Recording 1 of Configuration Number 46.

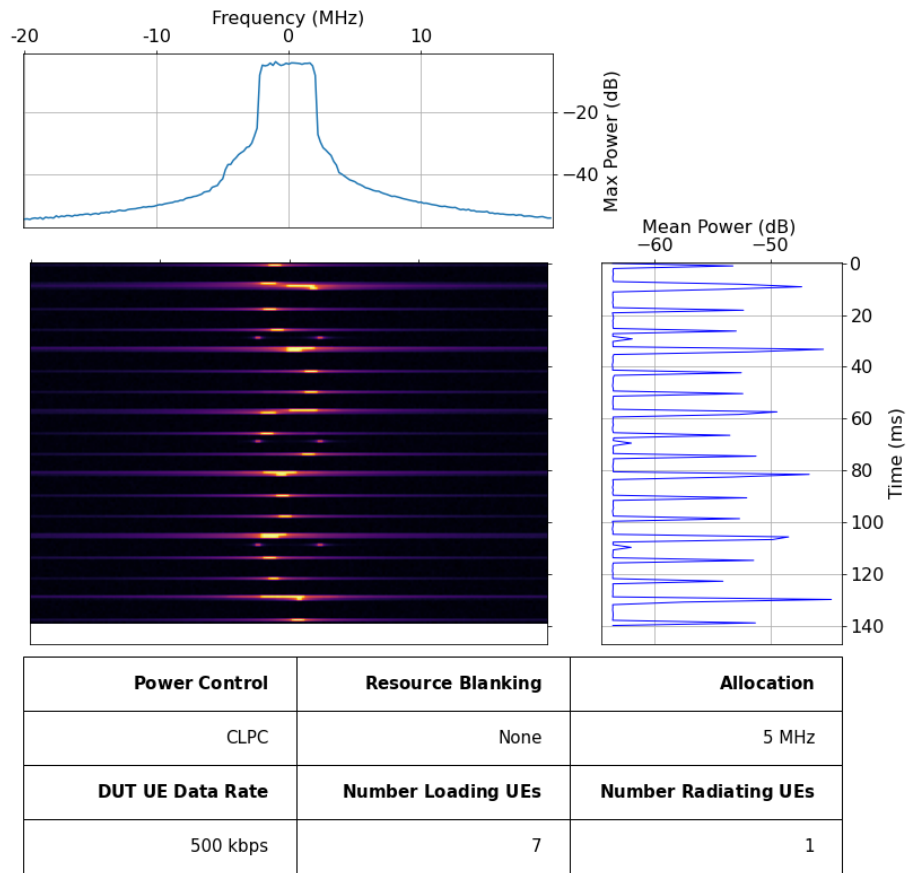


Figure B.47: 140 milliseconds of IQ Recording 1 of Configuration Number 47.

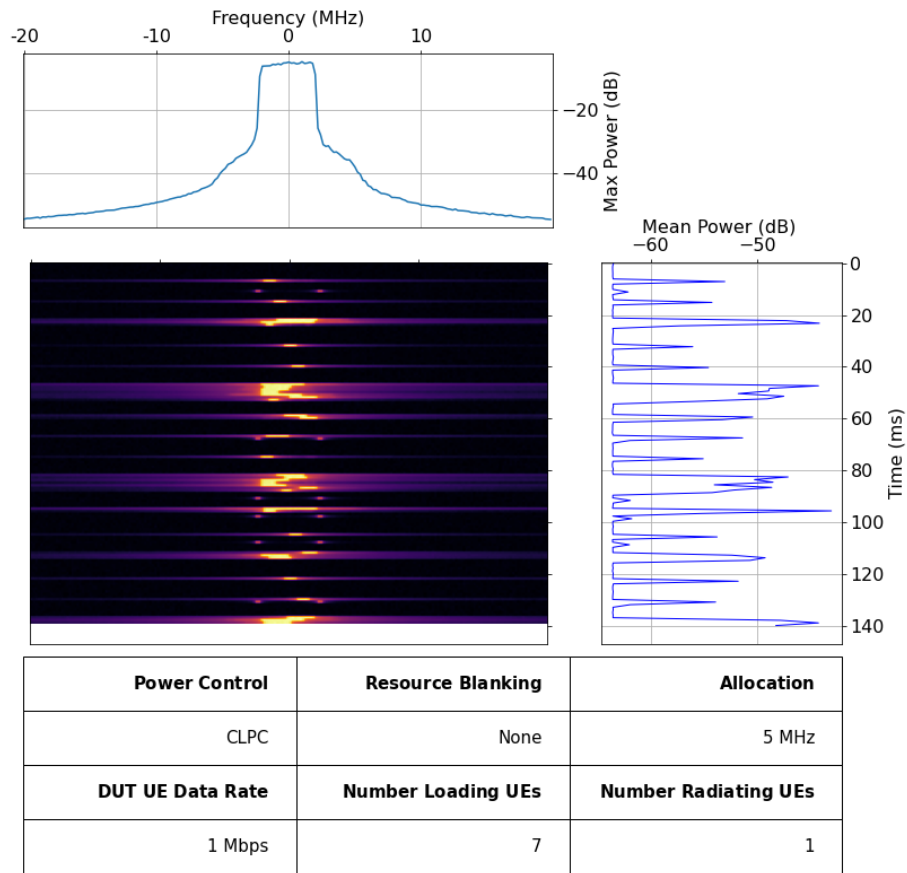


Figure B.48: 140 milliseconds of IQ Recording 1 of Configuration Number 48.

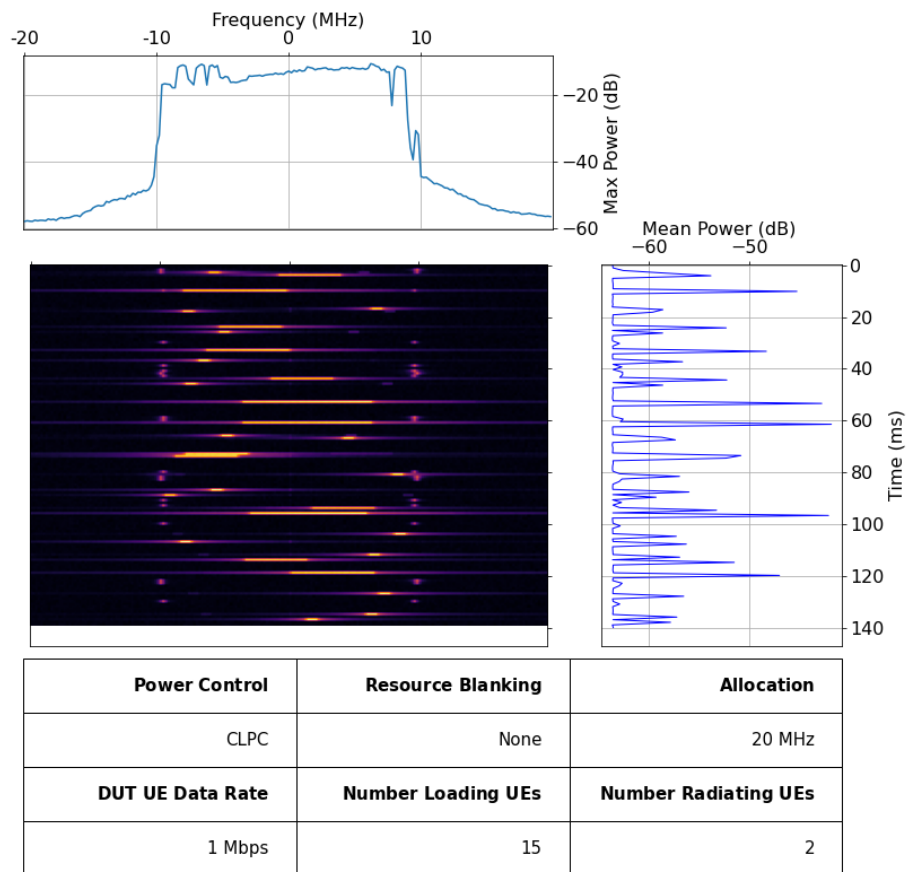


Figure B.49: 140 milliseconds of IQ Recording 1 of Configuration Number 49.

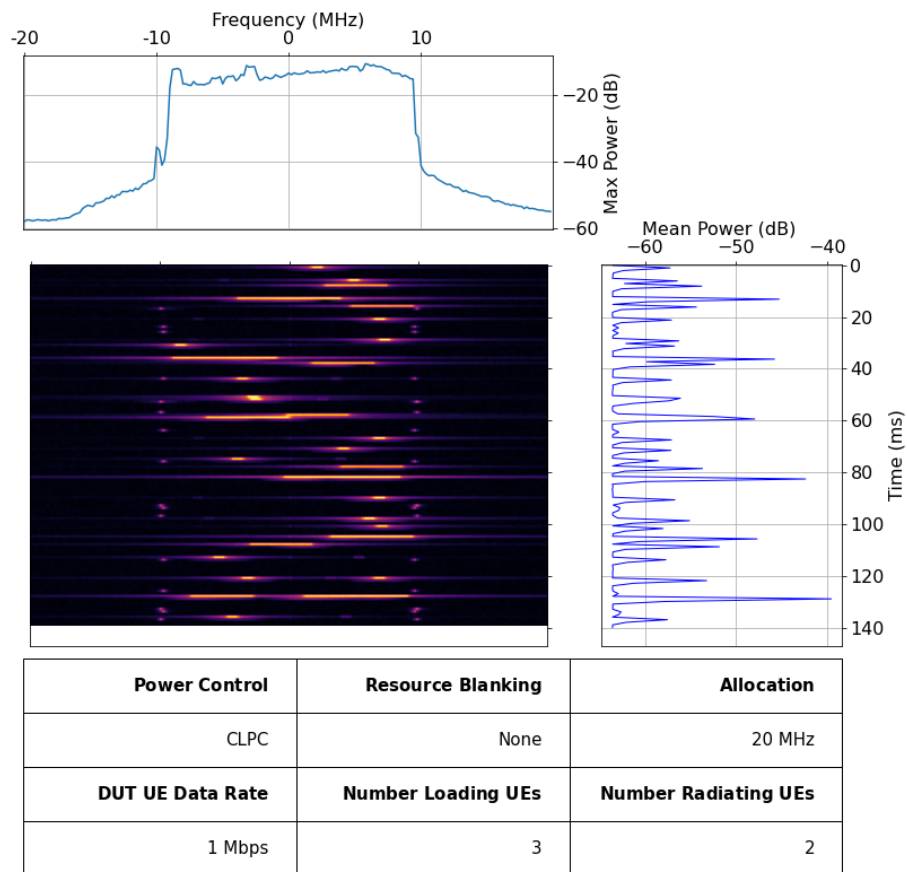


Figure B.50: 140 milliseconds of IQ Recording 1 of Configuration Number 50.

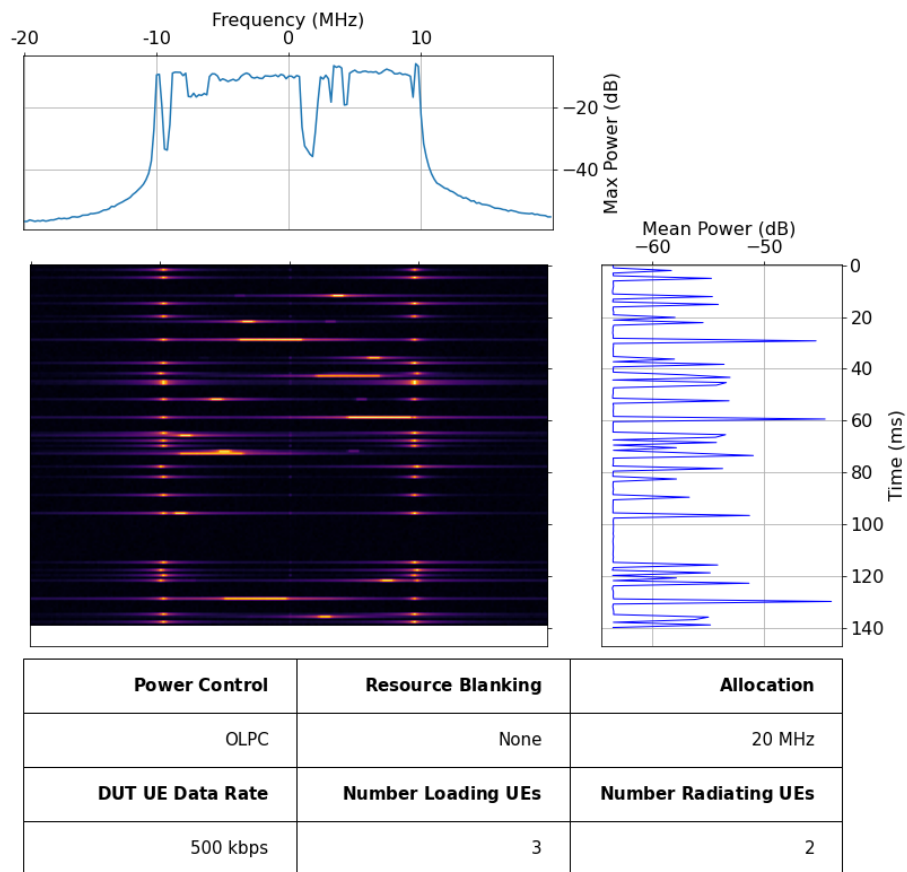


Figure B.51: 140 milliseconds of IQ Recording 1 of Configuration Number 51.

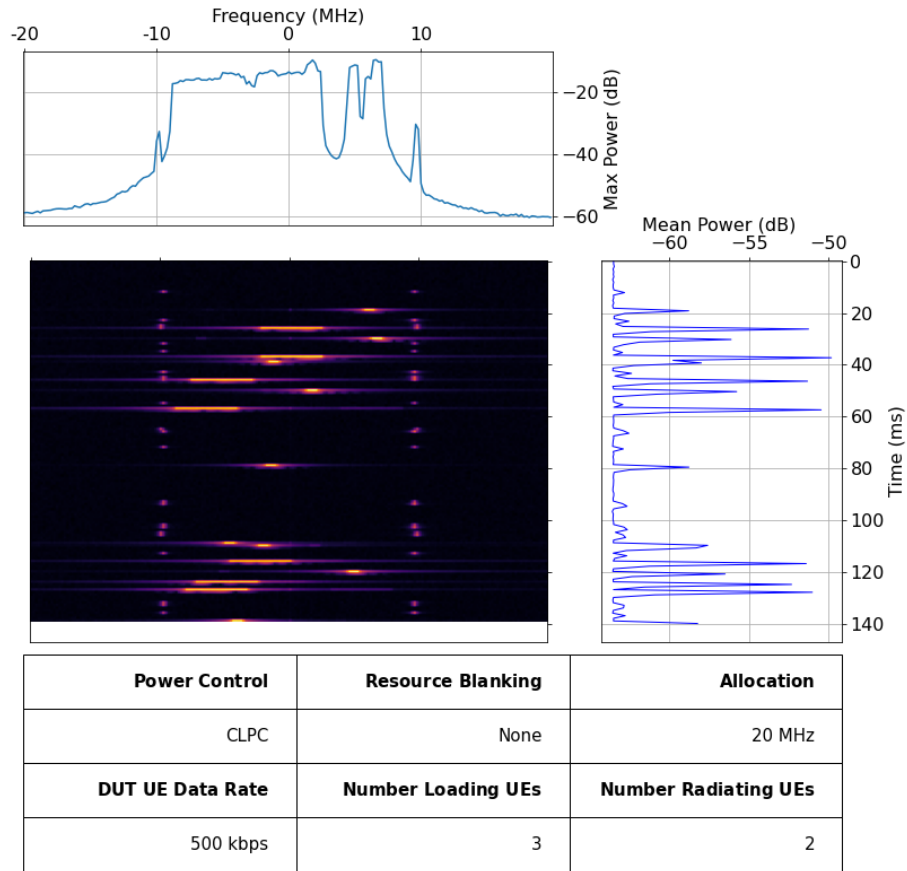


Figure B.52: 140 milliseconds of IQ Recording 1 of Configuration Number 52.

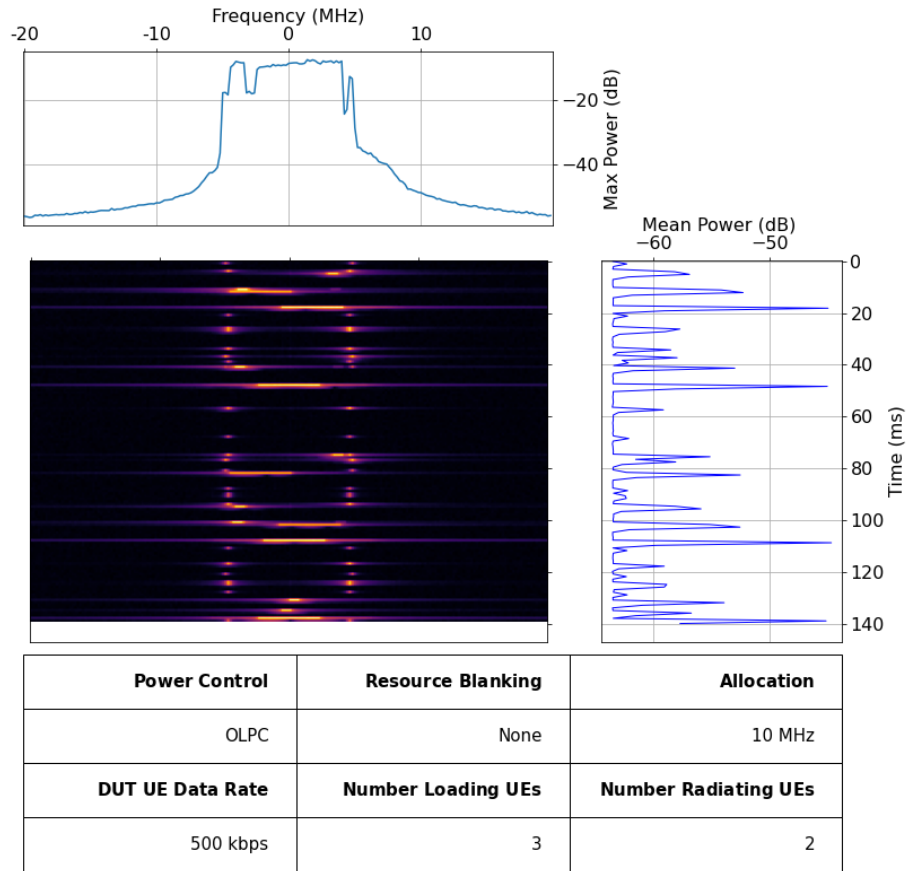


Figure B.53: 140 milliseconds of IQ Recording 1 of Configuration Number 53.

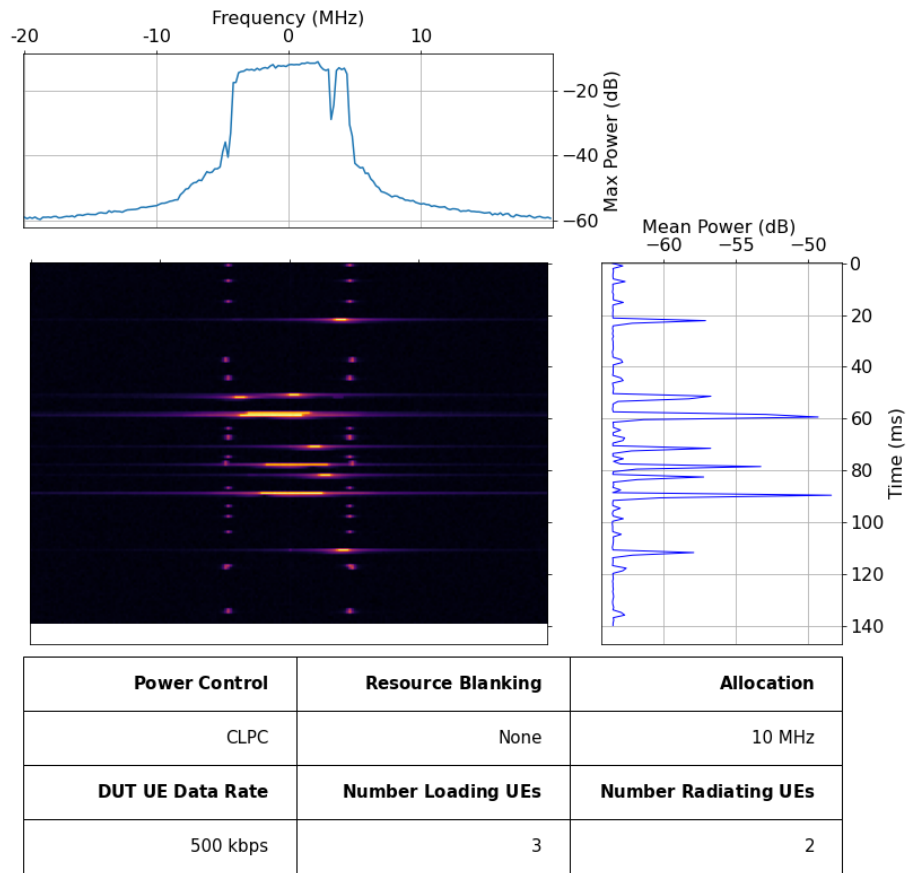


Figure B.54: 140 milliseconds of IQ Recording 1 of Configuration Number 54.

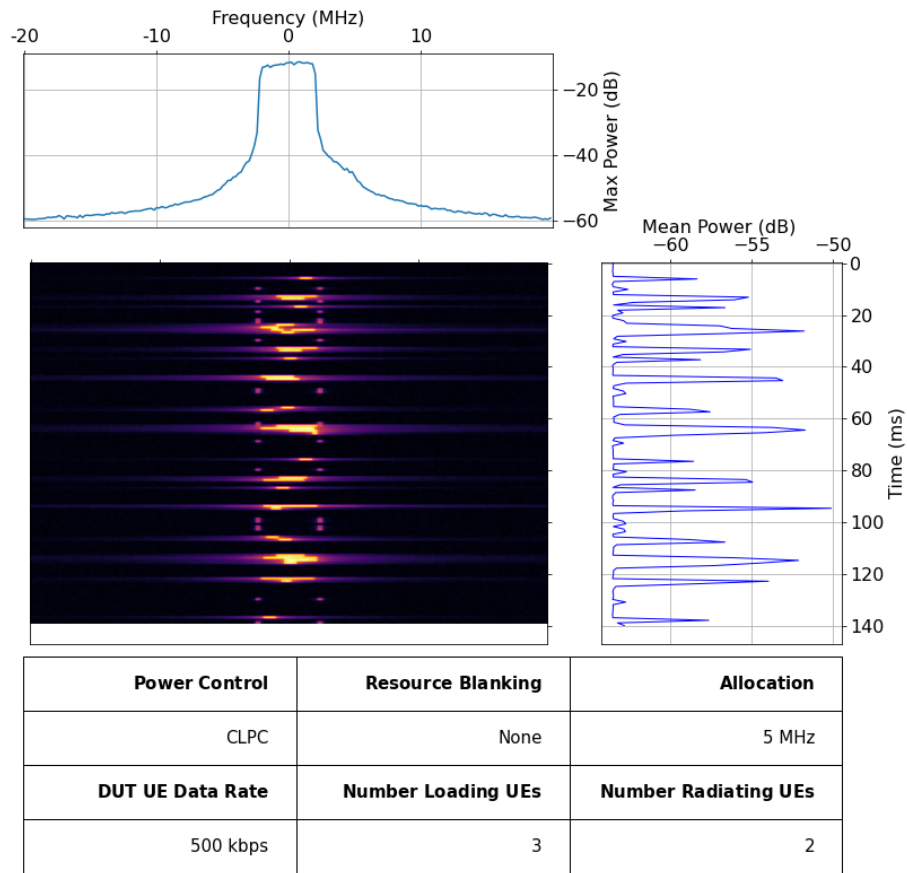


Figure B.55: 140 milliseconds of IQ Recording 1 of Configuration Number 55.

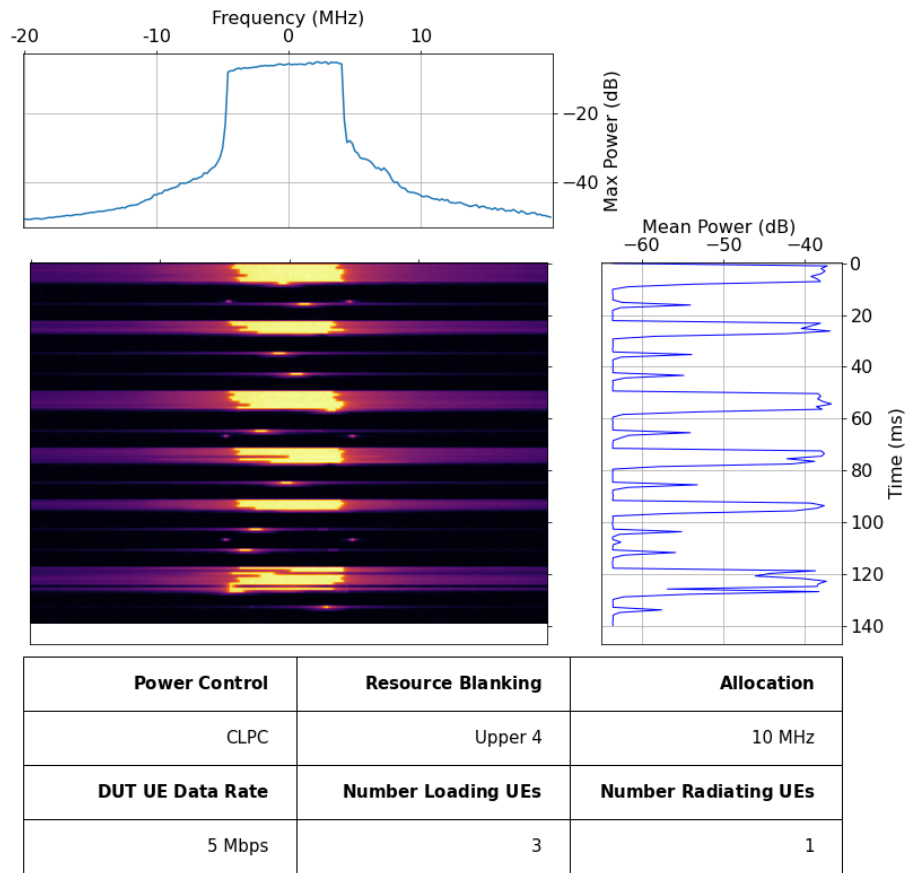


Figure B.56: 140 milliseconds of IQ Recording 1 of Configuration Number 56.

Bibliography

- [1] J. Coder, A. Wunderlich, M. Frey, P. Blanchard, D. Kuester, A. Kord, M. Lees, A. Sanders, J. Splett, L. Koepke, R. Horansky, D. McGillivray, J. Ladbury, J. Correia, V. Ramaswamy, J. Fevold, S. Lefebvre, J. Johnson, J. Carpenter, M. Lofquist, and K. Hartley, "Characterizing LTE User Equipment Emissions: Factor Screening," NASCTN, Tech. Rep. 2069, Sep 2019. [Online]. Available: <https://doi.org/10.6028/NIST.TN.2069>
- [2] E. D. Nelson and D. A. McGillivray, "In-Situ Captures of LTE for Aeronautical Mobile Telemetry System Evaluation," National Telecommunications and Information Administration, Tech. Rep. NTIA Report 21-553, March 2021. [Online]. Available: <https://www.its.bldrdoc.gov/publications/details.aspx?pub=3262>
- [3] 3rd Generation Partnership Project, "LTE: E-UTRA Radio Resource Control (RCC) (3GPP TS 36.331 version 13.0.0 Release 13)," 3GPP, Tech. Rep., 2016. [Online]. Available: https://www.etsi.org/deliver/etsi_ts/136300_136399/136331/13.00.00_60/ts_136331v130000p.pdf
- [4] "American National Standard For Methods Of Measurement Of Radio - Noise Emissions From Low-Voltage Electrical And Electronic Equipment In The Range Of 9 KHz To 40 GHz," American National Standards Institute, Tech. Rep., 2014. [Online]. Available: https://webstore.ansi.org/standards/ieee/ieeecsansic632014?gclid=CjwKCAjw1K75BRAEEiwAd41h1NMDFSTxoU8tLVO_oTJrsTb4wQZ3U0DdodYtVrBVgyVIQqSQw8dCRoCTJEQAvD_BwE
- [5] "Electromagnetic compatibility (EMC) - Part 4-3 : Testing and measurement techniques - Radiated, radio-frequency, electromagnetic field immunity test," American National Standards Institute, Tech. Rep., <https://webstore.iec.ch/publication/4209>. [Online]. Available: <https://webstore.iec.ch/publication/4209>
- [6] R. Horansky, J. Coder, and J. Ladbury, "LTE Handset Emissions: Radiation Pattern Measurements Final Test Report," NASCTN, Tech. Rep. 2056, Aug 2019. [Online]. Available: <https://doi.org/10.6028/NIST.TN.2056.pdf>
- [7] 3rd Generation Partnership Project, "Physical layer procedures (3GPP TS 36.213 Release 10)," 3GPP, Tech. Rep., 2011. [Online]. Available: https://www.etsi.org/deliver/etsi_ts/136200_136299/136213/10.03.00_60/ts_136213v100300p.pdf
- [8] Rohde & Schwarz, "R& S ZN-Zxxx Calibration Units Specifications," Rohde & Schwarz, Tech. Rep., 2019. [Online]. Available: https://scdn.rohde-schwarz.com/ur/pws/dl_downloads/dl_common_library/dl_brochures_and_datasheets/pdf_1/ZN-Zxxx_dat-sw_en_5214-7558-22_v0400.pdf
- [9] J. Kraus, Antennas, 2nd ed. Boston: McGraw-Hill, 1988.
- [10] Keysight Technologies, "Time Domain Reflectometry Theory, Application Note," Keysight, Tech. Rep., 2015.
- [11] Joint Committee for Guides in Metrology, "Evaluation of Measurement Data-Guide to the Expression of Uncertainty Measurement," International Bureau of Weights and Measures (BIPM), Tech. Rep., Sep 2008. [Online]. Available: <http://www.bipm.org/en/publications/guides/gum.html>

REPORT DOCUMENTATION PAGE

Form Approved
OMB No. 0704-0188

The public reporting burden for this collection of information is estimated to average 1 hour per response, including the time for reviewing instructions, searching existing data sources, gathering and maintaining the data needed, and completing and reviewing the collection of information. Send comments regarding this burden estimate or any other aspect of this collection of information, including suggestions for reducing the burden, to Department of Defense, Washington Headquarters Services, Directorate for Information Operations and Reports (0704-0188), 1215 Jefferson Davis Highway, Suite 1204, Arlington, VA 22202-4302. Respondents should be aware that notwithstanding any other provision of law, no person shall be subject to any penalty for failing to comply with a collection of information if it does not display a currently valid OMB control number.

PLEASE DO NOT RETURN YOUR FORM TO THE ABOVE ADDRESS.

1. REPORT DATE (DD-MM-YYYY) 10-5-2021			2. REPORT TYPE NIST Technical Note		3. DATES COVERED (From - To) 24-02-2018 - 11-05-2021	
4. TITLE AND SUBTITLE Laboratory Method for Recording AWS-3 LTE Waveforms				5a. CONTRACT NUMBER F1S0AG8229G001		
				5b. GRANT NUMBER		
				5c. PROGRAM ELEMENT NUMBER R20-670-0004		
6. AUTHOR(S) Aric W. Sanders, M. Keith Forsyth, Robert D. Horansky, Azizollah Kord, Duncan A. McGillivray				5d. PROJECT NUMBER 6702378		
				5e. TASK NUMBER 000		
				5f. WORK UNIT NUMBER 30-67-0670-02-00-00-00		
7. PERFORMING ORGANIZATION NAME(S) AND ADDRESS(ES) National Institute of Standards and Technology (NIST) Communications Technology Laboratory, NASCTN Program Office 325 Broadway Boulder, CO 80305				8. PERFORMING ORGANIZATION REPORT NUMBER NIST TN 2159		
9. SPONSORING/MONITORING AGENCY NAME(S) AND ADDRESS(ES) Edwards Air Force Base 412th Test Engineering Group, Spectrum Relocation Program 307 E Popson Ave, Ste 204 Edwards AFB, CA 93524-1180				10. SPONSOR/MONITOR'S ACRONYM(S) EAFB		
				11. SPONSOR/MONITOR'S REPORT NUMBER(S)		
12. DISTRIBUTION/AVAILABILITY STATEMENT Approved for Public Release. Distribution Unlimited.						
13. SUPPLEMENTARY NOTES						
14. ABSTRACT The focus of this work provides a library of actual long-term evolution (LTE) user equipment (UE) emissions with sufficient time resolution and dynamic range for use in spectrum sharing, and interference susceptibility studies. National Advanced Spectrum and Communications Test Network (NASCTN)'s "AWS-3 LTE impacts on AMT" study required the use of LTE waveforms from advanced wireless services 3 (AWS-3) equipment for playback in a susceptibility analysis. Thus, National Institute of Standards and Technology (NIST) and the NASCTN program office commissioned the work as part of the Edwards Air Force Base (EAFB) proposed and NASCTN steering committee approved test request to investigate the impact of LTE activities on aeronautical mobile telemetry (AMT) links. The recordings of the UE emissions are performed in the NIST Broadband Interoperability Testbed (NBIT) facility, where under laboratory conditions, a single UE (and subsequently a second UE) are in connection to a fully emulated LTE network with a carrier grade evolved Node B (eNB). NBIT's hybrid radio frequency (RF) testbed allows for a radiated free-space connection to the UE in conjunction with a cabled user equipment traffic generator (UTG) for control of cell loading conditions.						
15. SUBJECT TERMS NASCTN, LTE, RF Testing, Metrology, LTE waveform, waveform capture, lab capture, AWS-3						
16. SECURITY CLASSIFICATION OF:			17. LIMITATION OF ABSTRACT	18. NUMBER OF PAGES	19a. NAME OF RESPONSIBLE PERSON	
a. REPORT	b. ABSTRACT	c. THIS PAGE			Melissa Midzor	
UNCLASSIFIED	UNCLASSIFIED	UNCLASSIFIED	None	87	19b. TELEPHONE NUMBER (Include area code) (303) 497-3591	